Teknik Dergi
Technical Journal

TEKNİK DERGİ PUBLICATION PRINCIPLES

Teknik Dergi is a scientific and technical journal indexed by the Science Citation Index Expanded. Annually six issues are published, three in Turkish in the months of January, May and September, three in English in March, July and November. Its main principles of publication are summarized below:

1. Articles reporting original scientific research and those reflecting interesting engineering applications are accepted for publication. To be classified as original, the work should either produce new scientific knowledge or add a genuinely new dimension to the existing knowledge or develop a totally new method or substantially improve an existing method.

2. Articles reporting preliminary results of scientific studies and those which do not qualify as full articles but provide useful information for the reader can be considered for publication as technical notes.

3. Discussions received from the readers of the published articles within three months from publication are reviewed by the Editorial Board and then published together with the closing remarks of the author.

4. Manuscripts submitted for publication are evaluated by two or three reviewers unknown to the authors. In the light of their reports, final decision to accept or decline is taken by the Editorial Board. General policy of the Board is to get the insufficient manuscripts improved in line with the reviewers' proposals. Articles that fail to reach the desired level are declined. Reasons behind decisions are not declared.

5. A signed statement is taken from the authors, declaring that the article has not been published as a "journal article or book chapter". In case the Editorial Board is in the opinion that the article has already been published elsewhere with minor changes or suspects plagiarism or a similar violation of ethics, then not only that article, but none of the articles of the same authors are published.

6. Papers reporting works presented as conference papers and developed further may be considered for publication. The conference it was presented to is given as a footnote in the first page.

7. Additionally, a document signed by all authors, transferring the copyright to UCTEA Chamber of Civil Engineers is submitted together with the manuscript.

Teknik Dergi
Technical Journal

Teknik Dergi is indexed by
- Science Citation Index Expanded
- Scopus
- Journal Citation Reports / Science Edition
- Engineering Index
- Concrete Abstracts (American Concrete Institute)
- National Technical Information Service (US NTIS)
- CITIS
- Ulrich's International Periodical's Directory
- TÜBİTAK / ULAKBİM

Teknik Dergi is a peer reviewed open access periodical publishing papers of original research and interesting practice cases. It addresses both the research community and the practicing engineers.

Reviewers:

This list is renewed each year and includes reviewers who served in the last two years of publication.

CONTENTS

OBITUARY – ENDER ARKUN

It is with sorrow that we announce the passing of our dear friend and colleague Mr. Ender Arkun on April 23, 2020.

Following his involvement in the launching of Teknik Dergi in 1989, Mr. Arkun actively served in the Editorial Board for an uninterrupted period of thirty years. After the journal's move to bilingual publication three years ago, he also contributed to the final editing of the manuscripts in English.

Mr. Ender Arkun was born on March 23, 1940 in Kabul, Afghanistan, where his father was on temporary duty as a medical doctor. When he was four years old, the family moved back to Istanbul. He attended the English High School and later Robert College, where he was introduced to western culture and outlook. He later studied civil engineering at Yıldız Technical University.

After graduating in 1969, Mr. Arkun worked as a design engineer for an Italian contractor company in charge of the design and construction of the viaducts on the E5 highway. In 1971, he took office in the Scientific and Technical Research Council of Turkey (TUBITAK). During his two terms at TUBITAK (1971-1988 and 2000-2004), he served in various positions, as Researcher and Acting Chair of the Building Research Institute, as Deputy Secretary General and as Chair of the Construction Technology Research Group. He contributed to the document "Turkish Science Policies 1983-2003". Between the two periods of his TUBITAK service, he worked for eleven years for the private construction sector and served as the Secretary General of a leading construction company in Turkey. During his first period of TUBITAK employment, Mr. Arkun assumed a duty in the Turkish Standards Institute to serve as a member of the Civil Engineering Standards Coordination Group.

After leaving TUBITAK, he joined the Turkish Academy of Sciences (TUBA) and served as the Consultant to the Academy President for four years. His interview with Prof. Bernard Lewis at Princeton University is an important documentary produced by TUBA within the framework of a series titled "Those Who Cast Light on Science".

He was happily married to Sünter Arkun long enough to celebrate their golden anniversary. He had a daughter, a son and a grandson.

Mr. Arkun was a well-educated and well-balanced gentleman. He was known by his tolerant and friendly personality, which made him popular in both the social and business circles. His reliable and industrious character and his refined sense of humour made collaboration with him both productive and enjoyable.

The Editorial Board acknowledge the invaluable contributions of Mr. Ender Arkun to IMO Teknik Dergi and wish to extend their sincerest condolences to the Arkun Family.

Prof. Tuğrul Tankut
On behalf of the Editorial Board

Credit Success Rates of Certified Green Buildings in Turkey

Xhensila THOMOLLARI[1]
Vedat TOĞAN[2]

ABSTRACT

The green building rating systems have been used as a tool to evaluate the environmental impact of buildings since 1990. In Turkey, Leadership in Energy and Environmental Design (LEED) is in the first place concerning the total number of certified green buildings and then followed by Building Research Establishment Environmental Assessment Method (BREEAM) and German Sustainable Building Council (DGNB). This paper aims to give general information concerning the 287 certified green buildings, and to investigate an updated situation of credit success rates of 127 LEED new construction certified green buildings in Turkey. The results show that the certified green buildings in Turkey have a lower average percentage of credit success rates in indoor environmental quality, energy efficiency, and material and resources categories compared to the other groups. Also, despite the increasing number of the certified projects mostly office buildings through the years, it is noticed an unequal geographical distribution of the examples.

Keywords: Credit success, LEED, Sustainable Development, Turkey.

1. INTRODUCTION

For the developing countries, construction industry, among the other industries, has been leading industry that contributes significantly to the economic development. However, though it contributes to the economy, this sector has negative impacts on environment. For example, the building stock is responsible for using 40% of all raw materials, 17% of freshwater withdrawals, consuming around 40% of total energy used, and generating 40% of the total solid waste [1-3]. Therefore, to reduce these adverse effects, designing and building sustainable or green projects are getting more important day by day. Since 1990, building sustainability level has been measured by international green building rating systems. It is estimated that around 600 green rating systems exist globally [4]. In 1990, Building Research

Establishment Environmental Assessment Method (BREEAM) was the first rating tool with the aim to assess the building's performance through various criteria under several categories. After BREEAM, several international rating systems Leadership in Energy and Environmental Design (LEED), German Sustainable Building Council (DGNB), Comprehensive Assessment System for Built Environment Efficiency (CASBEE), High Quality Environmental (HQE) and national rating systems such as Green Globe in Canada, Green Star in Australia, BEAM in China and lately CEDBIK in Turkey etc., have been applied to evaluate the sustainability level of buildings. BREEAM-certified buildings have shown 3-30% less energy consumption than conventional structures [5], while LEED-certified ones consume 18-39% less energy than conventional ones [6, 7]. Some of the economic benefits are 1-25% occupant productivity increase, minimum 14% higher rate of return, 10% higher market value of the asset, and 5-10% higher rental rate [5, 7-9]. Therefore, the trend of designing and constructing green buildings started to spread worldwide.

All rating systems have continuously been upgrading and adopting the list of criteria to assess more accurately the sustainability aspects of buildings. For example, in 2013, LEED through the LEED v4 version made a lot of changes in the list of criteria and the attributed points for each category. Similarly, BREEAM made a significant update in 2014 and 2016 [4, 9, 10]. Fig.1 shows chronological development of the BREEAM and LEED systems' versions and illustrates the percentage of credits of each assessment category in the respective version.

a) BREEAM versionsevolution

b) LEED versionsevolution
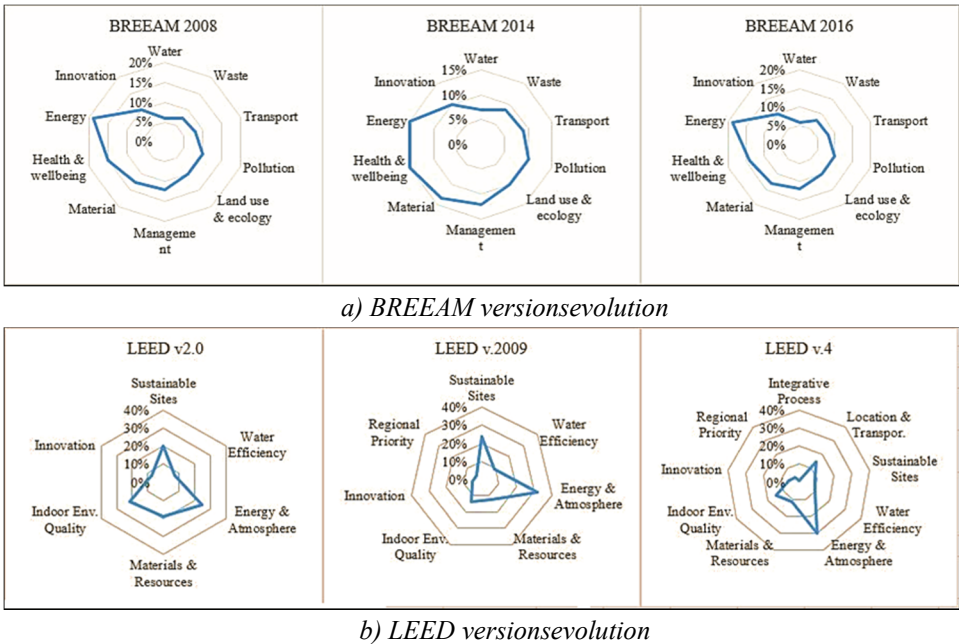
Figure 1 - Chronological development of BREEAM and LEED new construction scheme

The rating systems operating in Turkey are BREEAM, LEED, DGNB, and lately CEDBIK. There are 286 certified green buildings in Turkey, 242 of them are LEED, 43 of them are BREEAM, and one of them is DGNB certified, projects at the time of the study in October

2017. However, there was only one CEDBIK-certified project, since this national rating system was launched in the Turkish Market in 2016. The key features of these systems are introduced in Table 1. One main difference among these systems is the evaluation methodology. While BREEAM and DGNB use individual weightings for each assessment issue depending on the importance of the category, LEED and CEDBIK implement a simplified points system or scorecard. In 2015, Turkey was ranked in the 9th position regarding the total number of LEED-certified projects [11]. This ranking and the increased number of registered projects for certification under the LEED system (as seen in Fig. 5) indicate that interest in green construction practices in Turkey has been growing.

1.1. Literature Review

In the literature, there are many comparative studies related to different green building rating systems. These studies aimed to emphasize the differences between these rating systems by comparing them according to scheme typology, geographical distribution, indicators categories and attributed credits, standards used for establishing reference buildings during evaluation, etc. [4, 7, 12-17]. It can also be found several studies, in which the differences in the total obtained credits for a particular project evaluated according to various green rating systems, were pointed out [18, 19]. The different standards adopted in the rating systems used and the regional features of the state origins, where these rating systems were found, produced the variation on the results [18, 19]. There are limited studies in which the certified projects' allocation credits were analyzed. Ma and Cheng [20] examined 1000 projects in the United States certified by LEED-NC v2009. They used the percentage of average score method to explain the rate of credits achievement in individual subcategory criteria. Wu et al. [21] reviewed all the LEED v2.2 certified projects until its certification sunset date and concluded that the percentage of credit achievements in various categories varies in different countries. Moreover, Wu et al. [22] analyzed the credit allocation pattern of 3416 LEED v.2009 certified projects around the world. This study revealed that energy-related and material-related credits showed difficulty to achieve credits.

Wu et al. [23] investigated the credit achievement pattern of 4021 LEED v.2009 certified projects in the United States of America, China, Turkey, and Brazil. The results indicated that each country analyzed demonstrated different performance achievement in most rating categories including sustainable sites, water efficiency, energy and atmosphere, indoor environmental quality, and innovation in design. Also, Da Silva and Ruwanpura [24] compared the credit achievement of 42 LEED-certified projects in Canada with LEED-certified projects in the United States of America based on credit frequency indicators (CFIs). The study pointed out that factors such as climate conditions and regional location influence the credit achievement of the projects. Furthermore, there are several papers that were examined the credit achievements of Green Star certified projects. For instance, Xia et al. [25] analysed 388 certified building projects and Zuo et al. [26] examined 264 certified office projects with Green Star certificate located in Australia. The studies pointed out the easiest and most difficult categories to achieve credits during the certification process are based on the project types. Moreover, there is a lack of investigating LEED-certified projects in Turkey. Very few studies were carried out a partial analysis of particular samples of the certified projects in Turkey. Celik [27] evaluated 66 LEED-certified buildings in Turkey regarding their certification dates, the scores they have earned, their types and locations.

Bastanoglu[28] examined 52 Gold LEED new construction certified green buildings. Gokbayrak [29] assessed certified buildings under LEED new construction scheme in six different countries, among of which 102 certified projects in Turkey, and argued how the green building numbers, the projects' certificate types and its evaluation criteria are correlated with the countries' development levels. Also, Gunes [30] analysed 9 LEED and 6 BREEAM-certified projects, which have obtained a higher score at the time of preparing the study. On the other hand, Uğur and Leblebici [55] investigated in two green buildings certified as gold and platinum levels according to the LEED certification system in terms of construction and operating costs and property value. As implied from above, there is still a necessity for a full up-to-date investigation of the certified green buildings in Turkey.

Table 1 - Main features of BREEAM, LEED, DGNB and CEDBIK

	BREEAM	LEED	DGNB	CEDBIK
Country	UK	US	Germany	Turkey
Organizations	BRE	USGBC	DGNB	CEDBIK
No. of country implemented	77	160	20	1
Latest version	2016	2013	2017	2016
Categories	Management Health & Wellbeing Energy Transport Water Material Waste Land Use & Ecology pollution Innovation	Integrative Process Location and Transportation Sustainable Sites Water Efficiency Energy and Atmosphere Materials and Resources Indoor Environmental Quality Innovation Regional Priority	Environmental Economic Social-cultural and functional Technical Process Site	Integrative Process; Land use Water Efficiency Energy Efficiency Health and Comfort Materials and Resources Life on Property Operation and Maintenance Innovation
Evaluation method	Pre-weighted categories	Additive credits	Pre-weighted categories	Additive credits
Certificate level	Pass >30 Good >45 Very good >55 Excellent >70 Outstanding >85	Certified >40 Silver >50 Gold >60 Platinum >80	Bronze >50% Silver >65% Gold >80%	Certified >45 Good >65 Very good >80 Excellent >90
No. of certified buildings	563,461	110,315	1201	1
In Turkey	43	242	1	1

1.2. Research Objectives

This paper aims at i) investigating the situation of certified green buildings according to their distribution, certification level, and project types; and ii) presenting the more and less problematic categories and criteria to obtain credits. In contrast to above-mentioned studies in Turkey, larger sample size, i.e., 242 LEED, 43 BREEAM, 1 DGNB and 1 CEDBIK-certified green buildings, will be taken into consideration in this study. The results of this research can be useful to understand the situation of certified green projects in Turkey, and to point out the assessment categories that show higher or lower difficulty in earning credits. In this way, it can be understood which categories need further attention from the policymakers and design teams to obtain more credits in future projects.

2. METHODOLOGY

This research is organized into two main sections. In the first section, general statistical data related to 242 LEED, 43 BREEAM, 1 DGNB, and 1 CEDBIK-certified green buildings are illustrated. Later on, descriptive statistical analysis of credit achievements based on project types and rating categories of 127 LEED new construction certified projects is conducted. This paper focuses on LEED new construction system because i) this system is the well-developed versions of LEED [23], ii) the majority of green buildings in Turkey were certified under this system, iii) the data related to these projects were accessible online, and iv) the total number of projects certified by the newest version, i.e., LEED v4, at the time of the research was small. The small sample size can produce significantly biased results. Besides, LEED v.2009 is the first version of LEED that includes regional priority credits.
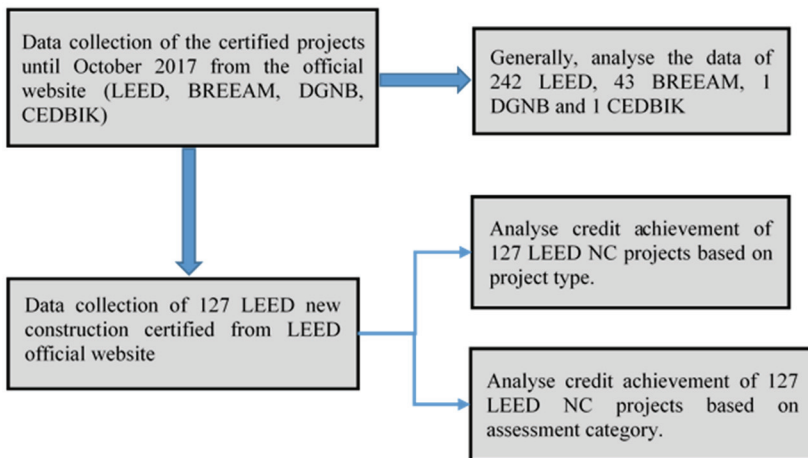
Figure 2 - Flowchart of the methodology

The analysis of this version can help to understand the performance of regional priority credits. On the other hand, the data related to BREEAM, DGNB, and CEDBIK-certified projects are partially reachable. The data used in the present study were retrieved from the official green building rating systems' websites in the directory of certified projects located in Turkey until October 2017. The general data (i.e., project name, total earned points, location, accredited date etc.) related to LEED-certified projects were retrieved in an excel spreadsheet downloaded from the official website [30]. Furthermore, the credit achievements in various categories for each project were obtained from the official website in the directory of certified projects located in Turkey [31]. The information about BREEAM, DGNB, and CEDBIK-certified projects were also collected from their official websites in the directory of certified projects located in Turkey [32-34]. Figure 2 presents the flow chart of the methodology followed in this study.

3. RESULTS AND DISCUSSIONS

3.1. General Statistical Data of the Certified Projects in Turkey

There were 242 LEED, 43 BREEAM, and 1 DGNB-certified projects at the time of the research conducted. Geographical distribution of LEED, BREEAM, DGNB, and CEDBIK-certified projects in Turkey is given in Fig. 3. Furthermore, Fig. 4 shows the percentage distribution of certified buildings according to geographical regions of Turkey. Turkey is located partly in Asia and partly in Europe and acts as a bridge between the two continents. The area of Turkey is divided into seven geographical regions according to their climate, location, flora and fauna, human habitat, agricultural diversities, transportation, topography and other characteristics.

The distribution of green building examples is in a linear relationship with the economic and demographic development of these geographical regions. It can be seen from Figs. 3- 4 and even from the literature [27, 30] that certified green buildings are mostly located in the western region of Turkey while there is a lack of certified green buildings in its other regions.
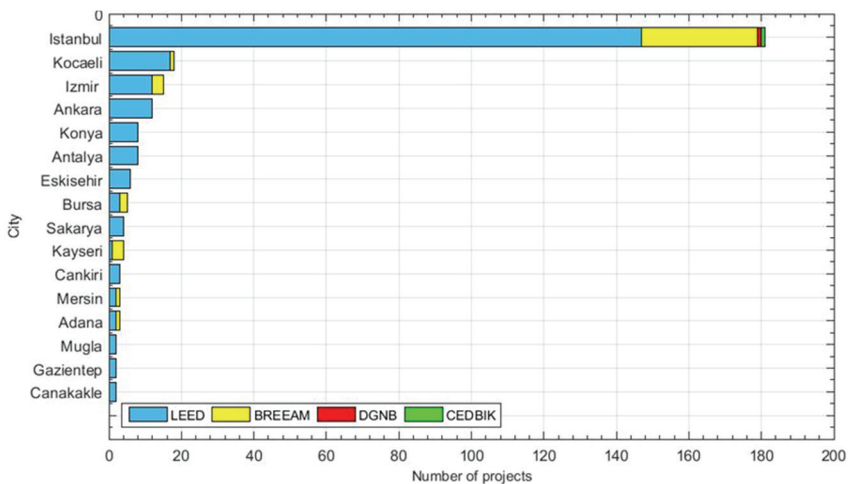
Figure.3 - Geographical distribution of certified projects

Figure 4 - Distribution of certified buildings in Turkey's geographical regions
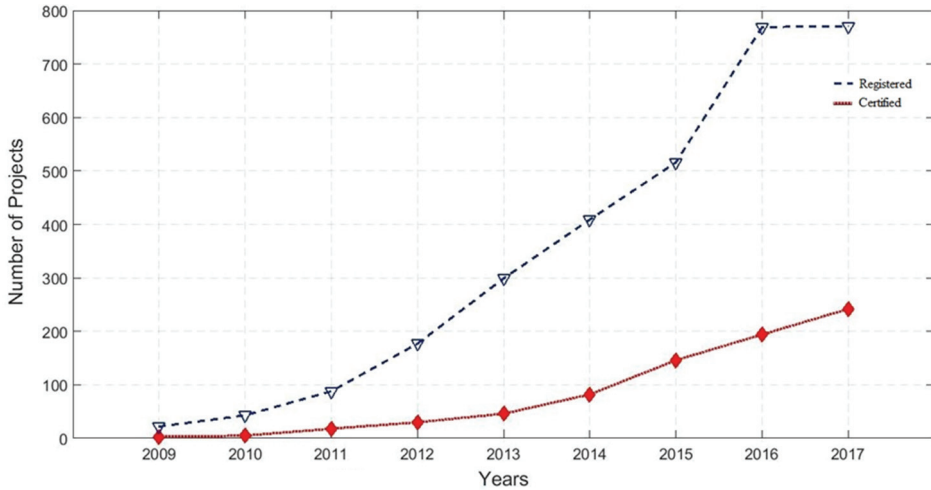
Figure 5 - Cumulative number of registered and certified LEED projects in Turkey

Aktas and Ozorhon [35] as well as Uslu et al. [36] concluded that investors operating in big cities are more willing to embrace green policies, and in addition to the aforementioned benefits, obtaining an international certificate for their buildings is used as a powerful tool to increase competitiveness in the market.

There was only one DGNB-certified project, a commercial building with a gold certificate and located in Istanbul, the most populated city of Turkey. Besides, there is a residential building that has a very good certification level located in Istanbul, certified by CEDBIK. Comparing the number of projects qualified by BREEAM, DGNB, and CEDBIK, the numbers of LEED-certified projects are higher. The certified and registered numbers of

LEED projects are illustrated by years in Fig. 5. The percentages of LEED projects under different version and scheme in Turkey are given in Fig. 6. It can be observed from Fig. 6 that the projects were mainly certified under LEED v.2009 version and new construction scheme.
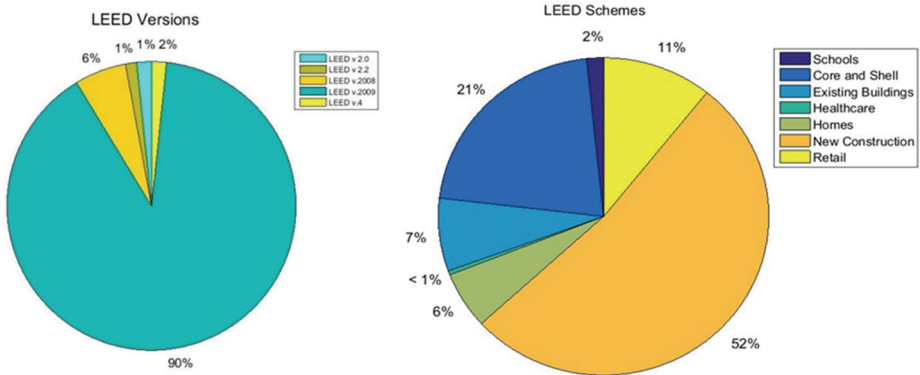
Figure 6 - The percentage of LEED-certified projects according to LEED version and scheme

BREEAM-certified projects in Turkey were evaluated under its international scheme. Their distribution according to the project types and phases is given in Fig. 7. Even in the BREEAM system, the dominating scheme is new construction. In addition, office and retail project types are encountered at a higher percentage. The distribution according to the level of certification is presented for LEED and BREEAM systems in Fig. 8. It is seen from Fig. 8 that most of LEED-certified projects have scored a total of 60-79 credits while most of BREEAM-certified projects were rated very good that means 55-70% accomplishment of total possible points was achieved.
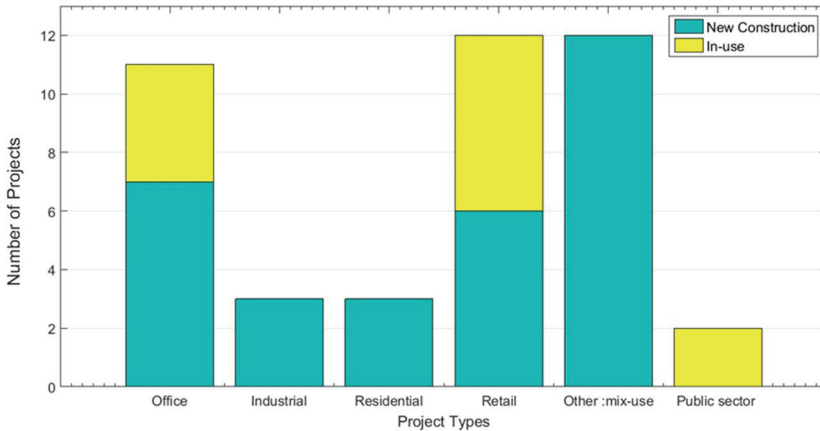
Figure 7 - BREEAM projects according to the project scheme and type
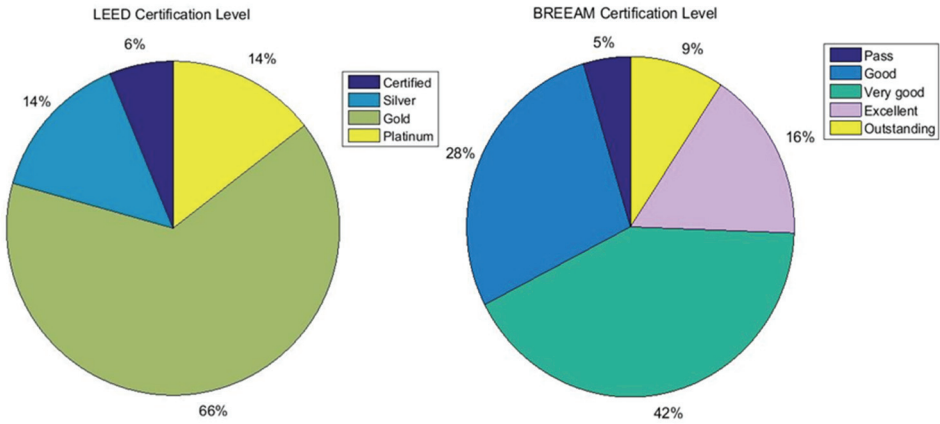
Figure 8 - LEED and BREEAM certification category distribution
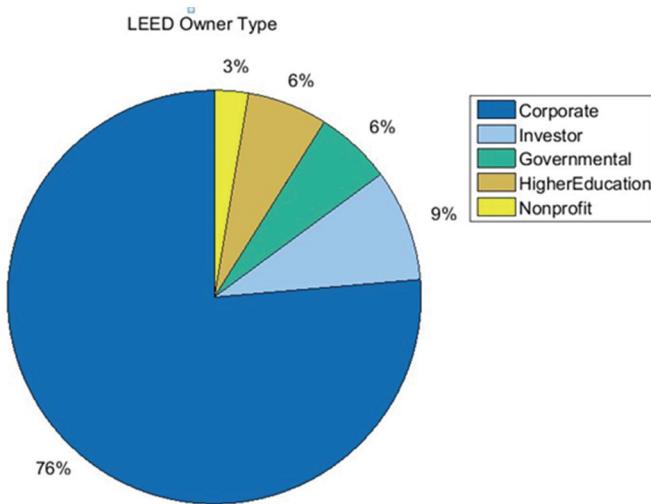
Figure 9 - Owner types in the LEED system

Fig. 9 shows the type of owners and their percentage for LEED-certified projects. It is understood that the private companies are more willing to invest in green buildings. Also, higher education institutions have invested in greener campus. This leads to increase indoor environmental quality as well as the productivity of occupants [35]. Even governmental authorities in Turkey are engaged in building more energy efficient offices and reducing the operational cost. Due to high level of electricity consumed for lighting purposes (20%), the Ministry of Energy and Natural Resources initiated the policy on "Transition to Efficient Public Lighting" to reduce the electricity bills in public institutions [37, 38].

3.2. Analysis of LEED New Construction Projects Based on Project Type

In this section, 127 LEED new construction certified projects were analysed. Only three of them are certified under LEED v2.2 version but the others are certified according to LEED V.2009. The LEED new construction scheme is selected for further analysis because this scheme is the most well-developed evaluation scheme and has a higher number of samples. A histogram is depicted in Fig. 10 for the frequency of points obtained by the projects under this scheme. As demonstrated in the histogram, the most frequently acquired points vary from 60 to 65. The distribution according to the project types is illustrated in Fig. 11. It can be assumed from Fig. 11 that office projects tend to be more certified due to lower payback value [39]. Also, office projects have a higher range of total earned credit with an average of 67.4. Higher operational cost characterizes this type of projects. Therefore, it is in the investor's benefit to increase the percentage of improvement in respective categories. Despite presenting 80% of the total building stock in Turkey, the certified residential building consists of only 17% of total certified projects [40].
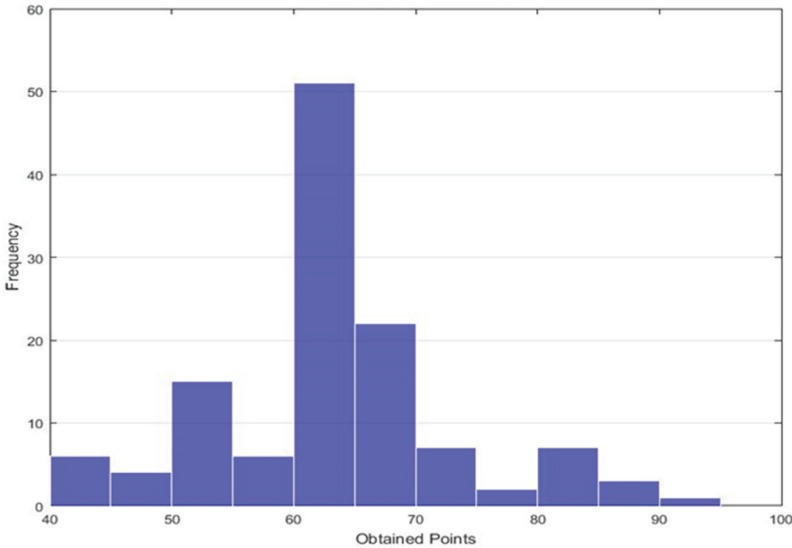
Figure 10 - Histogram of frequency of obtained points in the LEED New Construction

Fig. 12 is schematized according to data retrieved by [31, 41], and shows the percentage of improvement in different categories for each project type. The rate of improvement is calculated as a division of the project's performance with reference building's performance (as required in the LEED system) for a particular aspect. Each bar in Fig. 12 indicates the average percentage of improvement in each criterion for the corresponding project type.

In Figure 12, the numbers inside the bars represent the number of projects showing improvement in the related criterion. The average credit achievements of each project type in the associated categories are tabulated in Table 2. In projects like retail, office public

assembly, lodging (i.e., hotels, resorts), and core learning space, a generation of 5-13% onsite renewable energy is noticed.

Based on Figure 12 and Table 2, these projects are mainly located in metropoles, namely Istanbul, Ankara, Bursa, Çanakkale, Mersin, and Izmir. For the same category of project's type, a green power purchase of 35% is seen, but the number of projects is small, which are located in Istanbul, Bursa, Antalya, Mersin, and Izmir. They utilize renewable energy from green power plants, which mostly are found in the Mediterranean region.

For the material category, it can be implied that a maximum of 20% of recycling content of building materials is achieved for most of the project types. Also, locally produced materials are used in the same percentage. A higher percentage of improvement is reached in the subcategory division of construction and demolition debris, approximately 75%. Generally, an undesired performance is noticed in the following subcategories: reuse of existing building material, existing interior non-structural elements, and existing building structures and envelope. In these subcategories, only a limited number of projects have achieved a percentage of improvement of 50, 50, and 85%, respectively. Unfortunately, even the use of FSC–certified products and rapidly renewable materials are noticed in limited projects and in low percentages. In the indoor environmental quality category, in most of the project types, 75% of occupied spaces have daylight and 90% of live-in areas has a quality view. In the water efficiency category, an average reduction of 80% in potable landscape water use, 38% in indoor water use, and 50% in wastewater generation was achieved.
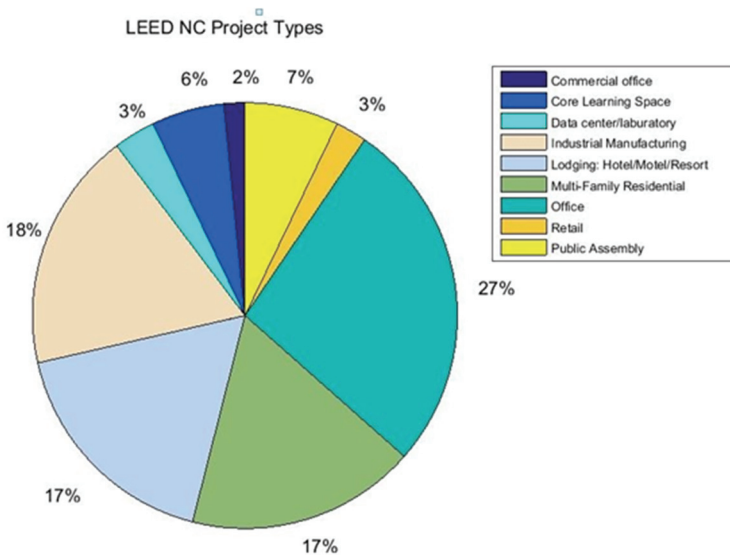
Figure 11 - The distribution of LEED New Construction projects according to project type
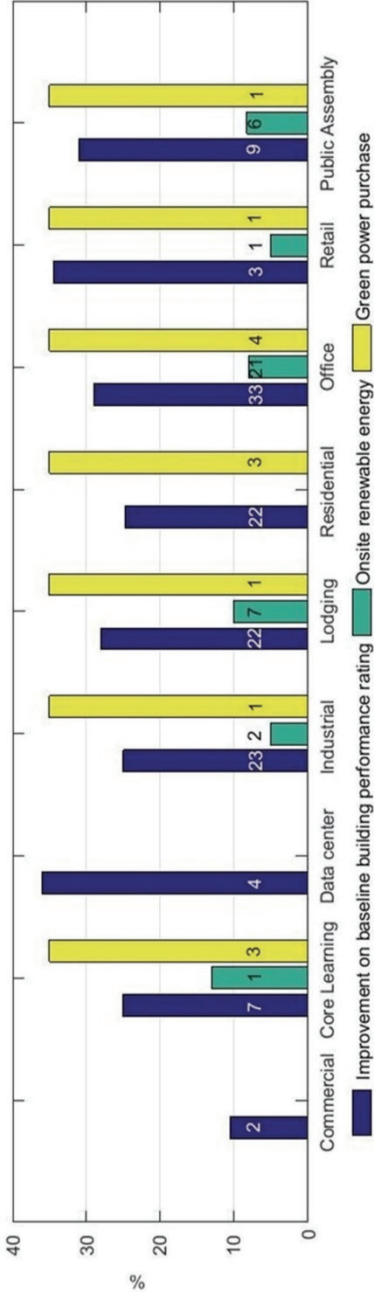
a) Energy & Atmosphere Category

b) Material & Resources Category

c) Indoor Environmental Quality Category
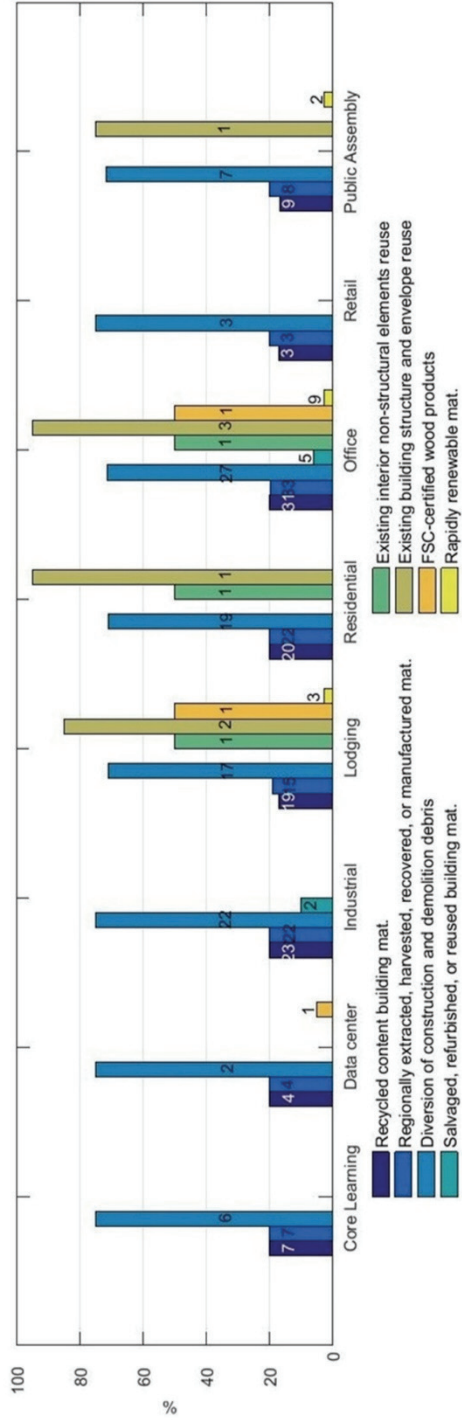
d) Water Efficiency Category
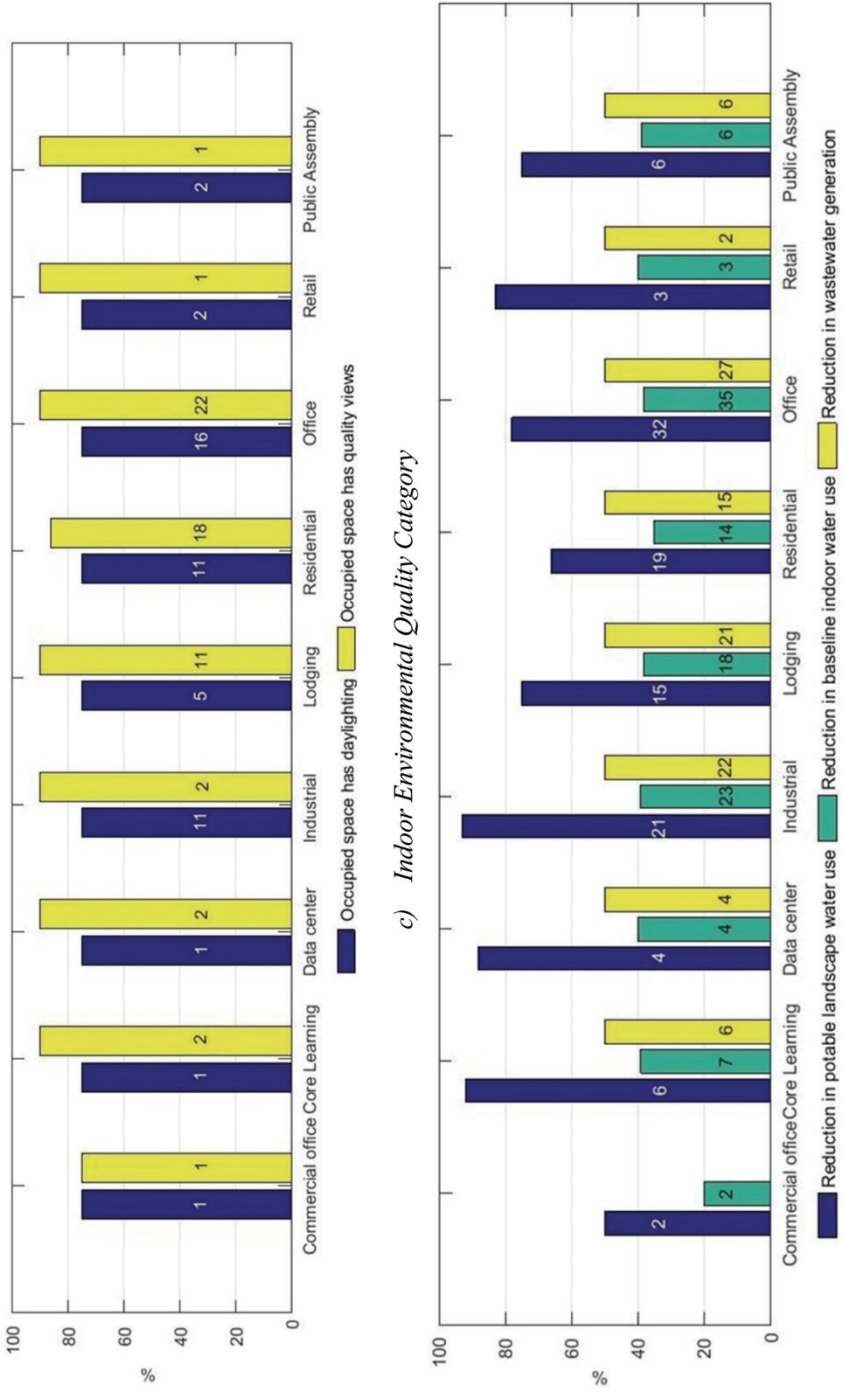
Figure 12 - The percentage of improvement in a) energy & atmosphere; b) material & resources; c) indoor environmental quality; and d) water efficiency categories for various project types

Table 2 - Average point obtained for each project type in every category

Category	Commercial office	Core Learning	Data center	Industrial	Lodging	Residential	Office	Retail	Public Assembly
Total average point	43	64.7	74	59.5	58	57.5	67.4	67.4	63.2
Sustainable site	9	20.3	20	16.5	18.9	19	19	18.3	20.2
Water efficiency	4.5	8.6	9.5	9.2	6.7	5.3	8	9.3	7.5
Energy & atmosphere	7.5	13.9	20.7	12.6	13.4	11.7	16.8	16.7	15.9
Indoor environmental quality	12	7.1	9.5	7.4	6.9	7.9	9	9.7	6.5
Material & Resources	6	5.7	5.25	5.6	4.8	5.5	6	5.7	5.3
Innovation	4	5.6	5.75	4.9	3.9	5	5	4	4.6
Regional Properties	-	3.6	3.25	3.3	3.5	3	3.6	3.7	3

3.3. Analysis of LEED New Construction Projects Based on Categories

For projects certified under LEED BD+C New Construction (NC), an investigation of most and least credit earned categories is conducted. Table 3 presents the information about the average percentage of credit secured by the LEED NC-certified projects in the following categories: regional priorities, innovation, water efficiency, sustainable site, indoor environmental quality, energy & atmosphere, and material & resources. Also, the most problematic and non-problematic criteria are highlighted.

Table 3 - Percentage of credit achievement in different categories of LEED NC-certified project

Category	Possible point	Average point	%	Level of difficulty	Subcategory	%
Regional priority	4	3.37	84	Less	Optimize energy performance	85
					Heat island effect - roof	54
				Higher	Construction waste management	1
					Site development - protect or restore habitat	1
Innovation	6	4.77	80	Less	Innovation in design	76
					LEED Accredited Professional	100

Table 3 - Percentage of credit achievement in different categories of LEED NC-certified project (continue)

Category	Possible point	Average point	%	Level of difficulty	Subcategory	%
Water efficiency	10	7.68	77	Less	Innovative wastewater technologies	85.5
				Higher	Water efficient landscaping	68.5
					Water use reduction	80.6
Sustainable site	26	18.69	72	Less	Alternative transportation	91.5
					Heat island effect -	81
				Higher	Brownfield redevelopment	0
					Light pollution reduction	15
Indoor environmental quality	15	7.88	52	Less	Construction IAQ management plan-during construction	85.5
					Low-emitting materials - paints and coatings	88.7
				Higher	Low-emitting materials - composite wood and agrifiber products	5.6
					Low-emitting materials - flooring systems	25.8
Energy& atmosphere	35	14.48	41	Less	Enhanced refrigerant management	71.8
					Measurement and verification	80
				Higher	On-site renewable energy	18.9
					Green power	14.5
Material & Resources	14	5.54	40	Less	Recycled content	89
					Regional materials	91
				Higher	Building reuse (maintain interior non-structural elements; maintain existing walls, floors, and roof)	4
					Certified wood	2.4
					Materials reuse	4

Wu et al. [23] investigated the credit achievements of LEED v.2009 certified projects, 89 in Turkey, 172 in China, and 75 in Brazil, respectively. While comparing the results of the present study with that of the above research, it can be concluded from Table 4 that the average credit achievement of the certified projects in Turkey in each category does not change with the increase of certified projects number.

Table 4 - Comparison of the results

Category	Possible point	Present study results	Wu et al. [23]
Innovation	6	4.77	4.58
Water efficiency	10	7.70	7.63
Sustainable site	26	18.69	18.80
Indoor environmental quality	15	7.88	7.88
Material & Resources	14	5.44	5.51
Energy& atmosphere	35	14.48	14.33

Analysis of the categories in a descending order based on the average percentage of credit achievement is discussed as follows:

Regional priority category shows an average percentage of 84% in credit achievement. From 4 possible credits, an average of 3.3 credits was obtained. Regional priority credits for LEED v.2009 scheme set by the USGBC for all the projects in Turkey include 2 credits concerning energy conservation, 1 credit for thermal comfort verification, 1 credit for recycling of non-structural materials, 1 credit for quantity control of storm water, and 1 credit for minimizing heat island effects [12]. While, in LEED v.4, generally for Turkey, criteria evaluated under regional priority category are the thermal comfort, sensitive land protection, reduced parking footprint, site development-protect or restore habitat, open space, rainwater management. The respective regional priority credits changed in different regions of Turkey because of LEED v.4, the assignment of regional priority credits is made based on geocoding. However, during the examination of credits earned in this category, the credits were attributed even in other criteria such as construction waste management and site development-protect or restore habitat.

Innovation category shows an average percentage of 84% in credit achievement. During the LEED certification process, the requirement of a LEED Accredited Professional is obligatory, that's why the fulfillment of this criterion was 100%. Also, in the other criterion of this category, a considerable average percentage of 76% was achieved. This high rate implies extensive implementation of innovative design techniques in the certified green building projects.

Water efficiency category shows an average percentage of 77% in credit achievement. Considering the growing population of Turkey and being a water-stressed country, the implementation of water conservation measures is necessary to reduce the demand for potable water. Some of the strategies used in these projects to earn credits in this category are the installation of low flow fixtures, rainwater harvesting system, greywater recycling, and water-wise landscaping [42].

Sustainable site category shows an average percentage of 72% in credit achievement. The majority of the projects are located in high-density urban zones. This creates the opportunity to easily reach a larger number of amenities and low-carbon public transportation vehicles around the projects site [43]. Consequently, it can be earned without any difficulty credits in this category. However, none of the buildings has gained points in the brownfield re-development sub-category. This situation may be driven by a lack of adequate policies which

can encourage the third parties to invest in the conversion of the brownfields through appropriate treatments to suitable construction sites.

Indoor environmental quality category shows an average percentage of 52% in credit achievement. In this category, some of the most important aspects of health and well-being of a person take place like air quality, thermal comfort, daylight availability and quality view. This moderate rate of achievement is not insufficient to ensure a healthy lifestyle considering that in the modern lifestyle a person spends approximately 90% of the time indoors [44, 45]. That's why, designing with green principals plays a positive role in reducing the rate of respiratory disease, sick building symptoms, and enhance occupant comfort and worker performance [46].

Material & Resources category shows an average percentage of 40% in credit achievement. This low rate indicates the handicap of the sustainable construction material supply chain and Construction and Demolition Waste (C&DW) recycling systems. One of the fundamental principles of sustainability is the responsible use of available resources reflected even in certification systems by encouraging the selection of eco-friendly and recyclable materials and appropriate waste management planning. Previous surveys in Turkish green construction industry pointed out the immaturity of sustainable material manufacturing industry and the lack of incentives for construction waste management as one of the reasons of the low performance in this category [47, 48]. Furthermore, Ulubeyli et al. [48] pointed out the limited number of C&DW recycling plants in Turkey. There are only two plants owned by private enterprises and one by Istanbul Municipality. The development of C&DW can be useful in the reduction of recycling process cost, reversing the adverse impact on the environment by reducing the transportation distance from construction site to the recycling plant and increasing awareness at the architect and contractors about salvaged and recycled building materials [49]. These obstacles have a negative impact on the initial cost of the projects and discourage investors to embrace green construction [50, 51].

Energy & Atmosphere category shows an average percentage of 41% in credit achievement. Despite the high importance showed by the government and the academic authorities toward minimization of non-renewable energy demand and encouraging onsite renewable energy, the average credit achievement in this category was not at the desired level. While performing an investigation for renewable energy performance for various countries, Arik [52] concluded that Turkey showed a good level for renewable energy incentives from the government like the enacting of the second Renewable Energy Law, namely Law No. 6094 in 2010 concerning the use of Renewable Energy Resources for the Generation of Electrical Energy. Unfortunately, for further development of renewable energy production, it is necessary to use a better electric power grid. Also, the absence of adequate binding policies and financing options possibilities for sustainability of renewable energy was pointed out even by Gurgun and Arditi [53]. Unfortunately, Turkey imports 72.5% of the total energy used, but the investments in renewable energy productions like 41 wind farms intend to lower this percentage [38]. Except for wind energy, there is a great possibility to produce geothermal energy and solar energy in Turkey, but it is required more attention and support from the government. Another criterion in this category that shows a low average percentage of achievement is green power purchasing. This result is incurred by the lack of green-e-certified renewable energy grid-source [53].

Table 3 points out the more promising criteria to earn more credits for projects located in Turkey. In this way, the design team during the certification process can focus on these criteria to increase the likelihood of higher certification rate. However, indoor environmental quality, energy & atmosphere, and material & resources categories are essential for designing and constructing a greener project, and further attention should be paid by the practitioners to improve the performance of their projects in categories [54].

The low percentage of credit achievement in particular categories implies the lack of proper green building development incentives and binding regulations by the policymakers to increase the opportunities to obtain higher certification level and consequently greener projects.

4. CONCLUSIONS

In the last decade, interest towards implementing green construction practice and the number of certified green buildings in the Turkish market has increased. In this study, a general overview of 287 certified green buildings was provided. Furthermore, the average credit achievement of 127 LEED new construction certified projects was investigated based on project types and assessed categories. Some of the key findings are:

- The examples of green buildings were mostly concentrated in densely populated and industrialized cities, especially in the western part of Turkey but in the eastern part of Turkey, the examples of green projects are rare.

- Project types characterized by high operational costs showed a higher certification level.

- The investigation performed for 127 certified projects under LEED v.2009 NC scheme indicated fewer credits earned categories and revealed the problematic criteria that hinder the acquiring of higher certification level.

- Even though the number of certified projects in Turkey has increased, the comparison of the present study results with the available ones demonstrated there is no improvement of average credit achievements in related categories.

- The categories showing lower average percentages in credit achievements for indoor environmental quality, energy & atmosphere, and material & resources are 52, 41, and 40%, respectively.

- Some criteria such as brownfield redevelopment, low-emitting materials, on-site renewable energy, materials reuse etc., are denoted as no inconsiderable level of credit achievements.

Knowing the updated LEED-certified projects performance at a country level orientates the policymakers to establish proper green building development incentives and binding regulations. Also, it can be implied from the results that further effort should be made by the practitioners during design stage to improve the performance of their projects in important categories such as indoor environmental quality, energy & atmosphere, and material & resources.

References

[1]   Dixit, M.K., Culp, C.H., & Fernandez-Solis, J.L. (2013). System boundary for embodied energy in buildings: A conceptual model for definition. Renewable and Sustainable Energy Reviews, 21, 153–164.

[2]   Yeheyis, M., Hewage, K., Alam, M.S., Eskicioglu, C., & Sadiq, R. (2013). An overview of construction and demolition waste management in Canada: A lifecycle analysis approach to sustainability. Clean Technologies and Environmental Policy, 15, 81–91.

[3]   Udawatta, N., Zuo, J., Chiveralls, K., & Zillante, G. (2015) Attitudinal and behavioural approaches to improving waste management on construction projects in Australia: Benefits and limitations. International Journal of Construction Management, 15(2), 137–147.

[4]   Doan, D.T., Ghaffarianhoseini, A., Naismith, N., Zhang, T., Ghaffarianhoseini, A., & Tookey, J. (2017). A critical comparison of green building rating systems. Building and Environment, 123, 243–260.

[5]   Vimpari, J., & Junnila, S. (2014). Value influencing mechanism of green certificates in the discounted cash flow valuation. International Journal of Strategic Property Management, 18, 238–252.

[6]   Scofield, J.H. (2013). Efficacy on LEED-certification in reducing energy consumption and greenhouse gas emissions for large New York City office buildings. Energy and Building, 67, 517–524.

[7]   Dobias, J., & Macek, D. (2014). Leadership in Energy and Environmental Design (LEED) and its impact on building operational expenditures. Procedia Engineering, 85, 132–139.

[8]   Dwaikat, L.N., & Ali, K.N. (2016). Green buildings cost premium: A review of empirical evidence. Energy and Building, 110, 396–403.

[9]   Darko, A., Chan, A.P.C., Owusu-Manu, D.G., & Ameyaw, E.E. (2017). Drivers for implementing green building technologies: An international survey of experts. Journal of Cleaner Production, 145, 386–394.

[10]   Rezaallah, A., Bolognesi, C., & Khoraskani, R.A. (2012). LEED and BREEAM; Comparison between policies, assessment criteria and calculation methods. In: Proceedings of the 1st International Conference Building Sustainability Assessment (BSA). Porto, Portugal.

[11]   LEED, LEED Homepage. (2017). Top 10 countries for LEED national profile: Turkey. Available from: https://www.usgbc.org/articles/top-10-countries-leed-national-profile-turkey, Assessed 07 October 2017.

[12]   Suzer, O. (2015). A comparative review of environmental concern prioritization: LEED vs other major certification systems. Journal of Environment Management, 154, 266–283.

[13]   Darko, A., & Chan, A.P.C. (2016). Critical analysis of green building research trend in construction journals. Habitat International, 57, 53–63.

[14] Awadh, O. (2017). Sustainability and green building rating systems: LEED, BREEAM, GSAS and Estidama critical analysis. Journal of Building Engineering, 11, 25–29.

[15] Hu, M., Cunningham, P., & Gilloran, S. (2017). Sustainable design rating system comparison using a life-cycle methodology. Building and Environment, 126, 410–421.

[16] Zhang, Y., Wang, J., Hu, F., & Wang, Y. (2017). Comparison of evaluation standards for green building in China, Britain, United States. Renewable and Sustainable Energy Reviews, 68, 262–271.

[17] Mattoni, B., Guattarib, C., Evangelisti, L., Bisegnaa, F., Gorib, P., & Asdrubali, F. (2018). Critical review and methodological approach to evaluate the differences among international green building rating tools. Renewable and Sustainable Energy Reviews, 80, 950-960.

[18] Rastogi, A., Choi, J.K., Hong, T., & Lee, M. (2017). Impact of different LEED versions for green building certification and energy efficiency rating system: A multifamily midrise case study. Applied Energy, 205, 732–740.

[19] Roderick, C., Mcewan, Y., & Alonso, D. (2009). Comparison of energy performance assessment between LEED, BREEAM and Green Star, in building simulation. In: Eleventh International IBPSA Conference. Scotland, p. 1167–1176.

[20] Ma, J., & Cheng, J.C.P. (2016). Data-driven study on the achievement of LEED credits using percentage of average score and association rule analysis. Building and Environment, 98, 121–132.

[21] Wu, P., Mao, C., Wang, J., Song, Y., & Wang, X. (2016). A decade review of the credits obtained by LEED v2.2 certified green building projects. Building and Environment, 102, 167–178.

[22] Wu, P., Song, Y., Shou, W., Chi, H., Chong, H.Y., & Sutrisna, M. (2017). A comprehensive analysis of the credits obtained by LEED 2009 certified green buildings. Renewable and Sustainable Energy Reviews, 68, 370–379.

[23] Wu, P., Song, Y., Yang, Y., Wang, X., Zhao, X., & HE, Q. (2018). Regional Variations of Credits Obtained by LEED 2009 Certified Green Buildings-A Country Level Analysis. Sustainability, 10(20), 1-18.

[24] Da Silva, L. and Ruwanpura, Y.(2009). Review of theLEED points obtained by Canadian bulding projects. Journal of Architectural Engineering, 15(2), 38-54.

[25] Xia, B., Zuo, J., Skitmore, M., Pullen, S., & Chen Q. (2013). Green Star Points Obtained by Australian Building Projects. Journal of Architectural Engineering, 19(4), 302-308.

[26] Zuo, J., Xia, B., Chen, Q., Pullen, S., & Skitmore, M. (2016). Green building rating for office buildings – lessons learned. Journal of Green Building, 11(2), 131-146.

[27] Celik, K. (2016). LEED certification systems and evaluation of their implementation in Turkey (in Turkish). Master Thesis. Istanbul Culture University, Turkey.

[28] Bastanoglu, E. (2017). Evaluation of LEED green building certification system practices: Europe and Turkey (in Turkish). Master Thesis. Istanbul Technical University, Turkey.

[29] Gokbayrak, (2016). A. Evaluation of green building criteria according to development level of countries (in Turkish). Master Thesis. Gazi University, Turkey.

[30] Gunes, S.B. (2017). Analysis of buildings with LEED and BREEAM green building certificate in Turkey (in Turkish). Master Thesis. Haliç University, Turkey.

[31] LEED, LEED Homepage. (2017). Directory of projects. Available from: https://www.usgbc.org/projects/list/?keys=turkey, Assessed 11 November 2017.

[32] BREEAM, BREEAM Homepage. (2017). Directory of projects. Available from: https://www.breeam.com/projects/explore/buildings.jsp?sectionid=0&projectType=& rating=&certNo=&buildingName=&client=&developer=&certBody=&assessor=&loc ation=&countryID=7&partid=10023&Submit=Search, Assessed 11 November 2017.

[33] CEDBIK, CEDBIK Homepage. (2017). Available from: https://cedbik.org/tr/cedbik-zirve-15-pg/cedbik-kongre-2016-16-pg/cedbik-kongre-2016-belgelendirme-18-pg, Assessed 11 November 2017.

[34] DGNB, DGNB Homepage. (2017) DGNB pre-certified and certified projects-Turkey. Available from: http://www.dgnb-system.de/en/projects/index.php?filter_Freitextsuche=&filter_Land=T%C3%BCrkei &filter_Bundesland=&filter_Standort=&filter_Jahr=&filter_Zertifizierungsart=&filte r_Nutzungsprofil=&filter_Zertifiziert_von_1=&filter_Verliehenes_Guetesiegel=&filt er_Architekt=, Assessed 11 November 2017.

[35] Aktas, B., & Ozorhon, B. (2015). Green building certification process of existing buildings in developing countries: Cases from Turkey. Journal of Management Engineering, 31(6), 05015002-05015002-9.

[36] Uslu, Y.D., Hancioglu, Y., & Demir, E. (2015). Applicability to green entrepreneurship in Turkey: A situation analysis. Procedia Social and Behavioural Sciences, 195, 1238–1245.

[37] Canitez, I.S. (2013). System approaches appropriate model for Turkey conditions relating to the sustainable building production process based on certification (in Turkish). Doctoral dissertation. Trakya University, Turkey.

[38] Komurlu, R., Arditi, D., & Gurgun, A.P. (2014). Applicability of LEED's energy and atmosphere category in three developing countries. Energy and Building, 84, 690-697.

[39] Olubunmi, O.A, Xia, P.B., & Skitmore, M. (2016). Green building incentives: A review. Renewable and Sustainable Energy Reviews, 59, 1611–1621.

[40] Saglam, N.G., Yilmaz, A.Z., Becchio, C., & Corgnati, S.P. (2017). A comprehensive cost-optimal approach for energy retrofit of existing multi-family buildings: Application to apartment blocks in Turkey. Energy and Building, 150, 224–238.

[41] Green Building Information Gateway (GBIG), GBIG Homepage. (2017). Available from: <http://www.gbig.org/collections/14544/buildings>, Assessed 11 November 2017.

[42] Thomollari, X., Bahadir, U., Togan, V., & Tokdemir, O.B. (2017). Reducing water consumption with sustainable building design: A case study. The Turkish Journal of Occupational / Environmental Medicine and Safety, 2(3), 444–453.

[43] Aktas, B. (2011). Converting existing buildings to green buildings: Implementations in Turkey. Master thesis. Boğaziçi University, Turkey.

[44] U.S. Environmental Protection Agency (EPA), EPA Homepage. (2016). Report on the Environment (ROE). Available from: https://cfpub.epa.gov/roe/chapter/air/indoorair.cfm, Assessed 18 January 2018.

[45] European Commission (EC), EC Homepage. (2003). Indoor air pollution new EU research reveals higher risks than previously though. Available from: http://europa.eu/rapid/press-release_IP-03-1278_en.htm, Assessed 18 January 2018.

[46] Kubba, S. (2017). Handbook of green building design and construction LEED, BREEAM, and Green Globes. (P. Jardim, Ed.) (Second). United States: Joe Hayton. p. 353-359.

[47] Ekincioglu, O., Gurgun, A.P., Engin, Y., Tarhan, M., & Kumbaracibasi, S. (2013). Approaches for sustainable cement production: A case study from Turkey. Energy and Building, 66, 136–142.

[48] Ulubeyli, S., Kazaz, A., & Arslan, V. (2017). Construction and demolition waste recycling plants revisited: Management issues. Procedia Engineering, 172, 1190–1197.

[49] Arslan, H., Cosgun, N., & Salgin, B. (2012). Construction and demolition waste management in Turkey. Intechopen, 313-332. http://dx.doi.org/10.5772/46110.

[50] Gundogan, H. (2012). Motivators and barriers for green building construction market in Turkey. Master thesis. Middle East Technical University, Turkey.

[51] Mohammadi, S. (2015). The future of green building contracts in Turkey. Master thesis. Middle East Technical University, Turkey.

[52] Arik, A. (2016). Sustainability of renewable energy policies: an evaluation in terms of EU countries and Turkey (in Turkish). Master thesis. Ordu University, Turkey.

[53] Gurgun, A.P., & Arditi, D. (2018). Assessment of energy credits in LEED certified buildings based on certification levels and project ownership. Building, 8(29), 1-20.

[54] Illankoon, I.M.C.S., Tam, V. W.Y., Le, K.N., Shen, L. (2017). Key credit criteria among international green building rating tools. Journal of Cleaner Production, 164, 209-220.

[55] Uğur, L.O, Leblebici N. (2019). Investigation of the effects of energy and water saving benefits on property value in LEED-certified green buildings. Teknik Dergi, 30(1), 8753-8776.

Geotechnical Risk Identification: Case Study of Flexible Retaining Wall Installation

Danute SLIZYTE[1]
Natalija LEPKOVA[2]
Rimantas MACKEVICIUS[3]

ABSTRACT

Analysis of the scientific literature has demonstrated that the risk of collapse or deformations of flexible retaining walls has not been the object of in-depth examination so far. The article presents an analysis of the main geotechnical risks, focusing on the installation of flexible retaining walls according to analysis by construction participants and their experiences. A case study was conducted to identify the risks of flexible retaining walls. In order to determine the risks of installation of flexible retaining walls, the authors of the article employed a face-to-face interview approach. Investigation of the data obtained during the face-to-face interview was based on brainstorming and the cause and effect diagram: five professionals who had monitored most of the risks were selected with the help of the face-to-face interview. The results of the investigation showed, that for specific and complicated projects the team of professionals should be composed of specialists from different fields of construction. Additionally, the respondents agreed with the opinion that the greatest loss in the given situation would be caused by a breakdown in the pressure pipe and pollution of the natural environment by wastewater. The novelty of the article on investigating the possibilities for identifying the risk of installation of flexible retaining walls and on suggesting risk identification steps.

Keywords: Flexible retaining wall, technical risk, cause and effect diagram.

1. INTRODUCTION

The article analyzes risk identification when installing flexible retaining walls. The article considers this problem, taking into account that not all risks are always assessed within the process of installing flexible retaining walls, which may result in collapse or deformations.

To determine and analyze risk, the concept has to be defined. Risk considers the probability of an event occurring and the consequences of the event, should it occur [1]. Emerging risk can be defined as the likelihood of loss, that is, the probability that a certain consequence will occur in a specific time and space under specified or insufficiently specified conditions [2]. This article adopts the definition of risk as the 'effect of uncertainties on objectives' given by ISO 31000:2009 [3]. The definition provides that uncertainties include events (that may or may not happen) and are caused by ambiguity or lack of information. It also includes both negative and positive impacts on objectives [3]. The article reports only negative effects.

Geotechnical risk has been analyzed in a number of scientific articles. Duncan [4] investigated safety and reliability in geotechnical engineering. Special attention was paid to uncertainty about the factors involved in safety against sliding. As an example, the stability of a cantilever retaining wall with silty sand backfill was analysed. Gibson [5] explored and compared four probabilistic methods for slope analysis and design. Brown [6] reviewed risk assessment and management practice in underground rock engineering. Swannell et al. [7] analysed the geotechnical risk management approach to boring machines tunnelling under squeezing ground conditions. Lacasse [1] showed how the concepts of hazard, risk, and reliability could help with making more secure decisions. The article shows examples of calculation taken from a wide range of geotechnical problems, including the hazard and risk of collapse related to railway traffic, mine slopes, and soil exploration. Mishra et al. [8] analysed tools for geotechnical real-time risk assessment and management and proposed a geotechnical risk management workflow diagram of intelligent deep mines. Xia et al. [9] focused on the issue of model uncertainty and differences in risk consciousness with different decision-makers in tunnel and underground engineering and proposed a risk decision model based on sensitivity analysis and tolerance cost, which can improve decision-making efficiency. Haddad et al. [10] performed a study based on the failure and stability of gravity retaining walls, which can be categorized into three different modes of failure in sliding, overturning, and foundation-bearing capacity. They introduced a relatively simple method of probabilistic analysis of the dimensions of gravity retaining walls which might lead to a more accurate understanding of failure. Risk management in the architecture, engineering, and construction industries remains a global issue. Lack of adequate risk management may cause difficulties in implementing the objectives of a project and negatively affect spatial planning and urban spatial design in the future. Yang et al. [11] analysed risk management in the field of health and safety using Building Information Modelling (BIM) and other BIM-related technologies. Li et al. [12] analysed site selection for underground petroleum storage. To reduce construction risk and cost during the construction of underground petroleum storage, they proposed a new site selection model for large underground petroleum storage based on the analytic hierarchy process (AHP) method and ideal point theory. Xue at al. [13] analysed rockburst hazard, which is an important issue affecting safe production at coal mines in China. They paid attention to the influence of the backfilling roadway driving sequence on coal pillar stability. Ahmasi et al. [14] presented a comprehensive framework to manage the main risk events of highway construction projects within three stages: (1) identification of

potential risks; (2) assessment and prioritization of identified risks based on fuzzy FMEA; (3) identification of appropriate response. Authors suggested the new expert system for identifying an appropriate risk response strategy for a risk event based on risk factor, control number and risk allocation. The proposed methodology is demonstrated for management of risk events in a construction project of Bijar-Zanjan highway in Iran. Valipour et al. [15] applied hybrid SWARA (Step-wise Weight Assessment Ratio Analysis) -COPRAS (COmplexPRoportionalASsessment) method for risk assessment in deep foundation excavation project through introducing new criteria for risk assessment. A case study of deep foundation excavation in Shiraz (Iran) was presented. The results have shown that the risks involving construction safety, unfavourable geological conditions, shortage of managerial experience, incomplete emergency plan and subsidence of ground are the most significant risks excavation projects in Shiraz.

To sum up, the risk of collapse or deformations of flexible retaining walls has not been widely examined.

This paper aims to identify the most common risks of installing flexible retaining walls. The analysis performed involves the face-to-face interview approach, brainstorming, and a cause and effect diagram. The article discusses a specific case of installing flexible retaining walls. This case study has been selected with reference to the results of the face-to-face interviews, showing that the parties involved in construction most frequently fail to assess the risk of installing the flexible retaining wall, which causes some problems in geotechnical applications in Lithuania. Identification of risks is important for risk analysis in order to reduce the number of emergencies. The face-to-face interview approach and the brainstorming method were chosen for analysis, as the knowledge and experience of experts in the field of installing flexible retaining walls allow a more thorough identification of possible risks. The major finding of the face-to-face interview approach was that the greatest loss is caused by breakdown in the pressure pipe. When analysing the case of installing the flexible retaining wall using the cause and effect diagram, all possible risks leading to the breakdown in the pipe are shown graphically.

The novelty of this article is investigating the identification of possible risks when installing flexible retaining walls and suggests risk identification steps in the risk management flow of the flexible retaining wall installation process.

The structure of the article is built as follows. Section 2 analyses geotechnical risks. The authors of the article present the case study and risk identification by applying the face-to-face interview approach in Section 3. Having analysed the data obtained during the face-to-face interview and clarifying the possible causes of breakdown in the pipe, brainstorming and the cause and effect diagram were used. Section 4 deals with risk identification in the risk management flow of the flexible retaining wall.

2. GEOTECHNICAL RISK IDENTIFICATION

Risk identification is very important in the risk management cycle. Once the risk has been identified, a decision has to be made regarding whether to take the risk if it is acceptable or to make some changes to reduce it if it is unacceptable.

To identify risk, the Swedish Geotechnical Society (SGF) [16] recommends employing methods for detecting hazards and considering possibilities. When opting for techniques and organizing a risk management team, one has to adhere to the following principles:

Risk identification is considered to be an engineering task:

- anyone who may be of benefit to the work should be engaged in it;
- the goals of the project have to be considered first;
- a unified approach should prevail, and therefore all aspects of the project have to be studied;
- necessary information should be collected;
- both hazards and consequences have to be investigated and distinguished from each other;
- risk should be analysed without emotions;
- there should be concentration on risk rather than on solving related problems.

    The result should be documented so that it can be used for the entire project.

The geotechnical risk of the project is a part of the risk of a construction project and is frequently one of the most controversial parts of the technical risks. 'Geotechnical risk – is the risk to buildings and construction work created by the site ground conditions' [17]. However, this is only one of many risks that are specific to geotechnical projects. Table 1 presents the specific risks and hazards of geotechnical projects. In general understanding, a hazard is something that can cause harm, e.g. electricity, chemicals, working up a ladder, noise, stress, etc. A risk is the chance, high or low, that any hazard will actually cause somebody harm. The geotechnical hazard can be named as building collapse, landslides and etc.

Table 1 - Specific risks and hazards of geotechnical projects (adapted by authors from Baynes' [18]).

Type of geotechnical risk		Hazard
Project management		Poor management of the entire geotechnical process
Contractual		Poor management of site investigation and contractor documentation
Technical	Analytical	Unreasonable analytical model selected
		Nonconformity of the structural scheme with design drawings
		Nonconformity of the structural scheme with construction stages; technological effects are not assessed
	Properties	Unreasonable design values selected
	Geological	Inherently hazardous ground conditions
		Unforeseen ground conditions
	Construction	Invalid construction type selected
		Invalid technology selected

Based on the experience gained in the field of designing and constructing geotechnical objects, the authors of the article propose five categories for analysing geotechnical risks, as depicted in Figure 1: water, soil, seismology, surrounding buildings and structures, and technological processes used during construction.

The first three types of risks are natural and most uncertain.

The risk of breakdown of the structure(Figure 1) took into account geotechnical research, design, and Eurocodes and standards for specific geotechnical works.

The analysis of water level and its variations in terms of time shows that the groundwater level is not constant in nature and is subject to various factors such as seasonal changes, floods, tides, and so on. Frequently, the maximum possible rise in groundwater is calculated according to standardized diagrams that may not meet local conditions.
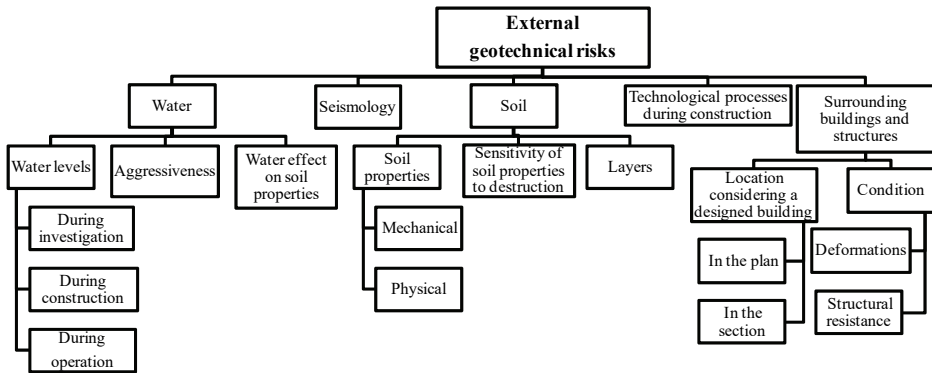
Figure 1 - External geotechnical risks

The following variations in water level may occur during construction:

- blocking the natural flow of water will result in a rise;

- the water flow may be artificially decreased if it interferes with construction processes.

Variations in soil moisture change the physical and mechanical properties of the soil more or less, which has a direct impact on the foundation works.

The soil is a naturally occurring dispersion substance whose properties are subject to the processes and conditions of formation, conditions of the study, and variations in those conditions. During testing, the mechanical and physical properties of the soil are determined by employing field (in situ) and laboratory methods. However, it should be noted that the test results largely depend on the qualifications and diligence of the staff involved in the investigation. Any inaccuracies in taking, transporting, preparing, and testing a specimen under laboratory conditions may cause serious distortion of the results. Thus, geotechnical studies often use accumulated information about the properties of similar soils and compare the findings with the results obtained. When in doubt, such results should be verified by additional testing. Attention should be drawn to the fact that soil properties are determined

only at separate points of the soil matter. Hence, it is important that attention is paid to the selection of representative specimens when describing the characteristics of a single layer.

Variations in the characteristics of soil exposed to the effects of cold or mechanical or dynamic factors are accepted as one of the soil properties. Therefore, soil properties described -in the geotechnical report can only be applied on the condition that the structure of the soil will not be destroyed during construction and afterwards.

Soil characteristics appear to be one of the greatest sources of risk (see Table 2). Information on the layout of soil layers during engineering geological explorations and the preparation of a geotechnical report is limited. The placement of layers is directly investigated in separate places in the construction site by drilling, and information can be indirectly obtained through the Cone Penetration Test (CPT), Standard Penetration Test (SPT), or other methods. Only at tested points are the soil boundaries and type known. Between the tested points, only assumptions can be made. Therefore, only at the time of construction, when excavating the foundation pit, is it possible to verify whether the soil and the depth of the soil conform to the geotechnical report.

Table 2 - Sources of foundation-related risk in construction [17].

Risks related to	%
Soil boundaries	22
Soil properties	20
Groundwater	13
Contamination	11
Obstructions	10
Site investigation	9
Services	6
Detailed design	5
Other	4

The seismic effect on the specific construction site cannot be measured. This is the most uncertain geotechnical external effect. Designing seismic districts is one of the greatest risks, and the assessment of these risks may lead to fundamental changes in geotechnical solutions. This effect is strictly regulated by separate normative standards.

For the rest of the risks related to the environment, the size of uncertainties greatly depends on the ability to collect information about the surrounding buildings and structures. Those opportunities will certainly be better if the builder's relations with neighbours are good and if the builder convinces them that the risk to their property will be reduced during construction by the provision of such information. In this case, there is a need for effective communication with neighbours in order to avoid frightening them about possible risks. Lack of communication is due to the fact that everyone treats risk differently [19].

The selected technological processes of construction can determine the level of risks. From a geotechnical point of view, efficient technological processes can increase risks on the construction site. For example, hammering or vibrating a sheet pile wall results in producing dynamic effects that will lead to the occurrence of thixotropic processes, the soil will dissolve, and the surrounding structures may lose their foundations in silty sand saturated with water. Therefore, at the engineering feasibility stage, one of the essential tasks is to select the most appropriate technological processes taking into account the risks involved.

The risks of the construction project have to be assessed at all stages of its development. Each of these stages addresses different problems of risk manageability [20]. Figure 2 shows a diagram describing the risks under consideration during the stages of developing a geotechnical project. Risk identification and analysis is a continuous process, because each of the steps may result in additional data that will reveal new risks. The earlier the risk is identified, the easier its management will be.

To solve geotechnical problems, as the first step, the designer has to collect as much information as possible about the site itself and about the immediate environment that can affect the building being designed. This will allow potential risks to be assessed at the initial stages of the project (planning stage and engineering feasibility stage). Based on the analysis of the initial information, the project manager will also be able to decide on the extent of the required geotechnical exploration for the planned facility.
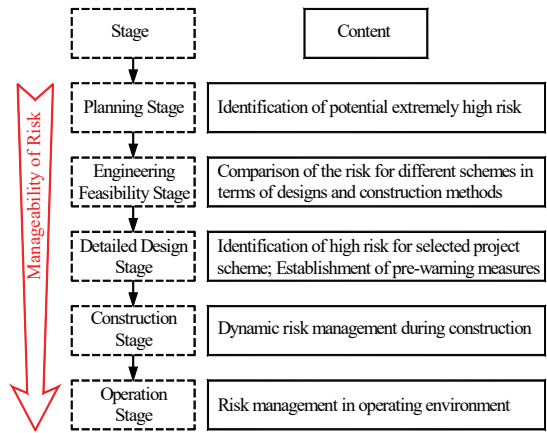
Figure 2 - Scheme for lifetime risk assessment by Huang and Zhang [20].

In different Member States of the European Union, investigation volumes are subject to the geotechnical category assigned to the object. This can be done using the process shown in Figure 3.

Subject to the category, the investigation volume and methods are regulated. A few geotechnical categories may form the object, which will depend on conditions for variations in the site and design constructions. It should also be considered that the situation must be monitored to determine whether there is a need to adjust the established geotechnical category during the whole construction process [22].
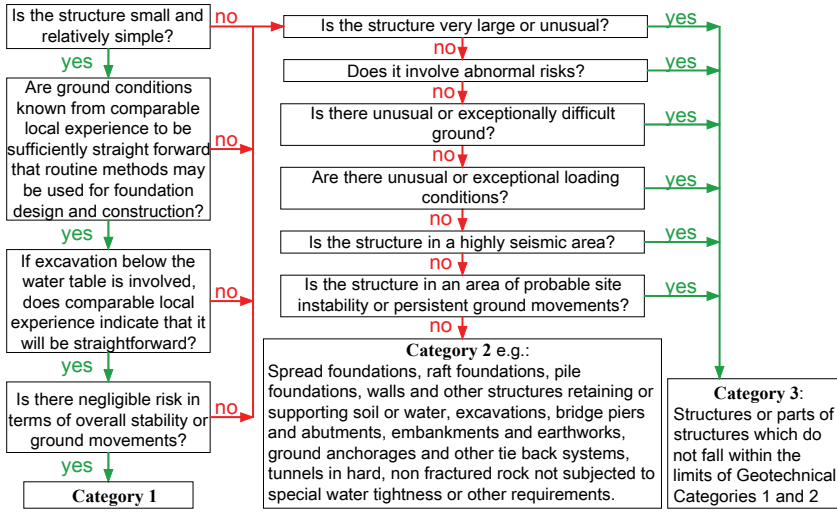
Figure 3 - The general decision tree for selecting a geotechnical category by Simpson and Driscoll [21].

However, even following recommendations can reveal some uncertainties. As a rule, for the objects of the second and third geotechnical categories, the mechanical properties of the soil are determined by laboratory tests. For example, in determining the indicators of the shear strength of the soil, their magnitude is subject to available comparable experience (see Table 3), according to EN 1997-2 [23]. Yet documents do not provide information on the type of comparable experience.

Table 3 - Direct shear test. The recommended minimum number of tests for one soil stratum [23].

Recommended number of tests[a]			
Variability in strength envelope	Comparable experience		
Coefficient of correlation on regression curve	None	Medium	Extensive
Coefficient of correlation < 0.95	4	3	2
0.95 ≤ coefficient of correlation < 0.98	3	2	2
Coefficient of correlation ≥ 0.98	2	2	1[b]

[a] One recommended test means a set of three individual specimens tested at different normal stresses.

[b] A single test and classification tests to verify compatibility with comparable experience. If the test results do not agree with the existing data, additional tests should be run.

To identify geotechnical risk, specific geotechnical issues that are not always successfully solved by referring to regulatory documents about this particular field of construction need

to be considered. Extensive experience of the parties involved in construction has to be taken into account. Thus, Chapter 3 applies the face-to-face interview approach followed by the construction participants analysing a certain case study and identifying the main problems using a cause and effect diagram.

3. RISK IDENTIFICATION APPLYING THE FACE-TO-FACE INTERVIEW APPROACH

3.1. Data Collection

The authors of this article mainly focus on identifying risks arising from the installation of a flexible retaining wall. Thus, to achieve this goal, the face-to-face interview approach, which is one of the methods recommended by ISO / IEC 31010: 2009 [24] was preferred, based on the argument that it has a lower non-response rate than other methods of surveying.

Furthermore, compared to other cases, the questioning technique enhances the opportunity to obtain more information and reduces the amount of time required to obtain the information. The face-to-face interview approach, being flexible, allows data collection using strictly structured to unstructured questions and very short to long answers [25].

The authors of this article conducted face-to-face interviews of 14 respondents with no time limit; each interview lasted approximately 30–50 minutes. All of the interviews were administered by the same person, who had 22 years of work experience in the field of designing geotechnical structures.

The types of experiences of the respondents and length of experience in their present positions and in total are listed in Table 4, below.

Table 4 - The demographics of the participants

Respondent	Type of Professional Experience	Experience in the present position (years)	Experience in total (years)
1	Associate Professor	37	37
2	Associate Professor	8	12
3	Architect	5	13
4	Geotechnical Designer	7	17
5	Geotechnical Designer	3	3
6	Geotechnical Designer	10	10
7	Geotechnical Expert	24	40
8	Structural Designer – Structural Project Manager (SPM)	15	20
9	Structural Designer – Structural Project Manager (SPM)	4	13

Table 4 - The demographics of the participants (continue)

Respondent	Type of Professional Experience	Experience in the present position (years)	Experience in total (years)
10	Structural Designer – Structural Project Manager (SPM)	10	19
11	Structural Designer – Structural Project Manager (SPM)	1	16
12	Structural Designer – Structural Project Manager (SPM)	8	9
13	Expert in Maintenance	8	12
14	Construction Manager	15	25

The interviewees were asked to list the types of geotechnical structures they designed based on the frequency and level of contribution of their experience.

In response to this enquiry, the top three types of geotechnical structures designed were revealed to be pile foundations (30%), retaining walls (26%), and shallow foundations (23%). The distribution of the geotechnical structures designed by the respondents is as depicted in Figure 4.
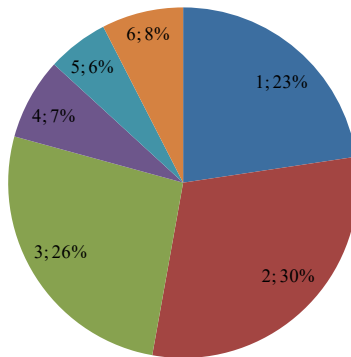
Figure 4 - Geotechnical structures most frequently designed by the respondents: 1 - shallow foundations; 2 - pile foundations; 3 - retaining walls; 4 - excavations, slopes, dikes; 5 - anchors; 6 - other types of geotechnical structures (floor, foundation underpinning, roads, collectors).

As can be seen from Figure 4, the most commonly used structure is pile foundations and the second choice is retaining walls.

The most commonly encountered problems identified by the respondents were related to retaining walls, loose soil, and water. However, very often, respondents related these problems to insufficient geological exploration, limited information about surrounding structures and engineering infrastructure, and their assessment at all stages of construction.

It is worth noting that underground barriers were mentioned as problems only by geotechnical engineers. The frequency of problems encountered in geotechnical structures as reported by the respondents is given in Figure 5.
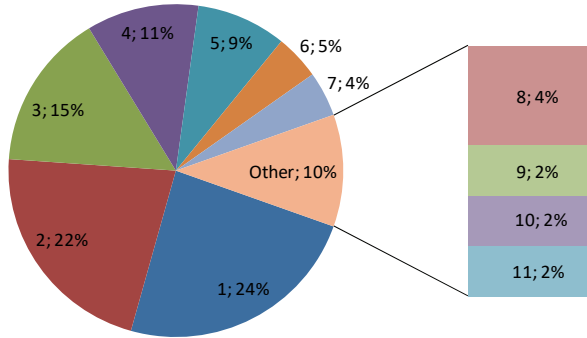
Figure 5 - Frequency of problems encountered related to:
1 - retaining walls; 2 - loose soil; 3 - water; 4 - limited information about surrounding structures and engineering networks; 5 - small number ground test; 6 - shallow foundations; 7 - foundation underpinning; 8 - dynamic loading; 9 - underground barriers; 10 - interaction between geotechnical and overhead structures; 11 - overall stability.

When answering the questions about quality mismatches specific to geotechnical structures and the usual reasons for their occurrence, 10 out of 14 respondents identified quality mismatch as a deviation inherent in geotechnical structures. Others mentioned sediment, insecure reinforcement in the project, insufficient depth, inadequate waterproofing, and concrete works.

The most significant reason for the appearance of poor-quality geotechnical structures, according to the respondents, was the geological conditions and their poor assessment or insufficient geological explorations. Workplace culture on the construction site and errors in design took second position. Errors in design were often (two times out of four) related to the inadequacies of technological processes with computational schemes. Also, tight work deadlines, incorrectly applied technology, misunderstandings, and corruption were also pointed out. The reasons for poor quality of the finished work and their respective weights are shown in Figure 6.

Insufficiency of geological and engineering investigations was cited as the most common cause of poor-quality work. Therefore, an additional enquiry was carried out with the aim of determining the causes of and reasons for complementary investigations in the design and construction stages. Only 11 of 14 interviewees responded to this line of enquiry: three respondents carried out the exploration when the properties of the soil at the site at the time of construction did not match the data provided in the report; six respondents did so when they lacked data in the design stage (insufficient depth of exploration, unspecified mechanical properties of the soil, filtration coefficient, etc.); two of them commissioned additional studies to clarify the characteristics of the loose soil for a reliable and cost effective design (Figure 7).
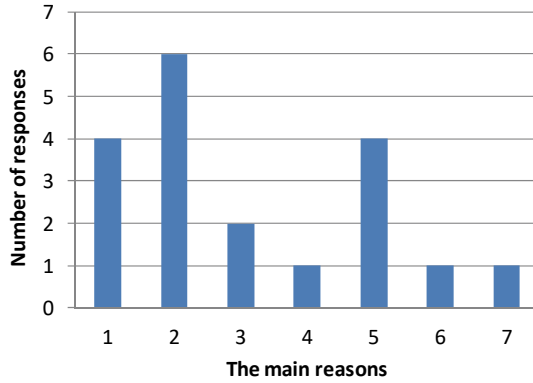
Figure 6 - The main reasons for low-quality geotechnical structures:
1 - workplace culture; 2 - geological conditions or poor evaluation of geological
conditions; 3 - busy work schedules; 4 - incorrect application of technology; 5 - errors in
design; 6 - misunderstandings; 7 - corruption.
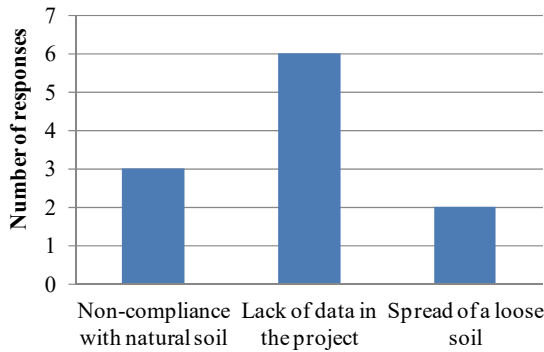
Figure 7 - Reasons for conducting additional geological and engineering investigations.
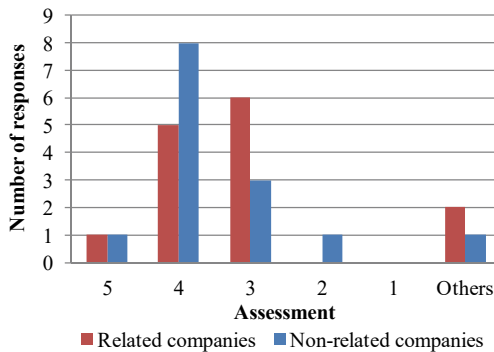
Figure 8 - Confidence in the experts

Geotechnical experts are frequently invited to participate at all stages of construction; however, the effectiveness of these sessions depends on the mutual trust between construction participants. Thus, the respondents were asked to assess their confidence in the experts, specifically confidence in experts from related companies and those from unrelated companies, that is, outsiders. Respondents were asked to rank their confidence levels using a 1 to 5 scale where 1 means 'no trust at all' and 5 means 'trust blindly and do not check the statements made'. The outcome of this enquiry is shown in Figure 8.

All respondents felt more confident when experts were independent, because they could more objectively assess the situation without 'linking' their opinions to a particular solution or the solutions of a particular company.

As 'other' answers, two options were distinguished:

- in the first option, regardless of the considered issue being discussed with the expert company, the experts were evaluated on an individual basis from 1 to 4 subject to the company and the designer;
- the second option was related to the companies: 1 to 3 (depending on the situation whether a decision or requests made by the expert have an effect on the selection of a geotechnical company and a certain type of foundation).

The provided answers suggest (see Figure 8) that extreme degrees of confidence in experts are rare: total mistrust never occurred and absolute confidence was a rare occurrence.

3.2. Geotechnical Risks of Installing Flexible Retaining Walls–Case Study

This section analyses the geotechnical risks of installing flexible retaining walls. Flexible retaining walls started to be applied in residential construction in Lithuania approximately 20 years ago. This was due to growing demand for the creation of underground parking space in developed urban areas. Therefore, it is no coincidence that the flexible retaining wall appears as the most common problem-related geotechnical structure. During the last 10 years, two accidents involving soil excavation and retaining walls have occurred on construction sites in Lithuania.

The second part of the interview was dedicated to the geotechnical risk of the stages in the installation of flexible retaining walls. The enquiry was aimed at determining the risks involved and the consequences incurred.

Assessment of the construction practice of flexible retaining walls led to the identification of seven stages of construction (Tables 5–9):

- Stage 1 – driving an H-beam into the designed position;
- Stage 2 – first-level excavation;
- Stage 3 – installing an anchor;
- Stage 4 – excavation up to the designed position;
- Stage 5 – installing piles next to the wall;
- Stage 6 – installing the first overlay;
- Stage 7 – installing the second overlay.

3.2.1. Interviews for the geotechnical risk of the steps in the installation of the flexible retaining wall

The respondents were asked to assess the compliance of the calculation scheme with the technological one and to identify the relevance of the aforementioned risks, consequences, and likely conditions to be observed at each stage and to recommend preventive measures to be undertaken to mitigate the risks.

Analysis of the calculation schemes showed that only two respondents underlined that pressure tubes sometimes formed intermediate cast-in-place that should affect the calculations of flexible retaining walls. Therefore, it was necessary to assess whether the load from the pipe could affect the retaining wall at all stages. As for the other stages, half of the respondents pointed out the following:

- in Stages 2 and 4, the calculated depth of the excavation has to be taken into account when estimating the possible inaccuracies of the excavation rather than accepting a standard size;

- in Stage 5, cast-in-place formation opposite the wall destroys the foundation of the retaining wall and therefore it is necessary to estimate this in the calculation scheme (Figure 9).
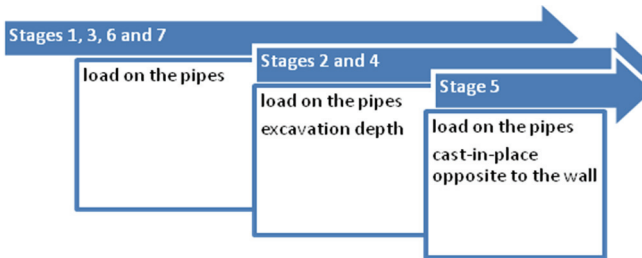
Figure 9 - Comments on the compliance of calculation schemes with technological schemes.
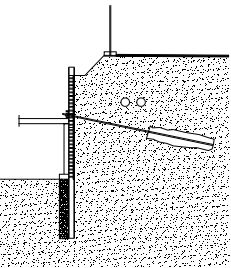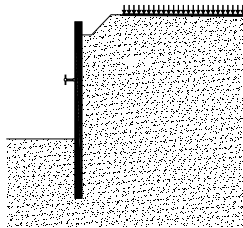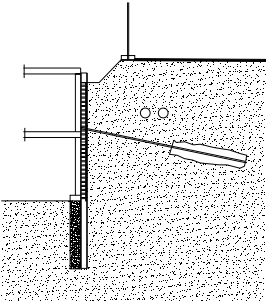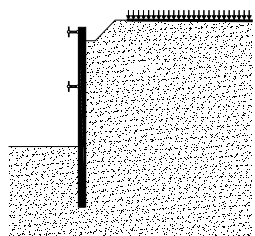
The tables below (Tables 5–9) show the summarized answers to the questions about risks arising and their consequences and conditions for the emergence of hazards occurring in each stage. The numbers in brackets next to the risks and conditions for risks indicate the number of respondents who named them.

The smallest number of risks were identified in Stages 6 and 7 (Table 5).

The most frequent ones involve the following:
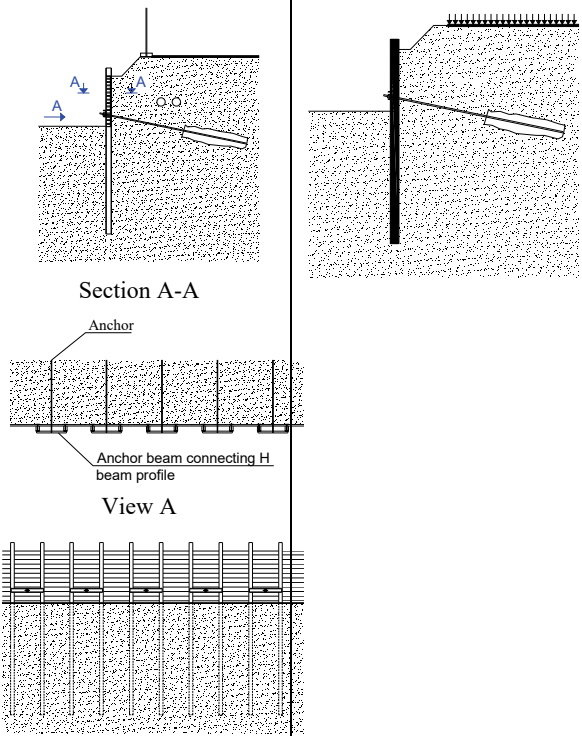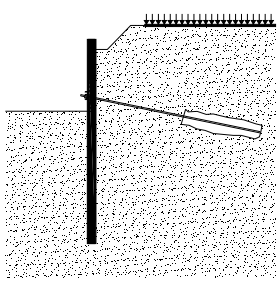
- too-deep excavation (Stages 2 and 4, Tables 8 and 9);

- deviations from designed anchors and beam anchors or insufficient bearing capacity (Stage 3, Table 6);

- foundation weakening caused by anchor installation (Stage 5, Table 7);

- H-beam deepening and related risks (Stages 1 to 3, Tables 6 and 8).

Table 5 - The analysis of risks, consequences, and conditions in the case study. Stages 6 and 7.

Stage 6 – Installing the 1st overlay		
Scheme / risk of the technological process	Calculation scheme / consequence	Description / conditions
Question		Concrete is poured on the grate, wall and overlay above formed cast-in-place In 28 days after laying concrete, temporary anchors are released
Responses Loosening anchors will move the wall (3)	Collapse or deformations of the retaining wall ⇒ crack in the pipe	Poor contact between the overlay and retaining wall (2)*
		Calculation scheme does not correspond to the actual situation of the overlay (1)
		Overlay design did not consider horizontal loads (2)
Stage 7 – Installing the 2nd overlay		
Question		Overlays are produced following concrete hardening (in 28 days after laying concrete) One-story wall is concreted
Responses The overlay will not accept horizontal loads (3)	Collapse or deformations of the retaining wall ⇒ crack in the pipe	Poor contact between the overlay (2) and retaining wall Overlay design did not consider horizontal loads (1)
*The brackets next to risks and conditions for risks indicate the number of the respondents who named them.		
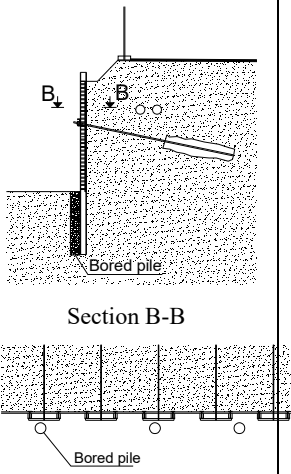
The most common opinion about potential risk was obtained by analysing Stage 4; foundation weakening within the process of forming cast-in-place pile was identified as a risk (Table 9).

Table 6 - The analysis of risks, consequences, and conditions in the case study. Stage 3.

Stage 3 – Installing an anchor		
Scheme / risk of the technological process	Calculation scheme / consequence	Description / conditions
Question Section A-A Anchor Anchor beam connecting H beam profile View A		Beam anchors connecting two neighboring H-beams are installed. Anchors the roots of which make ~ 20 cm in diameter are installed In 28 days, the anchors are pressed in up to the force provided in the project
Responses Insufficient bearing capacity of the anchor (3)	Collapse or deformations of the retaining wall ⇒ crack in the pipe	Clogged soil (1) Inappropriate anchor installing technology (2) Error in the project (1) Spoiled material (1) Anchors are fitted at a larger angle to protect pipes (1)
Pipes damaged during anchor installation (1)	Crack in the pipe	Clogged soil (1) Inaccurate information about the location of the pipe (1) Deviations from the project (2)
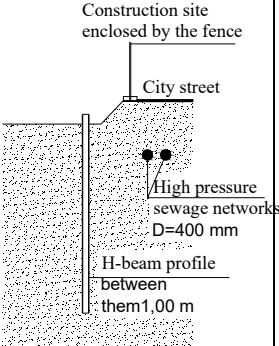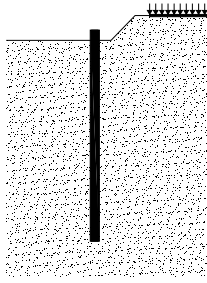
		Inappropriate anchor installing technology (1)
Big deformations or collapse of the beam anchor (5)	Collapse or deformations of the retaining wall ⟹ crack in the pipe	Deviations from installing H-beams: distance are too large (2)
		Too small profile of beam anchors has been selected (3)
		H-beams are interconnected only in pairs not using a continuous beam anchor (5)
Excessive deformations or collapse of H-beams (2)	Collapse or deformations of the retaining wall ⟹ crack in the pipe	Looser soil than that found during investigation (2)
		H-beams are interconnected only in pairs not using a continuous beam anchor (5)

Table 7 - The analysis of risks, consequences, and conditions in the case study. Stage 5.

Stage 5 – Installing piles next to the wall		
Scheme / risk of the technological process	Calculation scheme / consequence	Description / conditions
Question	Calculations of the retention walls of stage 4 are used	Formed cast-in-place bearing vertical loads of the retention wall are erected
Responses The foundations opposite the retention wall are weakened (7)	Collapse or deformations of the retaining wall ⟹ crack in the pipe	Cast-in-place formation is very close to the H-beam (2) Inappropriate cast-in-place formation technology, cast-in-place forming weakens the foundations (6)

| | | Loss of overall stability $\Rightarrow$ crack in the pipe | Cast-in-place formation is very close to the H-beam (2) |
| | | | Inappropriate cast-in-place formation technology, cast-in-place formation weakens the foundations (6) |

Table 8 - The analysis of risks, consequences, and conditions in the case study. Stages 1 and 2.

Stage 1 - H-beam deepening into the designed position			
	Scheme / risk of the technological process	Calculation scheme / consequence	Description / conditions
Question	Construction site enclosed by the fence / City street / High pressure sewage networks D=400 mm / H-beam profile between them 1,00 m		The site is enclosed inserting H-beams into the designed situation
Responses	Designed deepening is not achieved (2)*	Collapse of the retaining wall or deformations $\Rightarrow$ crack in the pipe	Clogged soil (1), inappropriate types of soil (strong clay, rubble) (1)
	H-beam inserted into the pipe (1)	crack in the pipe	
	Deviations of H-beams from the plan (2)	Project correction $\Rightarrow$ increase in costs	
	Solidified soil under the pipes (2)	Deformations of the foundation under the pipes $\Rightarrow$ crack in the pipe	Vibration (6)
	Solidified soil under the road (1)	Deformations of the foundation under the road $\Rightarrow$ deformations of the road	
	Collapse of pipe connections (1)	Crack in the pipe	
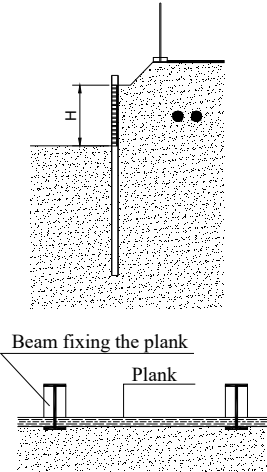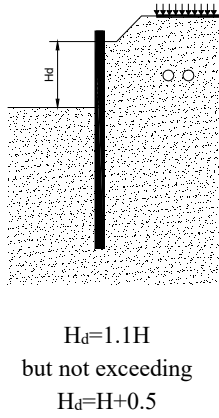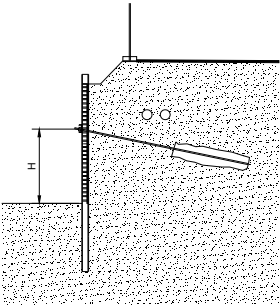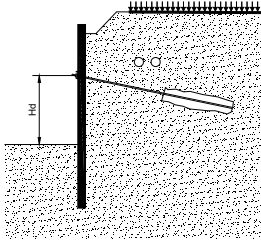
Stage 2 – 1st level excavation		
Question	Beam fixing the plank — Plank	H_d=1.1H but not exceeding H_d=H+0.5	Level 1 is excavated to be fitted with anchors To prevent sand crumbling, planks are embedded between H-beams
Responses	Cavities form between planks and soil matter form (2)	Soil moves behind the retaining wall ⇒deformations of pipe foundations ⇒ crack in the pipe	Crumbly, dry soil, recommendations are neglected when work is done' (3)
	Larger load than that expected in the road zone (1)	Collapse or deformations of the retaining wall ⇒ crack in the pipe	The project does not provide the possibility of carrying heavy loads, transport weight is not limited (1)
	Separate H-beams can enter the layer of the unexpected looser soil (3)	Collapse or deformations of the retaining wall ⇒ crack in the pipe	H-beams are not interconnected, insufficient soil investigation (4)
	Planks break (2)	Soil moves behind the retaining wall ⇒ deformations of pipe foundations ⇒ crack in the pipe	Distances between H-beams are larger than those provided in the project (2) Heavier load acting on the planks than that provided in the project (3)
	The excavation is deeper than that provided in the calculation scheme (4)	Collapse or deformations of the retaining wall ⇒ crack in the pipe	Improper control during construction (1) Misunderstandings between the construction parties (5)

Table 9 - The analysis of risks, consequences, and conditions in the case study. Stage 4.

Stage 4 – Excavation up to the designed position		
Scheme / risk of the technological process	Calculation scheme / consequence	Description / conditions
	  Hd=1.1H but not exceeding Hd=H+0.5m	Excavated up to the altitude of the designed foundation pit
Excavation is deeper than that provided in the computation scheme (5)	Collapse or deformations of the retaining wall ⇒ crack in the pipe	Improper control during construction (5) Misunderstandings between the parties of construction (2)
Loss of overall stability (2)	Collapse or deformations of the retaining wall ⇒ crack in the pipe	Too short anchors (1) Anchors are installed at a sharper angle of inclination than that provided in calculations (1) Overall stability is not verified (1)

On requesting recommendations regarding preventive measures that could be taken to reduce risks, experts' comments regarding all the design and construction stages of the retention wall involved remarks indicating that having a detailed project and sufficient time to prepare it, the collection of sufficient data on the environment and geological conditions, permanent structural monitoring, and close cooperation between all construction participants are the aspects that have a powerful effect on work quality and the reduction of errors. Reducing or eliminating pressure to decrease stress in the pipes was mentioned as a specific requirement for this structure during construction.

Additional preventive measures distinguished by stages are as follows:

Stage 1 includes the application of other technology for the installation of the retention wall, maintaining a safe distance to the pipes, conducting geotechnical studies of sufficient scope, and collecting a substantial amount of relevant data on the location and condition of the pipes.

Stage 2 covers control of the depth of the excavation and the careful installation of planks to minimize soil crumbling.

Stage 3 involves the process of making a continuous beam anchor that integrates H-beams and anchors into the common system; all anchors must be tightened and tested in accordance with the requirements for normative documents, the depth of the pipelines must be adjusted, a sufficient distance from the borehole for the anchor to the bottom of the pipeline must be maintained, the drilling angle must be monitored, and the designed injection area must be as far as possible beyond the pipelines.

Stage 4 keeps control of the excavation.

Stage 5 embraces the selection of cast-in-place formation technology that should minimally damage the foundations of H-beams and form cast-in-place as far from the H-beams as possible. The stage also points to forming cast-in-place with pauses to reduce temporarily weakened areas.

The interview was informal and had no time limit. Although the face-to-face interview approach was used and assisted in clarifying the situation, there was no respondent who should focus on all the risks listed in the table.

One of the respondent designers (Structural Project Manager) described situations and calculation schemes as logical and thoughtful and therefore did not face any risks in the process of installing flexible retaining walls. The surveyed architect, project manager (PM) distinguished only deviations from the design situation as risks that could affect architectural decisions.

The respondents agreed with the opinion that the greatest loss in the given situation would be caused by a breakdown in the pressure pipe and pollution of the natural environment by wastewater. Also, breakdown in the pressure pipe was mainly mentioned when assessing the final consequences of the risk.

3.2.2. Drawing the Cause and Effect Diagram

One of the major outcomes identified in the interviews was breakdown in the pressure pipe, which would lead to the greatest loss. After scrutiny of the data obtained from the interviews, to further clarify the possible causes of breakdown of the pressure pipe, a brainstorming session was held. Five experts who cited the majority of risks during interviews (one geotechnical expert, one designer (Structural Project Manager), two geotechnical designers, and one construction manager) were selected as participants. First, the participants were briefed about the case of breakdown of the pipes, and six categories of causes, namely technology, time, management, environment, people, and structures (geotechnology), were identified. Then they were asked to come up with as many causes of such an incident as possible. Finally, all the possible causes cited for the breakdown of the pressure pipe (the effect) were used to construct the cause and effect diagram (see Figure 10). The findings are summarized below:

Structural-geotechnical causes
- structural members of retention walls (H-beams, soil-retention planks, anchors);
- technological processes related to the installation and testing of structural members (vibration, cast-in-place formation opposite the retention wall technology);

- pit excavation (information included in the project, match with the calculation scheme, control over altitudes);
- initial information and the project (geological and engineering investigations, the place of the pipes in space, project finalization and application of technology used, the accuracy of calculation schemes, the amount and accuracy of all information).

Environmental causes

- accuracy and content of geological and engineering investigations;
- information on the surrounding buildings and structures;
- loads and impacts (e.g. transport, seismic, technological).

Technological causes

- technologies used in the construction of structures and their negative effects on the structures or their members.

Managerial causes

- poor organization;
- frequent changes in projects;
- excessive workloads;
- insufficient experience of installing BIM systems.

Time-related causes

- busy work schedules that disregard technologies.

Staff-related reasons:

- poor communication between stakeholders;
- lack of staff;
- errors in taking control of the project;
- errors in developing the geotechnical project.

Brainstorming disclosed that answers to the question of 'why it might happen' were based on:

- experience gained in the individual's and company's projects or acquired by analysing past failures in other projects;
- theoretical knowledge obtained during studies or on training courses;
- directions provided by regulatory documentation describing investigation, design, and installation.

Although the aim of the participants was to identify the risks of installing retaining walls and determining their causes while placing major focus on the retention wall as a geotechnical structure, other causes of risks related to technology, time, management, environment, and human resources were identified too. The selected team has to ensure the representation of all stakeholders and participants of construction- the composition of the team needs to be adjusted according to the intended goals. In this way, the project can be analysed in more detail.

Based on these observations, one can conclude that the proper selection of brainstorming participants can lead to good results when analysing geotechnical structures with respect to risks.
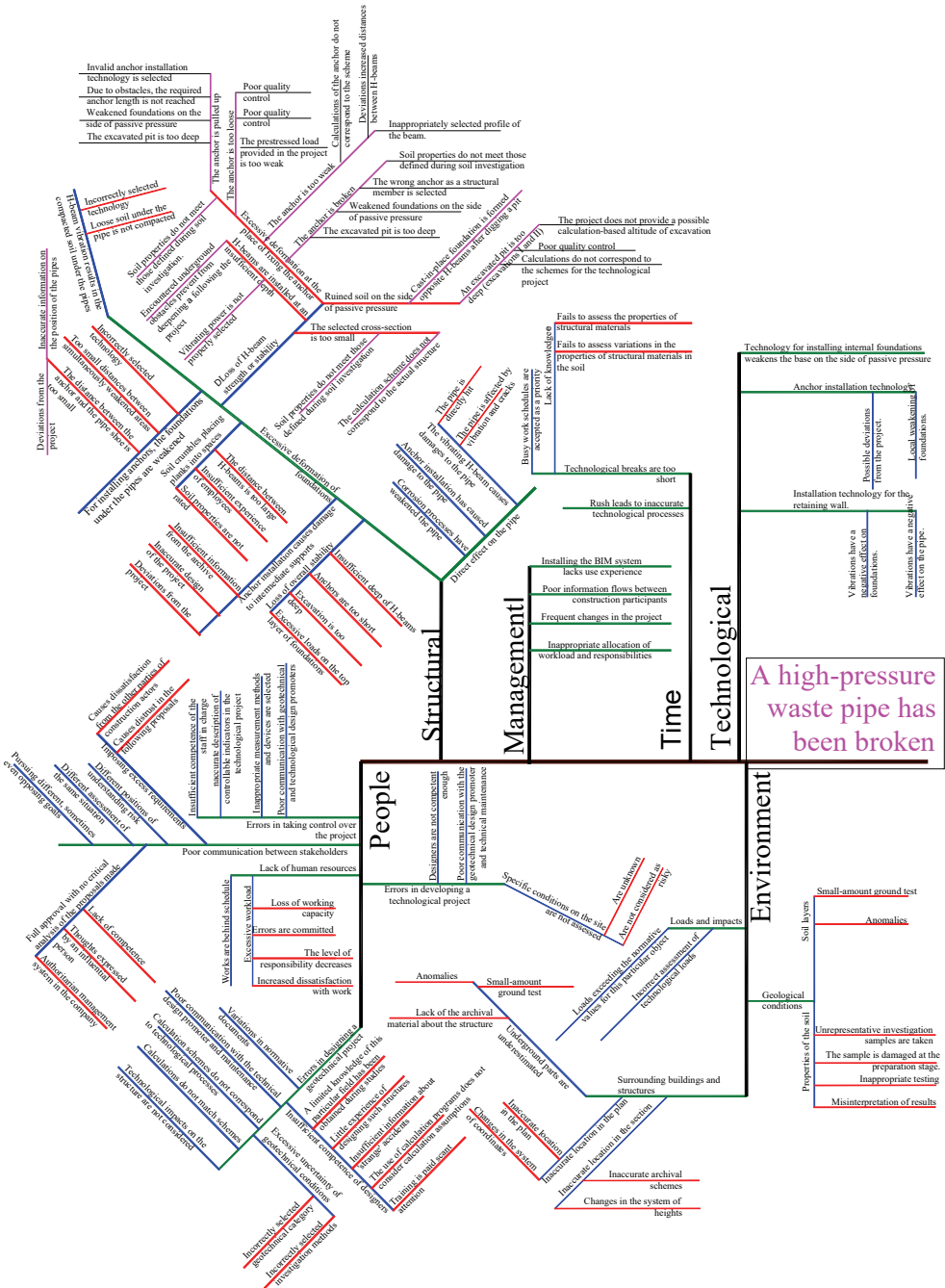
Figure 10 - The cause and effect diagram according to the information collected during brainstorming.

4. DISCUSSION

Based on the analysis carried out, the authors of the paper proposed risk identification of flexible retaining walls using a risk management flow based on Mishra et al. [8] and ISO/IEC 31010:2009 [24]. In the future, this chart (Figure 11) can be verified by analysing other geotechnical structures. For the effective application of risk identification in flexible retaining wall risk management flow, a well-prepared team representing all interested parties should be created.

Data collected on the investigated structure. A detailed project, including calculation schemes, descriptions of technology, and the work order, is developed, and all information on adjacent buildings and structures and data of geological engineering exploration are obtained.

The collected information assists in establishing the content, thus allowing the risk management objectives, criteria, and assessment programme to be identified and coordinated. If the required information is missing, data are added before proceeding to the next stage.

The purpose of risk assessment is to help make decisions based on the results of risk analysis, define the risks to be reduced, and set risk reduction priorities. Risk assessment includes one or a few options for changing risk and implementing these options.

First, the risks are identified, which involves all pre-selected construction participants and interested persons, for example, by applying the face-to-face interview approach. Brainstorming is used to identify risks. To facilitate risk management, the installation of the flexible retaining wall should be divided into technological stages.
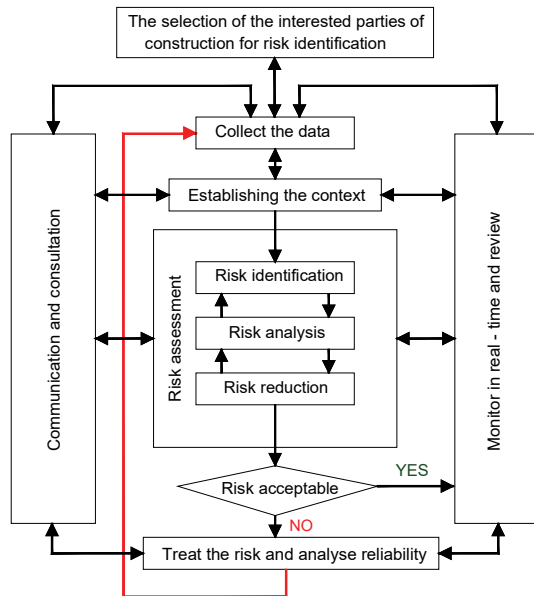
Figure 11 - Risk identification in flexible retaining wall risk management flow according to ISO/IEC 31010:2009 [24] and Mishra et al. [8]

At the stage of risk analysis, the probability of occurrence of the appropriate type of risk is estimated. The consequences established at the risk identification stage are also assessed; that is, their impact on the project and its related activities is evaluated.

The stage of selecting preventive measures, reducing risk, and analysing the reduced risk completes the risk assessment. Thus, the question of 'whether the risk is acceptable' arises.

The authors of the article propose that if the risk is not acceptable, the data collection stage should be performed again to acquire new data. It may involve material for additional geological engineering exploration or any other bonus information that may affect the risk of installing the retaining wall. Then, everything is repeated again. At the risk assessment stage, the processes of risk identification, analysis, and reduction are very closely interrelated and therefore have to complement one other.

The participants must be involved in information exchange, tutorials, risk monitoring, and review within the whole process. In order to identify risk, first of all, the selection of all construction participants involved has to be made. They may analyse geotechnical risks and related problems. The proposal is based on the analysis carried out in this article and on the observation that not all construction participants having experience in the field of construction - are able to identify geotechnical risk (see Section 3).

5. CONCLUSIONS

Analysis of the scientific literature with reference to the topic of the article shows that the risk of collapse or deformations of flexible retaining walls has not been widely analysed.

In order to determine the risk of installing flexible retaining walls, the authors of the article used the face-to-face interview approach, brainstorming, and a cause and effect diagram. A specific case study is presented.

The examination of the specific case (interviewing) demonstrated that the respondents identified risks and proposed additional preventive measures. The respondents expressed the same opinion about the given situation and agreed that the greatest loss would be caused by breakdown of the pressure pipe and pollution of the natural environment with wastewater. Also, breakdown in the pressure pipe was the most frequently mentioned option when assessing the final consequences of risks.

Investigation of the data obtained during the face-to-face interview was based on brainstorming and the cause and effect diagram: five professionals who had monitored most of the risks were selected with the help of the face-to-face interview. The thoughts expressed during brainstorming were used as the basis for drawing the cause and effect diagram.

The study found that the face-to-face interview approach could only be applied to risk identification in simple cases and was suitable for preliminary screening of the respondents involved in brainstorming. Thus, the face-to-face interview approach should provide an identical or similar situation in order to independently assess the competence of would-be respondents considering a particular issue.

Geotechnical experts are more trusted than other construction participants when expressing their positions on objects not related to it or the company that employs them. Cooperation is also smoother if reasoned statements are made.

Acknowledgements

Conflicts of Interest

The authors declare no conflict of interest.

References

[1] Lacasse, S. Hazard, Reliability and risk assessment – research and practice for increased safety. *NGM 2016 Reykjavik Proceedings.* Paper presented at the 17th Nordic Geotechnical Meeting. Challenges in Nordic Geotechnics, 25–28 May 2016.

[2] Flage, R., Aven, T. Emerging risk – Conceptual definition and relation to black swan type of events. *Reliab. Eng. Syst. Safe., 144*, 61–67, 2015.

[3] ISO 31000:2009(E). *Risk management – Principles and guidelines*.

[4] Duncan, J.M. Factors of safety and reliability in geotechnical engineering. *J. Geotech. Geoenviron., 126(4),* 307–316, 2000.

[5] Gibson, W. Probabilistic methods for slope analysis and design. *Aust. Geomech. J.*, *46(3)*, 1–12, 2011.

[6] Brown, E.T. Risk assessment and management in underground rock engineering—an overview. *J. Rock Mech. Geotech. Eng, 4(3)*, 193–204, 2012.

[7] Swannell, N., Palmer, M., Barla, G., Barla, M. Geotechnical risk management approach for TBM tunnelling in squeezing ground conditions. *Tunn. Undergr. Sp. Tech., 57*, 201–210, 2016.

[8] Mishra, R.K., Janiszewski, M., Uotinen, L.K.T., Szydlowska, M., Siren, T., Rinne, M. Geotechnical Risk Management Concept for Intelligent Deep Mines, *Procedia Eng, 191*, 361–368, 2017.

[9] Xia, Y., Xiong Z., Dong, X., Lu, H. Risk assessment and decision-making under uncertainty in tunnel and underground engineering. *Entropy, 19(10)*, 549, 2017.

[10] Haddad, A., Eidgahee, D.R., Naderpour, H. A probabilistic study on the geometrical design of gravity retaining walls. *World J. Eng., 14(5)*, 414–422, 2017.

[11] Zou, Y., Kiviniemi, A., Jones, S.W. A review of risk management through BIM and BIM-related technologies. *Safety Sci., 97,* 88–98, 2017.

[12] Li, Z., Xue, Y., Qiu, D., Xu, Z., Zhang, X., Zhou, B., Wang, X. AHP-ideal point model for large underground petroleum storage site selection: an engineering application. *Sustainability, 9(12)*, 2343, 2017.

[13] Xue, Y., Cao, Z., Du, F., Zhu, L. The influence of the backfilling roadway driving sequence on the rockburst risk of a coal pillar based on an energy density criterion. *Sustainability, 10(8)*, 2609, 2018.

[14] Ahmadi, M.; Behzadian, K.; Ardeshir, A.; Kapelan, Z. Comprehensive Risk Management Using Fuzzy FMEA and MCDA Techniques in Highway Construction Projects. *Journal of Civil Engineering and Management* 2017, 23 (2), 300-310, DOI: 10.3846/13923730.2015.1068847.

[15] Valipour, A.; Yahaya, N.; Md Noor, N.; Antuchevičienė, J.; Tamošaitienė, J. Hybrid SWARA-COPRAS Method for Risk Assessment in Deep Foundation Excavation Project: An Iranian Case Study. *Journal of Civil Engineering and Management* **2017**, 23(4), 524–532, DOI: https://doi.org/10.3846/13923730.2017.1281842

[16] SGF (Swedish Geotechnical Society). *Risk Management in Geotechnical Engineering Projects – Requirements: Methodology*. Report 1:2014E. 2nd ed. Linköping: Swedish Geotechnical Society. 2017. Available online: http://www.sgf.net/web/page.aspx?refid=4567 (accessed on 5 March 2018).

[17] Clayton, C.R.I. (ed.) *Managing Geotechnical Risk - Improving Productivity in the United Kingdom,* 2001.

[18] Baynes, F.J. Sources of geotechnical risk. *Q. J. Eng. Geol. Hydrog., 43*, 321–331, 2010.

[19] Sartain, N., Mian, J., Free, M. Presenting uncertainty clearly: challenges in communicating geotechnical risk. *Geotechnical Safety and Risk V,* 739–751, 2015.

[20] Huang, H., Zhang, D. Quantitative geotechnical risk management for tunneling projects in China. *Geotechnical Safety and Risk V,* 61–75, 2015.

[21] Simpson B & Driscoll R, *Eurocode 7: A Commentary.* CRC Ltd, Watford. 179 p, 1998.

[22] EN-1997-1 Eurocode 7: *Geotechnical Design – Part 1: General Rules.* 168 p.

[23] EN-1997-2 Eurocode 7 – *Geotechnical Design – Part 2: Ground Investigation and Testing.* 196 p.

[24] ISO/IEC 31010:2009. *Risk Management – Risk Assessment Techniques*. International Organization for Standardization, Geneva.

[25] Dikčius, V. *Marketing Research. Theory and Practice.* Vilnius, Lithuania, 187 p, 2003 [in Lithuanian].

Assessment of the Disaster Recovery Progress through Mathematical Modelling

S. Ümit DİKMEN[1]
Rıfat AKBIYIKLI[2]
Murat SÖNMEZ[3]

ABSTRACT

Natural disasters, especially major earthquakes, cause widespread devastation in the built environment. Hence, the major component of the recovery in its aftermath constitutes a chain of projects starting at different times, having different costs and durations. In this study, the post disaster recovery curve modelled through a mathematical approach taking into account these properties of the projects. The approach followed is based on the project S-curve concept that provides the opportunity to simulate the progress by outlining the project spending. Well-known mathematical functions are adapted to model the project spending and the handover processes. Monte Carlo simulation is performed to evaluate the general behavior of the recovery curve using the model developed. Weibull distribution is used to generate the model's parameters. Results of Monte Carlo simulation demonstrate that the recovery process exhibits an S-shape; the duration of initial portion and the slope of the bulk portion being significantly governed by the level of preparedness of the community.

Keywords: Disaster, recovery curve, mathematical modelling, S-curve, Monte Carlo Simulation.

1. INTRODUCTION

Ever since, Bruneau et al (2003) introduced the model conceptualizing the resilience and the recovery of the societies following a major disaster, the model has found wide acceptance among both the academicians and administrators [1]. In their work, researchers presented a mathematical framework that paved road for the development of methodologies to measure the resilience also. Hence, possibly owing to the simplicity of the model, various approaches

---

1 MEF University, Civil Engineering Department, Istanbul, Turkey - dikmens@mef.edu.tr - https://orcid.org/0000-0002-4003-1368

2 Duzce University, Civil Engineering Department, Duzce, Turkey - rifatakbiyikli@duzce.edu.tr - https://orcid.org/0000-0003-1584-9384

3 Sakarya University, Institute of Natural Sciences, Sakarya, Turkey- murat.sonmez2@ogr.sakarya.edu.tr - https://orcid.org/0000-0003-2328-6817

to measure resilience have been developed and put in use (e.g. Cimellaro et al, 2010a&b) [2,3]. A comprehensive review of these studies can be found in the book on urban resilience by Cimellaro (2016) [4].

The model of Bruneau et al simply indicates that a sudden drop, namely a loss, in the functionality of the built environment and the society will take place in a disaster which will then be recovered in a period $t_t = t_r\text{-}t_0$ through some path (Figure 1). In Figure 1, t_0 and t_r correspond to the event date and the date total recovery is achieved, respectively. Likewise, in the same figure, F_d indicates the remaining functionality following the disaster. Subsequently, the area above the recovery curve between times t_0 and t_r signifies the loss of resilience, R, with respect to a specific disaster. Whereas, the area below the recovery curve is a measure of the resilience of the disaster hit community. Hence, the recovery curve is an important element in the resilience studies. Also, both the extent of loss, $100\%\text{-}F_d$ and the recovery period, t_t, as well as the shape of the recovery curve are important parameters in modeling and assessing the resilience and recovery of a community after a disaster.
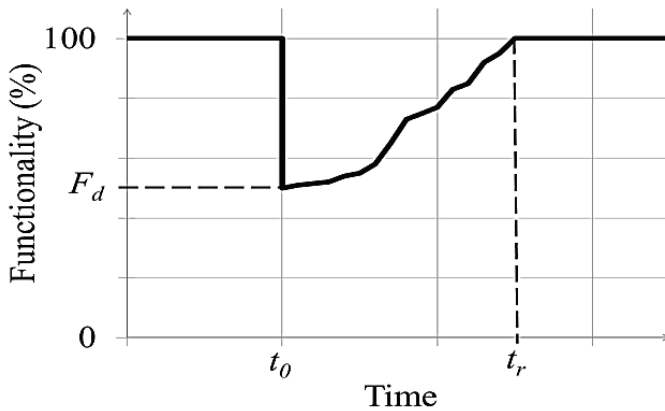
Figure 1 - Conceptual representation of resilience (adapted from Bruneau et al 2003)[1]

Bruneau et al (2003) proposed that resilience has four components, namely technical, organizational, social and economic [1]. They involve many parameters of different difficulty levels to quantify. Researchers indicated that the first two components are related to the resilience of critical physical systems such as hospitals and lifelines. While, the last two components are more related to the affected community, such as housing. Thus, the term resilience covers a wide spectrum of topics ranging from human care to reconstruction and/or repair of the built environment. Generally, the major portion of the devastation by a disaster, regardless of its nature, is in the built environment. Therefore, to a great extent, full recovery, namely full functionality of the disaster hit community will require the revival of the built environment to the standards and scope prior to the disaster, including and of course but not limited to the satisfaction of housing needs.

Thus, another angle to look into the subject of functionality is the level of damage incurred in the built environment. This is especially true in the case of earthquakes. During a major earthquake, extensive damages and collapses in the built environment takes place [5]. Yet, it

is very difficult to estimate the extents and composition of the structures and facilities damaged before the disaster [6]. While some structures will become functional with minor or major repairs, others may be in a condition beyond repair. Furthermore, the damaged structure can be a structure with low replacement cost and short implementation time or a facility with high replacement cost and duration [7]. The common point among all these efforts is that, they all are projects of different cost magnitude and duration. Hence, the major component of the recovery from a disaster will constitute a chain of projects starting at different times, having different costs and different durations. In this respect, if the full recovery of the damaged inventory is considered as a "project", the projects in the chain can be termed as "sub-projects". In other words, all sub-projects will have the objective to make good some function lost in the built environment during the disaster. Therefore, the shape of the recovery curve will be analogous to the progress curve of the overall recovery project, i.e. the chain of sub-projects.

Cimellaro et al (2006) suggested that the recovery curve can be represented by three different forms, namely linear, exponential and trigonometric [8]. In their work, the linear recovery is attributed to the recovery of an average prepared community. They also stated that if the community is well prepared the recovery curve will take the form of the exponential (convex) curve, while the recovery of an unprepared community will follow a trigonometric (concave) path (Figure 2).
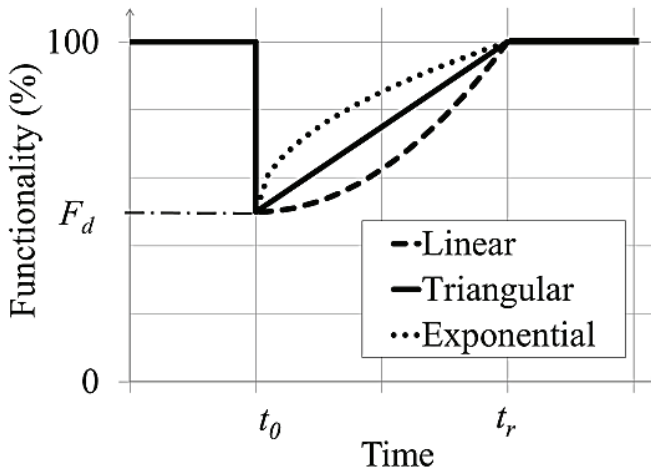
Figure 2 - Recovery functions (adapted after Cimellaro et al (2006, 2010) [2,3,8])

In project management, especially in construction project management, the cash flow of projects, in general, follow a curve known as S-curve. In other words, it can be stated that an S-curve is a mathematical form to represent the cash flow of a project (Kenley, 2005) [9]. By analyzing the S-curves, the management team can identify visually if a project is on time or delayed and in or over budget. In this respect, the S-curve constitutes one of the basic concepts in project management. The use of estimated S-curves is a common practice among the owners, contractors and administrations in project planning, especially for forecasting the

cash flow. With this token, assuming that the recovery process in the aftermath of a disaster consists of a number of small projects, i.e. sub-projects, one can construct the project spending curve by combining the S-curves and subsequently the functionality contribution of the sub-projects, as named earlier.

The objective of this study is the investigation and assessment of the trend of the disaster recovery curve using a mathematical model based on the project S-curve. The form of the S-curve is selected in accordance with the earlier S-curve models developed. Then a Monte Carlo simulation type analysis is performed to observe the general behavior of the recovery curve based on the hypothesized model.

2. THE MATHEMATICAL MODEL

Researchers analyzing past data have determined that cumulative cash flows during the course of a project, especially in construction projects, display an S-shaped curve. A typical S-curve of a construction project starts gradually with a small slope basically covering the mobilization and initial works, such as excavation (Figure 3). Then the curve has a higher slope when the bulk of the production takes place, such as structural works, interior finishes and the façade works. Finally, the rate of increase of the curve slows down nearing the end of the project when most of the efforts at site are devoted to finalizing various cost items and the commissioning activities of the facility.
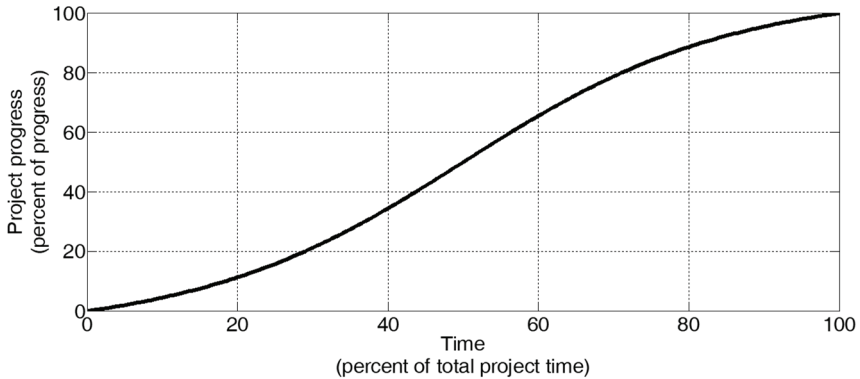
Figure 3 - Typical Project S-curve

Although, this shape generally applies to most of the projects, it should be noted that some variations can exist having impact on the shape of the curve, namely the cumulative cash flow curve at completion of a project may not be as smooth as the one shown in Figure 3. However, historical data prove that the spending at most of the projects closely follows a trend signified by the S-curve. In this respect, analyzing historical data researchers have proposed various mathematical expressions for the S-curve (Hudson &Maunick, 1974; Peer, 1982; Kenley & Wilson, 1986; Miskawi, 1989; Khoshrowshahi, 1991; Bousbaine and Elhag, 1999) [10,11,12,13,14,15,16]. Amongst various curves proposed, a well-known curve is the one developed by The Department of Health and Security of the United Kingdom (DHSS)

based on Hudson's studies on the subject (Hudson, 1978) [17]. A detailed treatment of the S-curve, including comparison of generic S-curves derived by various researchers, is given in the book on construction financing by Kenley (2005) [9]. A graphical summary of some the S-curves proposed by various researchers are given in Figure 4. Obviously, some differences exist between the proposed curves due to factors such as the composition and characteristics of the data set used, business culture of the country data collected. For instance, the DHSS curves are based on the construction of health care facilities with total value of about 12m £ at the time of the study. On the other hand, Miskawi and Khoshrowshahi curves represent some upper and lower bounds, which require selection of a parameter particular to the method for the determination of a project specific curve.
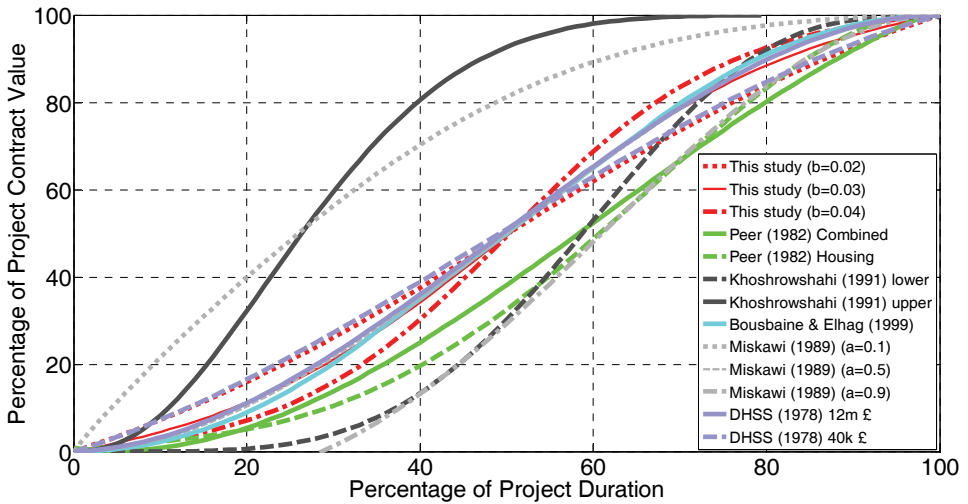
Figure 4 - S-curves proposed by various researchers

For the purposes of this study, a generic S-curve, assumed to be valid for all projects, namely the sub-projects, as defined earlier, is used. This curve is mathematically represented by the so-called logistic function in the following form,

$$E_{sp}(t) = \frac{C_{sp}}{1+ae^{-bt}} \qquad (1)$$

Where a and b are constants. Constants a and b determine the rate of increase and the shape of the curve. The limiting value C_{sp} is the total expenditure for the sub-project. If b is positive, as in our case, the curve will demonstrate an increasing trend. Time passed from the incision of the project, evaluated as the percentage of the total duration of the sub-project, appears as t in the equation. If the abscissa values, expenditure $E_{sp}(t)$, are normalized with respect to total sub-project expenditure, C_{sp} and the horizontal axes values, time t, normalized with respect to the total sub-project duration, we obtain a normalized generic S-curve in terms of percentages of progress and total project duration. The logistic curve has a single inflection point. The curve has two equal regions of opposite concavity with respect to this point. The

coordinates of the inflection point are $\left[\frac{\ln a}{b}, \frac{c_{sp}}{2}\right]$. Further detailed information about the properties of the logistic curve can be found in books on calculus and differential equations.

If variable a is equal to unity than the point of inflection of the S-curve will be at zero time and at half the expenditure of the sub-project conserving the concave symmetry around the abscissa. Hence, the S-curve calculated in this fashion is then shifted in the positive direction by half the duration of the sub-project. The S-curves for different combination of values of variable b and a is constant and equals to unity are given in Figure 5.
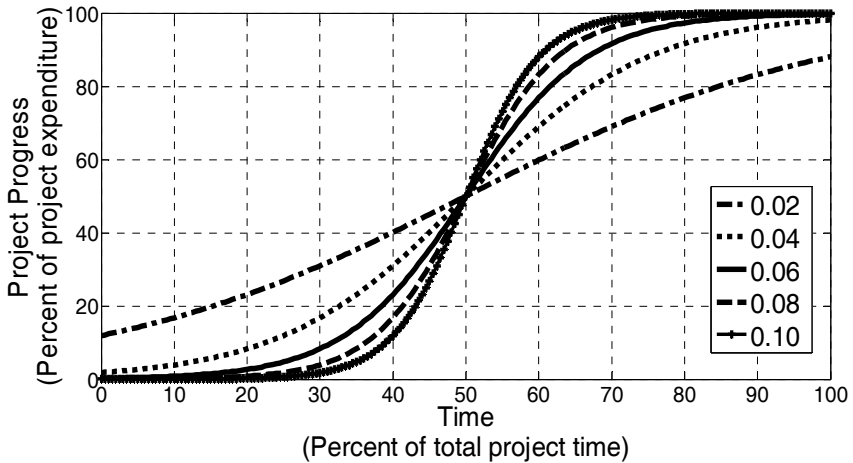
Figure 5 - Normalized generic project S-Curve

The curves for $b=>0.06$ are asymptotic with negligible values at 0 and 100% points in time, while for lesser values of b curves exhibit some finite value at these ends. Namely, these curves are asymptotic near the 0 and 100% and above. On the other hand, the curves with $b=>0.08$ have sustained negligible progress value for time percentages less than 30% and higher than 70%, which is not usual for the projects rolling normally. However, the curves in real life are not asymptotic at the beginning and at the end of a project as demonstrated in Figure 4. Hence, b value for the generic S-curve needs to be $=<0.04$; the abscissa values of the curves $b=<0.04$ can be adjusted by prorating to 100% expenditure. The S-curves adjusted in this fashion with $b=0.02$, 0.03 and 0.04 are demonstrated in Figure 4 together with the curves proposed by others. The curve with $b=0.03$ matches very closely with the DHSS curve for 12m £ projects as well as exhibits an average trend with respect to the other curves.

Furthermore, cash flow data of 38 different disaster recovery projects realized in Turkey were analyzed. These projects were constructed by The Housing Development Administration of Turkey between 2007 and 2014. Each individual project consists of a number of apartment buildings, social and technical infrastructure as well as landscaping. The average completion cost of the projects were about 20.0 million USD. It is also important to note that groups of several projects were constructed for the recovery of different earthquakes. The percent of realization vs percent of time graphs of these projects are shown in Figure 6 together with

their average. The generic S-curve with $b=0.03$ is also included in this figure. The close match of the $b=0.03$ curve with the average percent of realization vs percent of time of the recovery projects is remarkable. Therefore, considering the closeness of match with the DHSS curve and the average curve of the 38 earthquake recovery projects, $b=0.03$ was set to be used in generic S-curve definition.
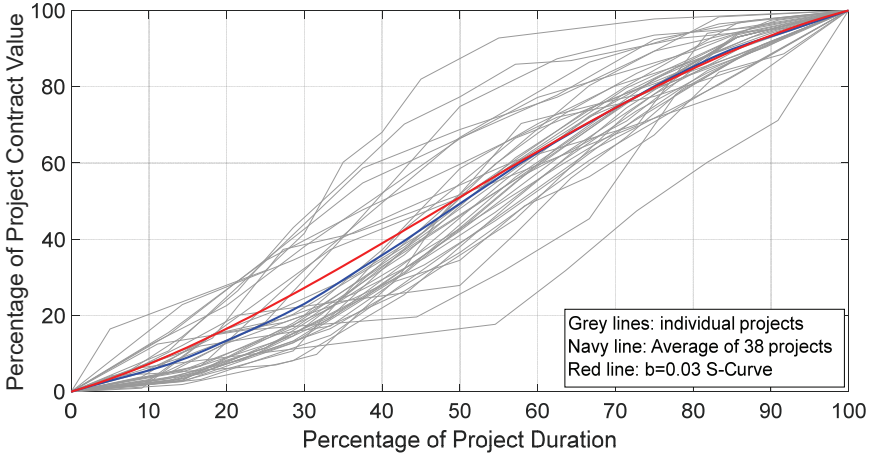
Figure 6 - Comparison of the b=0.03 S-Curve with data from projects realized in Turkey

The project progress curve or the recovery curve will be the summation of the n number of sub-projects necessary for full recovery. This can be mathematically represented as,

$$E(t) = \sum_1^n E_{sp_n}(t) = \sum_1^n \frac{C_{sp_n}}{1 + a_n e^{-b_n t}} \tag{2}$$

As shown in the equation, each sub-project will have different values for variables a, b and C_{sp} signified by subscript n. Furthermore, each sub-project will have a different start time and duration that will be reflected by variable for time, t.

For the simulation purposes, the sub-project costs C_{sp_n} can be randomly determined using an appropriate distribution function. Similarly, one can determine the start time and the duration of each sub-project randomly. Subsequently the function $E(t)$ can be evaluated using $a=1$ and $b=0.03$ (as determined earlier), which then can be shifted to the interval between t to t + sub-project duration.

The achieved functionality rate of each sub-project will not be the same also. Based on their contracts, while in some projects the commissioning of the project is at the end of the project duration, in some projects partial handovers to the owner can take place during the course of the project. Hence, the expenditure curve obtained by Eq. 2 will not be the same as the progress of functionality. This can be achieved by multiplying Eq. 1 of each sub-project by a function, such as an exponential function of the following form,

$$H(t) = e^{st} \tag{3}$$

where, s is a constant that determines the rate of increase, in turn the shape of the curve. t is time as before. The handover curves for $s=0.05$ and $s=1.0$ is shown in Figure 7. The $s=1.0$ curve can be considered for the handover at the end of the project as in the case of single buildings. Similarly, $s=0.05$ curve can be considered as the gradual handover almost from the start. The rate in the analysis will be selected between these values randomly.
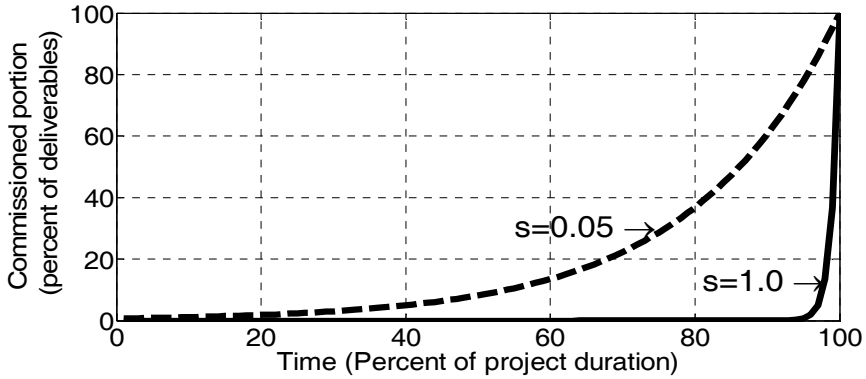
Figure 7 - Handover function

Now, we can write the functionality equation for each sub-project as,

$$F_{sp_n}(t) = E_{sp_n}(t) * H_{sp_n}(t) \tag{4a}$$

or for the entire recovery process as,

$$F(t) = \sum_1^n E_{sp_n}(t) * H_{sp_n}(t) = \sum_1^n \frac{C_{sp_n}}{1+a_n e^{-b_n t}} * e^{s_n t} \tag{4b}$$

As noted above, Weibull distribution is used to determine distribution of the variables in this case. Weibull distribution is a flexible distribution model that can be characterized by two parameters, namely shape and scale factors, to display different probability distribution functions (Figure 8). When the shape factors approaches to 1.0, the probability density curve takes the form of an exponentially decaying curve. While on the other when the shape factor is greater than 1.0, the probability density function will be approaching towards a normal distribution with the mean depending upon the scale factor.

Rules about the ranges of the variables should also be set so that they reasonably replicate the real life cases. Thus, it is essential to observe the following limiting conditions regarding the sub-project S-curves,

- The total value of the sub-projects cannot exceed the total expenditure for recovery as given in Eq. 2

- The duration of each sub-project cannot exceed the overall recovery period,

- The completion date of any sub-project cannot be after the full recovery date

- The start date of each individual sub-project cannot be earlier than the disaster date

Considering these limitations, two sample cases were evaluated assuming that 250 and 1000 sub-projects are needed for full recovery. Furthermore, for each case Weibull distribution with shape factors 1.0 and 2.0 were used to determine the sub-project cost, time of start of each sub-project and the duration of the sub-project. The resulting curves are displayed in Figure 9. Another constraint used in the analysis is that the sub-projects will have durations of 3.0-90.0% of the total recovery period. The 3% duration will correspond to approximately 1-2 months for recovery periods 3-5 years, which is a reasonable period when repair projects are considered.
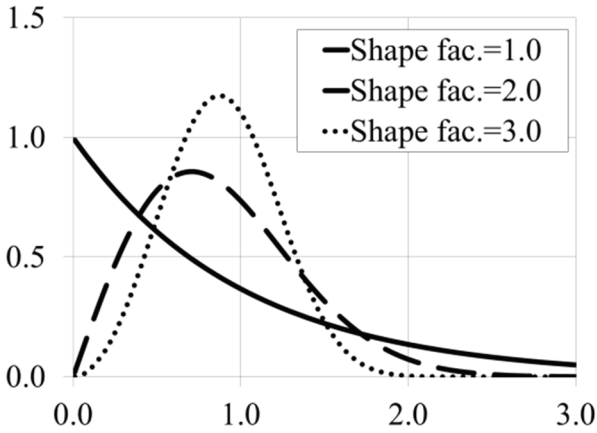
Figure 8 - Probability density curves for Weibull distribution (Scale factor =1.0)
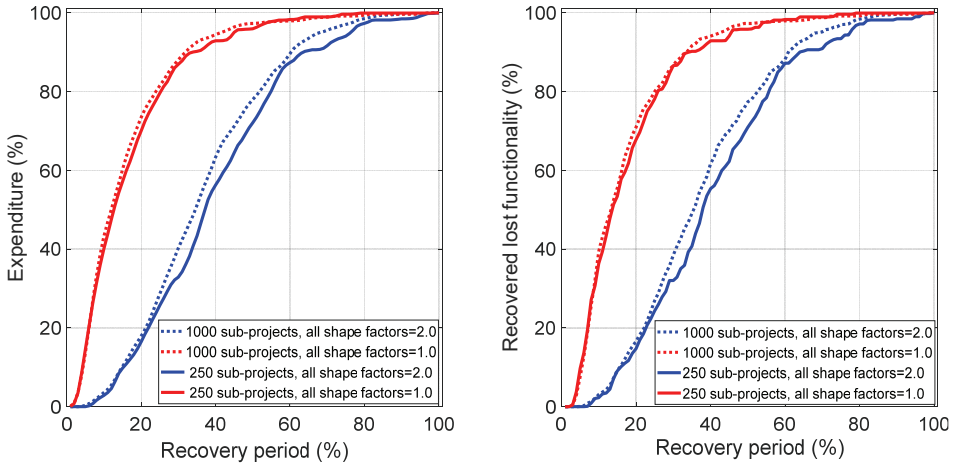
Figure 9 - Expenditure (left pane) and recovered lost functionality (right pane) curves

3. MONTE CARLO SIMULATION AND DISCUSSION OF RESULTS

A Monte Carlo simulation study is conducted to observe the behavior of the recovery curve proposed by Eq. 4 with respect to the variations in the distribution of cost, duration and the start time of the sub-projects. Monte Carlo simulation is a computer based mathematical technique. It allows the user to account for the variability of the factors in the process. Hence, the process involves a variation analysis by constructing models of possible results through the substitution of a range of values for any variable or factor that has inherent uncertainty. Afterwards, each time using a different set of random values from the probability functions results are calculated for a large number of times.

Table 1 - Case combinations considering Weibull shape factors for cost, duration and start time of the sub-projects

Case id	Weibull shape factor		
	Sub-project cost	Sub-project Duration	Sub-project start time
111	1.0	1.0	1.0
112	1.0	1.0	2.0
122	1.0	2.0	2.0
222	2.0	2.0	2.0
221	2.0	2.0	1.0
211	2.0	1.0	1.0
212	2.0	1.0	2.0
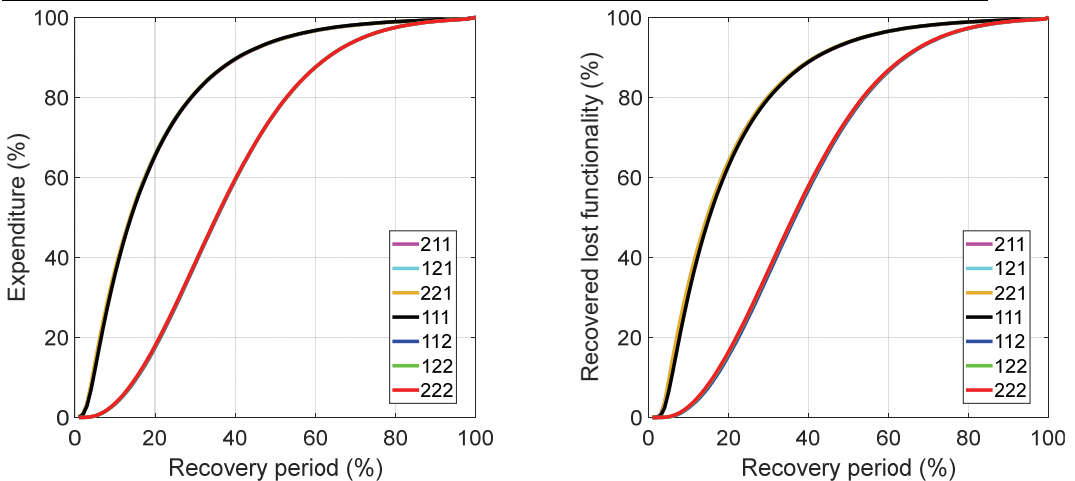
Figure 10 - Progress (left pane) and Functionality (right pane) curves (scale factor for sub-project duration taken as 1.0)
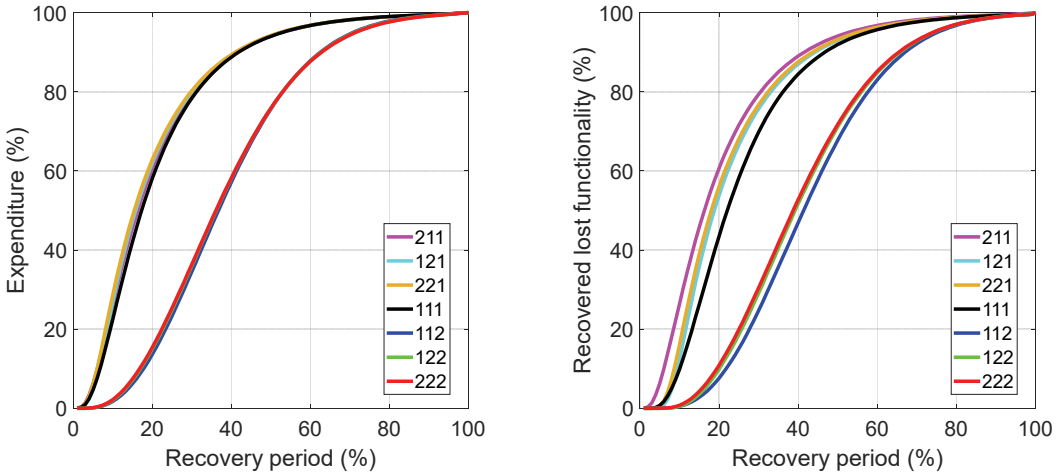
Figure 11 - Progress (left pane) and Functionality (right pane) curves (scale factor for sub-project duration taken as 5.0)

For the selection of the sub-project monetary sizes, two different random distribution schemes by varying the shape factors were employed. The combinations based on these parameters are determined and tabulated (Table 1). On the other hand, the shape factor was only varied for the sub-project duration, namely by using 1.0 in the first analysis set and by using 5.0 in the second set. For all cases, the simulations were made for 2500 trials and the mean curves calculated for the two different shape factors of the sub-project duration (Figures 10 and 11).

The observations and findings from the results of the simulations can be summarized as follows,

- All fourteen simulation cases, utilization of different statistical distributions of sub-project values yielded very similar shaped average recovered functionality curves with respect to the recovery period. They all yielded S-shaped curves, as would be expected. Earlier results, either analytically derived or recorded from actual case studies, reported in a number of valuable studies support this trend of the recovery period (e.g. Ouyang and Wang, 2015; Zobel, 2013; Porter, 2016) [18,19,20]. However, a variation in the spread of curves exists.

- The curves seem to accumulate in two groups regardless the scale factor (Figures 10 and 11). The common factor in each group is the shape factor of the sub-project value. The group with the shape factor=1.0 for the subproject values displays a faster recovery curve as compared to the other group with shape factor=2.0 for the sub-project values. The shape factor of the sub-project duration and the start time seem not to have a significant effect on the outcome. This is indeed reasonable and an expected outcome. Because shape factor=1.0 for the sub-project values reflect that majority of the sub-projects will have relatively low budget activities, i.e. repair or small projects. Whereas the shape

factor=2.0 can be deemed to represent less number of repair works and higher number higher budget sub-projects.

- Furthermore, to investigate the possible impact of number of sub-projects two additional simulations were made using 25 and 500 sub-projects for the cases 111 and 222 with shape factor=2.0. Both the expenditure and the recovered lost functionality curves had coincided with the previous simulations with 250 sub-projects.

- The build-up of recovery of lost functionality curve starts slowly and grows faster in the later stages. It is important to note that the generic recovery curve includes the impact of the sub-projects only and excludes the preparatory works, such as planning and contracting works. In that respect, it should be expected that the initial slow period will be extended accordingly. However, this extension will be closely related to the preparedness of the community to deal with the processes after the disaster.

- Towards the end of the recovery period, the curves display a slower progress. That is basically due to the commissioning and handover processes of the sub-projects. In this respect, it can be hypothesized that at the curvature point, around 90-95% recovery, "substantial recovery" is achieved.

- Hence, the S-curves can be split into three parts considering the curvature points, concave and convex of these curves. The three parts can be identified as the initial period, the main recovery period and the substantial recovery period.

- Assuming that at the substantial recovery period stage, the community has returned back to almost full functionality, the main governing factors of the recovery curve are the duration of the initial period and the slope of the main recovery period. Based on the findings above, both the length of the initial period and the main recovery period will be mainly governed by the monetary sizes of the sub-projects. Hence, for instance at places where the risk of a major earthquake exists, it will be appropriate to strengthen first the structures within the modal monetary value group of the risky stock in the built environment. Such a strategy will increase the resilience of the community and shorten the overall recovery period.

4. CONCLUSION

In this study, the recovery curve of a community, in the aftermath of a destructive event such as a major earthquake is evaluated through mathematical modelling. The mathematical model used is based on the project S-curve concept that is widely accepted and widely utilized in the project management community, especially in the construction industry.

Results of Monte Carlo simulation demonstrate that the recovery process exhibits an S-shape, the duration of initial portion and the slope of the bulk portion being significantly governed by the level of preparedness of the community. Namely, the higher the level of preparedness, the shorter will be the recovery process. Hence, a viable strategy in increasing the pace of the recovery, namely resilience, to be considered would be the strengthening of the group of structures (including infrastructure) that are in the modal monetary value group among the risky sub-projects. Thus, by reducing the damage of these structures in the event of a major disaster, the recovery process can be significantly expedited. Furthermore, the recovery of the community will start earlier as compared to less prepared cases.

Symbols

a, b	= constants
C_{sp}	= Total expenditure (cost) for the sub-project
E(t)	= Expenditure function of project
$E_{sp}(t)$	= Expenditure function of sub-project
F_d	= Remaining functionality following disaster
H(t)	= Handover function of sub-project
R	= lost resilience
s	= a constant that determines the rate of increase
t	= Time
t_0	= Event date
t_r	= Date total recovery achieved
t_t	= Total duration of recovery

Acknowledgements

References

[1] Bruneau, M., Chang, S., Eguchi, R. Lee, G., O'Rourke, T., Reinhorn, A., Shinozuka,M., Tierney, K., Wallace, W., von Winterfelt, D., (2003). "A framework to Quantitatively Assess and Enhance the Seismic Resilience of Communities", *EERI Spectra Journal*, 19, (4), 733-752

[2] Cimellaro, G.P., Reinhorn, A.M., Bruneau, M. (2010a) "Seismic resilience of a hospital system" *Structure and Infrastructure Engineering*, Vol. 6, Nos. 1–2, February–April 2010, 127–144

[3] Cimellaro, G.P., Reinhorn, A.M., Bruneau, M. (2010b) "Framework for analytical quantification of disaster resilience" Engineering Structures 32 (2010) 3639–3649

[4] Cimellaro, G.P. (2016) "Urban Resilience for Emergency Response and Recovery Fundamental Concepts and Applications" Springer International Publishing Switzerland

[5] Güler, H.G, Sözdinler, C.Ö., Arikawa, T., Yalçıner, A.C. (2018) "Tsunami AfetiSonrasıYapısalveYapısalOlmayanÖnlemlerveFarkındalıkÇalışmaları: JaponyaÖrneği", *TeknikDergi*, 8605-8629

[6] Şengöz, A., Sucuoğlu, H., (2009) "2007 Deprem Yönetmeliğinde Yer Alan "Mevcut Binaların Değerlendirilmesi" Yöntemlerinin Artıları ve Eksileri", *Teknik Dergi*, 4609-4633

[7] Yanmaz, Ö., Luş, H., (2005) "Yapı Güçlendirme Yöntemlerinin Fayda-Maliyet Analizi", *Teknik Dergi*, 3497-3522

[8] Cimellaro, G.P., Reinhorn, A.M., Bruneau, M. (2006) "Quantification of Seismic Resilience", Proceedings of the 8th U.S. National Conference on Earthquake Engineering, April 18-22, San Francisco, California, USA

[9] Kenley, R. (2005), *Financing Construction – Cash Flows and Cash Farming,* Taylor and Francis e-Library, ISBN 0-203-46739-6.

[10] Hudson, K. W. and Maunick, J. (1974). Capital expenditure forecasting on health building schemes, or a proposed method of expenditure forecast. Research report, Surveying Division, Research Section, Department of Health and Social Security, UK.

[11] Hudson, K. W. and Maunick, J. (1974). Capital expenditure forecasting on health building schemes, or a proposed method of expenditure forecast. Research report,

[12] Peer, S. (1982). 'Application of cost-flow forecasting models'. *Journal of the Construction Division*, ASCE, Proc. Paper 17128, 108(CO2): 226–32.

[13] Kenley, R., and Wilson, O. D. (1986) "A construction project cash flow model-An idiographic approach." *Construction Management and Economics*, 4(3), 213–232.

[14] Miskawi, Z. (1989) "An S-curve equation for project control." *Construction Management and Economics*, 7(2), 115–124.

[15] Khosrowshahi, F. (1991) 'Simulation of expenditure patterns of construction projects *Construction Management and Economics* 9(2): 113–132.

[16] Boussabaine, A. H. and Elhag, T. (1999). 'Applying fuzzy techniques to cash flow analysis'. *Construction Management and Economics* 17: 745–755.

[17] Hudson, K. W. (1978). 'DHSS expenditure forecasting method'. *Chartered Surveyor—Building and Quantity Surveying Quarterly* 5: 42–45.

[18] Ouyang, M., Wang, Z. (2015) "Resilience assessment of interdependent infrastructure systems: With a focus on joint restoration modeling and analysis", *Reliability Engineering and System Safety*, 141(2015)74–82, doi.org/10.1016/j.ress.2015.03.011

[19] Zobel, C.W., (2013) "Analytically comparing disaster recovery following the 2012 derecho", *Proceedings of the 10th International ISCRAM Conference – Baden-Baden, Germany, May 2013 T. Comes, F. Fiedrich, S. Fortier, J. Geldermann and T. Müller, eds.*

[20] Porter, K. (2016) "Damage and Restoration of Water Supply Systems in an Earthquake Sequence", *Structural Engineering and Structural Mechanics Program, Department of Civil Environmental and Architectural Engineering, University of Colorado*, SESM 16-02, July 2016.

Modeling Pavement Performance Using LTPP Database for Flexible Pavements

Mostafa M. RADWAN[1]
Mostafa A. ABO-HASHEMA[2]
Moatafa D. HASHEM[3]
Hamdy B. FAHEEM[4]

ABSTRACT

In many countries, incredible investments have been made in constructing roads that require conducting periodic evaluation and timely maintenance and rehabilitation (M&R) plan to keep the network operating under acceptable level of service. The timely M&R plan necessitates accurately predicting pavement performance, which is an essential element of road infrastructure asset management systems or Pavement Management Systems (PMS). Consequently, there is always a need to develop and to update performance prediction models embedded in PMS applications. This study focuses on developing distress prediction models for flexible pavements located in non-freeze climatic zone, which represent most of the Middle East countries using data extracted from the Long-Term Pavement Performance (LTPP) program. Six distress performance prediction models were developed in this study for both wet- and dry-non-freeze climatic zones, which are Fatigue (Alligator) cracking, longitudinal cracking, transverse cracking, raveling, bleeding, and rut depth models. These models can play an important role assisting decision makers in predicting pavement performance, identifying M&R needs, rational budget planning and resource allocation.

Keywords: Prediction models, distress models, ltpp, statistical modeling, flexible pavement, non-freeze climatic zone.

---

1 Nahda University, Faculty of Engineering, Beni Suef, Egypt - mostafa.yaseen@nub.edu.eg
  https://orcid.org/0000-0002-6246-1609
2 Fayoum University, Faculty of Engineering, Fayoum, Egypt - maa03@fayoum.edu.eg
  https://orcid.org/0000-0002-8301-0946
3 Minia University, Faculty of Engineering, Minia, Egypt - mostafa.deeb@mu.edu.eg
  https://orcid.org/0000-0001-8564-5550
4 Minia University, Faculty of Engineering, Minia, Egypt - hamdyfaheem@mu.edu.eg
  https://orcid.org/0000-0002-9841-6519

1. INTRODUCTION

Road network represents the powerful engine of economy to all countries, which requires conducting periodic evaluation and timely maintenance and rehabilitation (M&R) plan to keep the network operating under acceptable level of service [1, 2]. The timely M&R plan necessitates accurately predicting pavement performance, which is a key element of road Pavement Management Systems (PMS). The performance models calculate the future conditions of pavement based on which PMS optimizes several M&R treatments and estimates the consequences of maintenance operations on the future pavement condition during the life-span of the pavement [3, 4]. At the network level, pavement performance prediction is needed for programming M&R activities, while at the project level it is needed for determining the most appropriate M&R actions to be taken for a specific project, such as preventive maintenance, rehabilitation, or reconstruction [5, 6].

Consequently, there is always a need to develop and to update performance prediction models embedded in PMS applications. Early PMSs did not have pavement performance curves rather they evaluated only the current pavement condition. Later, the simplified pavement performance curves were introduced based on the engineering opinions on the expected design life of different M&R actions [7]. The only predictive variable of these performance curves was the pavement age. The development of pavement performance is explicitly complicated as the pavement performance is subjected to a large number of parameters of pavement performance. There are two streams of pavement performance modeling, which are deterministic and stochastic approaches. The major differences between deterministic and stochastic performance prediction models are model development concepts, modeling processor formulation, and output format of the models [8].

There are different types of deterministic models, such as mechanistic models, mechanistic-empirical models, and regression models. The mechanistic models draw the relationship between response parameters such as stress, strain, and deflection [8]. The mechanistic-empirical models are often developed in connection to design systems and therefore have not been widely applied in PMS but have the potential to be applied at a network level. On the other hand, the regression models draw the relationship between a performance parameter (e.g., pavement distresses) and the predictive parameters (e.g., pavement thickness, pavement material properties, traffic loading, and age) [8, 9].

This study focuses on developing regression models through deterministic approach to predict pavement performance. These prediction models allow highway authorities to predict the pavement performance and consequently identifying the M&R timely activities. Several performance prediction models have been introduced over the years, some of which are simple and others are quite complex. Many of these models are developed for application in a particular region or country under specific traffic and climatic conditions; hence, they cannot be directly applied in other countries or conditions. Therefore, this study comes to target specific climate condition. Table 1 shows selected published pavement distress models.

Hence, this study comes to develop pavement distress prediction models for roads located in wet- and dry-non-freeze climatic zones, which represent most of the Middle East countries using data extracted from the Long-Term Pavement Performance (LTPP) program. Therefore, the developed models can be utilized in the Middle East region experiencing the same climatic condition. This study is considered as a crucial attempt to develop such models

for the Middle East region due to lack of resources led to unavailability of such models in most of the Middle East countries. However, calibration of the developed models is recommended using local pavement performance data, whenever performance data is available.

Table 1 - Selected Pavement Distress Prediction Models

Model Formula	Abbreviations	Reference
$RD = \sum_{i=1}^{Nsublayers} \varepsilon_p^i h_i$	RD = Rut Depth, mm ε_p^i = plastic strain h_i = layer thickness, mm	ARA, 2004 [10]
Ln RD $_{dry}$ = 0.681 + 0.114 (Ln KESAL) + 0.007 (D > 32 C°)	KESAL = Standard Traffic Axle loads, thousands D> 32 C° = Number of days maximum temperature > 32 C°	Naiel, 2010 [6]
Ln RD $_{wet}$= 0.9 + 0.19 (AC %) - 0.077 (SN) +0.063 (Ln KESAL)	RD = Rut Depth, mm SN = Structural Number KESAL = No. of Standard Traffic Axle loads	Naiel, 2010 [6]
$N_{100}^{rut} = \frac{1}{0.9533 \times rut^{-0.0209}} \times (\frac{rut}{a})^{\frac{1}{b}}$	Nrut$_{100}$ = the average annual ESALs per lane rut = the total rutting on the surface used to define failure, mm. a , b = parameters estimated from FWD test as the surface curvature index SCI300 in [μm] measured during the fall (autumn), first time after the pavement structure is built.	Göransson and Den Svenska, 2009 [11]
Nf = 0.00432 xβf1 xC $x(\frac{1}{\varepsilon_t})^{3.291 \times \beta f2} (\frac{1}{E})^{0.854 \times \beta f3}$	Nf = the maximum allowable number of repetitions βf1, βf2, βf3 = calibration factors C = laboratory to field adjustment factor ε_t = critical tensile strain E = the stiffness of the AC surface layer	AI, 1982 [12]
% Fatigue cracking = $\frac{0.021}{0.027 + e^{(-0.851 \times Df)}}$	FC = fatigue cracking in percent of entire lane area, (%). Df = cumulative fatigue damage	Ali and Tayabii, 1989 [13]
(FC)wet = exp(-6.539 + 0.078 x age + 0.00187 x KESAL + 0.000673 x precip + 0.0914 x temp + 15097 x epsilon.t + 0.0272 x ft)	FC = fatigue cracking in percent of entire lane area, (%) age = pavement age, years. KESAL = the yearly ESALs, thousands. precip = mean annual precipitation, mm. temp = mean annual temperature, °C epsilon.t = the critical tensile strain. ft = yearly freeze-thaw cycle	Ker et al., 2007 [14]

Table 1 - Selected Pavement Distress Prediction Models (continue)

Model Formula	Abbreviations	Reference
(FC)dry=exp(-48.411 + 0.119 age + 0.025 x precip + 1.774 x temp + 2729 x epsilon.t + 0.0272 x ft)	FC = fatigue cracking in percent of entire lane area, (%) epsilon.t = the critical tensile strain. ft = yearly freeze-thaw cycle	Ker et al., 2007 [14]
(FC)freeze = exp(-5.944 + 0.00583 x precip + 41.768 x epsilon.t - 0.002 x visco + 0.4 x trange)	Visco = viscosity of the AC layer, p. trange = the difference of maximum and minimum mean annual temperature, ºC	Ker et al., 2007 [14]
(FC)nonfreeze = exp(-7.87 + 0.102 x age + 0.00219 x KESAL + 0.00102 x precip + 0.0472 x temp + 15172 x epsilon.t + 0.0476 x ft)	FC = fatigue cracking in percent of entire lane area, (%) epsilon.t = the critical tensile strain. ft = yearly freeze-thaw cycle	Ker et al., 2007 [14]

Such models would help highway authorities, located in non-freeze climatic zones, to precisely predict pavement performance and hence using these predictions in identifying the M&R activities. Based on the data available in the LTPP, six distress prediction models were developed in this study, for both wet- and dry-non-freeze climatic zones, as follows:

– Fatigue Cracking model
– Longitudinal Cracking model
– Transverse Cracking model
– Raveling model
– Bleeding model
– Rut depth model

The precision and accuracy of the distress prediction models are affected by the type of the mathematical model. Therefore, a comprehensive statistical analysis should be performed to get a model with high accuracy. A stepwise regression analysis was conducted to come up with the most effective factors that could affect such models. Consequently, a Statistical Package for Social Science (SPSS) program was used to develop such models. To check the reliability of the model, some measures of the statistical accuracy are used as follows [15, 16]:

- The Standard Error (SE), which is a measure of the statistical accuracy of an estimate,
- The coefficient of determination (R^2), which is defined as the proportion of the variance in the dependent variable that is predictable from the independent variable(s).

In statistics, normality tests are used to determine if a data set is well-modeled by a normal distribution and to compute how likely it is for a random variable underlying the data set to be normally distributed. If the data is normally distributed, analysis of variance (ANOVA) test is used. However, Kruskal-Wallis or Mann-Whitney tests is used for non-normal data.

2. BACKGROUND OF LTPP

The Long-Term Pavement Performance program (LTPP) is the largest pavement performance research program ever undertaken, gathering data from more than 2,000 pavement test sections over a 20-year test period. The single most significant product of the LTPP program is the pavement database - the largest and most comprehensive collection of research-quality performance data on in-service highway pavements ever assembled.

The Long-Term Pavement Performance program is one of the significant research regions of the Strategic Highway Research Program (SHRP). The initial five years of the LTPP program were finished under the subsidizing and course of SHRP. Since 1991, the Federal Highway Administration (FHWA) has proceeded with the administration and subsidizing of the program. The LTPP program is overseen by the LTPP Team under the Office of Infrastructure Research and Development [17, 18, 19].

The LTPP program has two complementary experiments to meet the objectives. First, the General Pavement Studies (GPS) use existing pavements as originally constructed or after the first overlay and focus on the most commonly used structural designs for pavement. The second set of LTPP experiments is the Specific Pavement Studies (SPS) whose test sections allow critical design factors to be controlled and performance to be monitored from the initial date of construction. The results will provide a better understanding of how selected maintenance, rehabilitation, and design factors affect pavement performance. The consolidated GPS and SPS programs comprise of more than 2,500 test segments situated on all through North America built in four climate zones: wet-non-freeze, dry-non-freeze, wet-freeze, and dry-freeze. The LTPP program screens and gathers asphalt execution information on every single dynamic site. The gathered information incorporates data on seven modules: Inventory, Maintenance, Monitoring (Deflection, Distress, and Profile), Rehabilitation, Materials Testing, Traffic, and Climatic. The LTPP Information Management System (IMS) is the focal database where every one of the information gathered under the LTPP program are put away. This database is persistently being produced as more information is gathered and handled [17, 18].

3. OBJECTIVE AND METHODOLOGY

The main objective of this study is to develop pavement distress prediction models for flexible pavements located in wet- and dry-non-freeze climatic zones, which represent most of the Middle East countries using LTPP database. This study focuses on developing such models for the Middle East countries experiencing wet- and dry-non-freeze climatic zones, to be used in their PMS; while calibration of the developed models is recommended based on local condition of a country whenever the pavement performance data is available.

Therefore, four main steps were conducted to achieve the objective of this study. Data collection and preparation using LTPP database was the first main step. The second step was statistical analysis that came to play the role of judgment on all possible factors that could affect developing such models as well as their significance. Developing and optimizing the pavement distress prediction models using SPSS software were the third step. The validation process was the last essential step.

4. DATA COLLECTION AND PREPARATION

The LTPP dataset was the main source of data in this study, which includes data until year 2016. Therefore, LTPP sites, located in wet- and dry-non-freeze climatic zones, were selected to obtain the required data according to specific criteria as follows:

–   Sites located in wet- and dry-non-freeze climatic zones.

–   Only overlaid sections were chosen to simulate newly constructed pavement.

–   Rural sections were selected to represent main roads.

–   Design period or data range was selected for 25 years, starting from 1991.

Accordingly, 43 and 57 LTPP sites were selected for wet- and dry-non-freeze climatic zones, respectively. Data collection step was then started. There are numerous factors related to the occurrence of the pavement problems. However, this study selected some factors that are considered as the most important factors related to pavement problems especially for fatigue cracking, longitudinal cracking, transverse cracking, raveling distress, bleeding distress, and rutting distress. These factors are summarized as follows:

–   Air temperature (Ta), ºC

–   Pavement age since overlay (PA), years

–   Traffic loading represented by Equivalent Single Axle Load (ESAL), No. of Axles

–   Annual Precipitation, mm

–   Available pavement distresses, area (sq.m.) or length (m)

–   Asphalt pavement thickness (T), mm

–   Material characteristics:

    –   Resilient modulus of subgrade soil (Mr), MPa

    –   % Passing the #200 sieve (0.075 mm) of subgrade soil (P_{200}),

    –   % Air voids of asphalt mix (V_a),

    –   % Asphalt content in the mix (P_b)

    –   % Moisture content of base/subbase courses (MC_b),

    –   % Moisture content of subgrade soil (MC_S), and

    –   Plasticity index of subgrade soil (PI)

All data were collected on different dates during the 25-year data range. The collected data have been filtered through a screening process to come up with feasible data that could be used to develop the required models. The criteria for screening process are selected as follows:

1.   Unavailability and/or insufficient of some distresses data

2.   Absence of material characteristics data

3.   Abnormal data patterns, e.g. distress density should be increased with time not decreased.

Table 2 - Selected Non-Freeze LTPP Sites

Site ID	State	Site ID	State
Wet-Non-Freeze Climatic Zone			
12-3997	Florida (FL)	28-2807	Mississippi (MS)
12-3996	**Florida (FL)**	28-3081	Mississippi (MS)
12-4106	Florida (FL)	37-1024	North Carolina (NC)
12-4107	Florida (FL)	37-1030	North Carolina (NC)
12-4108	**Florida (FL)**	37-1802	North Carolina (NC)
12-4097	Florida (FL)	40-1017	Oklahoma (OK)
12-9054	Florida (FL)	40-4163	Oklahoma (OK)
13-4096	Georgia (GA)	40-4087	Oklahoma (OK)
13-4112	Georgia (GA)	40-4161	Oklahoma (OK)
13-4113	Georgia (GA)	40-4165	Oklahoma (OK)
13-4111	**Georgia (GA)**	45-1025	South Carolina (SC)
13-4420	Georgia (GA)	5-3048	Arkansas
1-1021	Alabama (AL)	**48-3729**	**Texas (TX)**
1-4126	Alabama (AL)	**48-1113**	**Texas (TX)**
1-4129	Alabama (AL)	**48-1116**	**Texas (TX)**
1-1001	Alabama (AL)	**48-1093**	**Texas (TX)**
1-1019	Alabama (AL)	48-1068	Texas (TX)
24-1632	**Maryland (MD)**	48-1060	Texas (TX)
28-1001	Mississippi (MS)	48-3609	Texas (TX)
28-3028	Mississippi (MS)	**51-1023**	**Virginia (VA)**
28-3091	**Mississippi (MS)**	51-2021	Virginia (VA)
Dry-Non-Freeze Climatic Zone			
4-1002	Arizona (AZ)	**35-0108**	**New Mexico (NM)**
4-1003	Arizona (AZ)	35-0103	New Mexico (NM)
4-1006	Arizona (AZ)	**35-0104**	**New Mexico (NM)**
4-1007	Arizona (AZ)	35-0106	New Mexico (NM)
4-1015	Arizona (AZ)	35-0105	New Mexico (NM)
4-1017	Arizona (AZ)	**35-1112**	**New Mexico (NM)**
4-1021	Arizona (AZ)	35-0107	New Mexico (NM)
4-1024	Arizona (AZ)	35-0109	New Mexico (NM)
4-1025	Arizona (AZ)	35-0110	New Mexico (NM)
4-0113	**Arizona (AZ)**	35-0112	New Mexico (NM)
4-1062	Arizona (AZ)	**35-0101**	**New Mexico (NM)**
4-0160	Arizona (AZ)	48-1111	Texas (TX)
4-1065	Arizona (AZ)	48-1061	Texas (TX)
4-6055	Arizona (AZ)	48-1076	Texas (TX)
6-8151	California (CA)	48-3769	Texas (TX)
6-2004	California (CA)	48-6060	Texas (TX)
35-0101	New Mexico (NM)	**48-1048**	**Texas (TX)**

Sites to be selected for validation process

Consequently, 42 LTPP sites out of 43 were selected for wet-non-freeze climatic zone; and 34 LTPP sites out of 57 were selected for dry-non-freeze climatic zone, as shown in Table 2. Furthermore, fatigue cracking, longitudinal cracking, transverse cracking, raveling distress, bleeding distress, and rutting distress were selected for model development. The unit of distress data recorded in the LTPP database is based on the distress types. The unit of area is accounted for fatigue, raveling, and bleeding; on the other hand, the unit of length or depth is accounted for longitudinal, transverse, and rutting distress. In addition to the collected distress data, distress density was calculated by dividing the length or area of distress by the area of examined section based on the PAVER system [20].

Comprehensive database was then created to be used for model development and validation process. The database was split into two categories of dataset. The first category is for model development, which represents 79% of all databases, and the second category is for validation process, which represents 21% of all database, as shown in Table 2. The validation data of 21% is considered reasonable statistically and the validation sites were selected to represent most of the original data and most of the sites. It is noteworthy that the developed models should not be exposed to the validation dataset while developing the models.

5. DEVELOPMENT OF PAVEMENT DISTRESS PREDICTION MODELS

This part deals with the process of developing fatigue cracking, longitudinal cracking, transverse cracking, raveling distress, bleeding distress, and rutting distress models. Since ESAL is a function of time or age, either ESAL or age would be selected as independent variable in the developed models. Sample of collected data is shown in Table 3 and Table 4 for wet- and dry-non-freeze climatic zones, respectively, for different LTPP sites shown in Table 2.

Table 3 - Sample of Collected Data using Wet-Non-Freeze LTPP Sites for Different LTPP Sites

%Density	T_a, C^o	PA, Years	M_r, MPa	P_{200} (%)	%V_a	%MC_b	%MC_s	PI
Fatigue Cracking Model								
0	24.30	4	114	-	-	4	7	-
6.67	19.40	14	73	3.50	-	4	7	2
16.67	21.90	16.16	65	9.40	-	3	15	-
Longitudinal Cracking Model								
0	24.29	4	114	-	-	4	7	-
0.05	19.29	5.83	124	30.7	-	9	10	-
17.0	18	6.42	95	-	-	-	-	-
Transverse Cracking Model								
0	20.00	0.18	-	-	-	15	-	8
0.7624	16.40	4.52	-	83.00	-	15	4	6
7.8756	20.30	7.02	25	15.60	-	14	-	-

Table 3 - Sample of Collected Data using Wet-Non-Freeze LTPP Sites for Different LTPP Sites (continue)

%Density	Ta, C°	PA, Years	Mr, MPa	P$_{200}$ (%)	%Va	%MC$_b$	%MC$_s$	PI
Raveling Model								
0	13.50	0.12	20	25.40	4.593	4	18	12
12.5041	19.40	4.7	73	3.50	6.993	4	7	2
36.9383	24.30	13	-	-	-	-	5	-

Rutting Model

Rut Depth mm	Ta, C°	PA, Years	ESAL	Annual Precipitation, mm	%Va
6	15.89	5.92	711	1778.5	7.091
8	16.89	15.3	59	1679.30	5.823
10	15.60	12	40	1290.30	7.09
15	19.79	9.66	106	1418.59	3.993

Table 4 - Sample of Collected Data using Dry-Non-Freeze LTPP Sites for Different LTPP Sites

%Density	Ta, C°	PA, Years	Mr, MPa	P$_{200}$ (%)	%Va	T, mm	%MC$_b$	%MC$_s$	PI
Fatigue Cracking Model									
11.8	17.6	15.5	87	-	-	221	5	11	30
36.67	19.1	15.58	37	-	-	53.3	3	7	0
37.7	18.5	17.41	114	-	-	63.5	2	9	9
Longitudinal Cracking Model									
2.84	-	15.5	88.6	29.5	-	-	5	-	30
6.45	-	16	72.3	23.6	-	-	2	-	0
8.17	-	17.1	64.4	22.8	-	-	-	-	-
Transverse Cracking Model									
0	-	0	5794	51	-	-	2	-	0
2.84	-	15.5	88.6	29.5	-	-	5	-	30
4.18	-	18.09	101.8	28.5	-	-	5	-	0
Bleeding Model									
0	-	1.2	45	24.9	1.87	-	3	-	6
7.21	-	8.21	105.5	28.5	3.62	-	2	-	0
27.37	-	12.58	75	9.6	12	-	1	-	-

Rutting Model

Rut Depth mm	Ta, C°	PA, Years	ESAL	Annual Precipitation, mm	%Va
4	16.10	8.416	12	294.6	6.12
5	17.70	15.5	4	343.4	6.12
7	23.10	16.58	768	41	16.3
11	22.70	18.25	925	121.9	16.3

5.1. Stepwise Regression Test

Stepwise regression test was performed within 95% confidence interval to come up with the most effective factors that could affect fatigue cracking, longitudinal cracking, transverse cracking, raveling distress, bleeding distress, and rutting distress. The decision would be made based on p-value for all considered factors. A small p-value (typically ≤ 0.05) indicates strong evidence against the null hypothesis, so the null hypothesis is rejected. A large p-value (> 0.05) indicates weak evidence against the null hypothesis, so fail to reject the null hypothesis [21]. Table 5 and Table 6 depict the results of p-value of the considered factors for wet- and dry-non-freeze climatic zones, respectively.

Table 5 - P-value using Wet-Non-Freeze LTPP Sites

	Fatigue Cracking	Longitudinal Cracking	Transverse Cracking	Raveling Distress	Rut Depth
Ta	0.54337	0.42071	0.97183	0.27308	0.46982
PA	**0.01447**	0.89778	0.52564	**0.03860**	nil
ESAL	nil	nil	nil	nil	**0.02762**
Mr	0.66094	**0.03473**	0.49485	0.88260	0.79112
P_{200}	0.66620	0.14896	0.95062	0.30984	-
Va	0.87726	0.14831	nil	**0.01427**	**0.05558**
T	0.98640	0.28561	nil	nil	0.90004
MC_b	0.79172	**0.00194**	**0.03165**	0.66059	nil
MC_S	**0.00960**	0.61107	0.10406	0.24776	nil
PI	0.57023	0.26024	**0.04055**	0.12184	nil
P_b	nil	nil	nil	nil	nil

nil means that this factor is not considered in testing

As shown in Table 5, fatigue cracking model is affected by pavement age and moisture content of subgrade soil for wet-non-freeze climatic zone. On the other hand, pavement age, air temperature, and plasticity index of subgrade soil are the factors that affect fatigue cracking model for dry-non-freeze climatic zone, as shown in Table 6. It could be concluded that moisture condition-related factors of subgrade soil affect the occurrence of fatigue cracking.

On the other hand, longitudinal cracking model is affected by resilient modulus of subgrade soil and moisture content of base/subbase courses for wet-non-freeze climatic zone while pavement age and % passing the #200 sieve (0.075 mm) of subgrade soil are the factors affecting longitudinal cracking model for dry-non-freeze climatic zone. It could be concluded that too much fine aggregate experiences this type of crack.

Table 6 - p-value using Dry-Non-Freeze LTPP Sites

	Fatigue Cracking	Longitudinal Cracking	Transverse Cracking	Bleeding Distress	Rut Depth
Ta	**0.00740**	nil	nil	nil	**0.00111**
PA	**0.01515**	**0.00000**	**0.00351**	**0.00003**	nil
ESAL	nil	nil	nil	nil	**0.00010**
Mr	0.43891	0.93581	0.14276	0.93685	0.14071
P_{200}	nil	**0.01896**	0.12448	0.54376	-
Va	nil	nil	nil	**0.01832**	**0.00000**
T	0.38696	nil	nil	nil	nil
MC_b	0.28823	0.66000	0.82018	0.17165	nil
MC_S	0.17819	nil	nil	nil	nil
PI	**0.01646**	0.75348	0.26137	0.22060	nil
P_b	nil	nil	nil	nil	0.53185

nil means that this factor is not considered in testing

For transverse cracking model, it is affected by moisture content of base/subbase courses and plasticity index of subgrade soil for wet-non-freeze climatic zone while pavement age is the only factor affecting transverse cracking model for dry-non-freeze climatic zone.

Raveling and bleeding distress models are affected by pavement age and % air voids of asphalt mix for wet- and dry-non-freeze climatic zones, respectively. Finally, rut depth is affected by ESAL and Va for wet-non-freeze climatic zone. On the other hand, ESAL, Ta and V_a are the factors that affect rut depth for dry-non-freeze climatic zone.

5.2. Regression Analysis

Multiple regression analysis technique was applied to develop fatigue cracking, longitudinal cracking, transverse cracking, raveling distress, bleeding distress and rut depth prediction models for wet- and dry-non-freeze climatic zones using SPSS software. Several trials were made to develop the required models that best represent the relation between the distresses with related factors. Table 7 shows regression analysis for developed models using non-freeze LTPP sites.

Table 7 - Regression Analysis for Developed Models using Non-Freeze LTPP Sites

Distress Model	Climate	Estimate	Parameters				R^2	df	Mean Squares
			A	B	C	D			
Fatigue Cracking	Wet	Value	-10.356	1.936	1.422	-	0.884	3	488.633
		SE	2.263	0.359	0.251	-			
	Dry	Value	-45.281	9.260	2.101	6.135	0.465	4	482.729
		SE	120.087	20.856	8.318	4.457			
Longitudinal Cracking	Wet	Value	14.201	-5.320	0.365	-	0.318	3	7.152
		SE	116.202	38.766	0.698	-			
	Dry	Value	24.258	22.118	-0.078	-	0.478	4	31.956
		SE	7.389	0.109	7.385	-			
Transverse Cracking	Wet	Value	-10.725	1.146	-9.164	-	0.980	3	0.072
		SE	1.851	0.188	1.873	-			
	Dry	Value	0.048	0.203	-	-	0.755	1	420.013
		SE	0.147	0.11	-	-			
Reveling Distress	Wet	Value	-2.075	-0.902	0.823	-	0.323	3	19.273
		SE	1.924	1.037	0.468	-			
Bleeding Distress	Dry	Value	4.708	1.042	1.203	-	0.820	3	1588.807
		SE	8.933	0.283	0.299	-			
Rut Depth	Wet	Value	10.097	-0.987	0.478	-	0.233	3	693.294
		SE	2.664	0.474	0.229	-			
	Dry	Value	21.338	0.009	-1.055	0.255	0.479	5	411.999
		SE	0.317	0.210	4.384	0.002			

5.2.1. Fatigue Cracking Model

Table 7 indicates that the model has R^2 value of 0.884 and 0.465 based on the obtained data from LTPP for wet- and dry-non-freeze climatic zones, respectively. Therefore, the proposed distress model of fatigue cracking could be written as follows:

Wet-non-freeze zone:

$$\%Fatigue\ Cracking = e^{(-10.356+1.936\sqrt{PA}+1.422\sqrt{MC_S})} \tag{1}$$

Dry-non-freeze zone:

$$\%Fatigue\ Cracking = e^{(-45.28+9.26\sqrt{PA}+2.1\sqrt{PI})} + 6.14\cos Ta \tag{2}$$

5.2.2. Longitudinal Cracking Model

Table 7 indicates that the model has R^2 value of 0.318 and 0.478 based on the obtained data from LTPP for wet- and dry-non-freeze climatic zones, respectively. Therefore, the proposed distress model of longitudinal cracking could be written as follows:

Wet no-freeze zone:

$$\%Longitudinal\ Cracking = e^{(-22.896-0.185\log MC_b-28.073\sqrt{Mr})} \tag{3}$$

Dry no-freeze zone:

$$\%Longitudinal\ Cracking = 24.258 + 22.118\sin\sqrt{PA} - 0.078P_{200} \tag{4}$$

5.2.3. Transverse Cracking Model

Table 7 indicates that the model has R^2 value of 0.980 and 0.755 based on the obtained data from LTPP for wet- and dry-non-freeze climatic zones, respectively. Therefore, the proposed distress model of transverse cracking could be written as follows:

Wet no-freeze zone:

$$\%Transerve\ Cracking = e^{(-10+1.146\sin PI-9.164\cos MC_b)} \tag{5}$$

Dry no-freeze zone:

$$\%Transverse\ Cracking = 0.048 + 0.203\ PA \tag{6}$$

5.2.4. Raveling Distress Model

Table 7 indicates that the model has R^2 value of 0.323 based on the obtained data from LTPP for wet-non-freeze climatic zones. Therefore, the proposed distress model of raveling distress could be written as follows:

Wet no-freeze zone:

$$\%Raveling = -2.075 - 0.902\sin PA + 0.823Va \tag{7}$$

5.2.5. Bleeding Distress Model

Table 7 indicates that the model has R^2 value of 0.820 based on the obtained data from LTPP for dry-non-freeze climatic zones. Therefore, the proposed distress model of bleeding distress could be written as follows:

Dry no-freeze zone:

$$\%Bleeding = 4.708 + 1.043\,PA + 1.203\,V_a \tag{8}$$

5.2.6. Rut Depth Model

Table 7 indicates that the model has R^2 value of 0.233 and 0.479 based on the obtained data from LTPP for wet- and dry-non-freeze climatic zones, respectively. Therefore, the proposed rut depth model could be written as follows:

Wet no-freeze zone:

$$Rut\ Depth = 10.097 - 0.987\,Ln(ESAL) + 0.478V_a \tag{9}$$

Dry no-freeze zone:

$$Rut\ depth = 21.39 + 0.009ESAL - 1.05Ta + 0.255V_a \tag{10}$$

6. VALIDATION PROCESS

Once the models were developed, validation process should start using LTPP data sets different from the database used in the development process. The second category of dataset was used for validation process, which represents 21% of entire database.

Predicted values were calculated using the developed models; however, the actual or measured values were obtained from the selected LTPP sites. Table 8 and Table 9 show the results of measured and predicted values of fatigue, longitudinal, transversal, raveling, bleeding and rutting for wet- and dry-non-freeze climatic zones, respectively. The results indicate that the predicted values are fairly close to the measured values at the corresponding LTPP sites.

Table 8 - Measured and Predicted Distress Density for Wet-Non-Freeze LTPP Sites

%Fatigue Cracking		%Longitudinal Cracking		%Transverse Cracking		%Raveling		Rut Depth, mm	
M	P	M	P	M	P	M	P	M	P
0.00	0.01	0.00	0.23	0.10	0.0531	0.14	0.74	4	4.77
0.59	0.39	0.00	0.00	0.00	0.3756	0.00	0.63	12	12.09
7.46	8.29	0.00	0.00	0.00	0.00	9.83	6.81	6	8.56
0.00	0.04	2.18	1.27	0.00	0.00	0.35	0.59	7	9.43
0.00	0.05	0.00	0.00	0.00	0.10	0.00	0.00	17	13.71

Table 8 - Measured and Predicted Distress Density for Wet-Non-Freeze LTPP Sites (continue)

%Fatigue Cracking		%Longitudinal Cracking		%Transverse Cracking		%Raveling		Rut Depth, mm	
2.23	1.64	0.00	0.00	0.00	0.02	0.00	0.00	12	10.54
1.79	2.48	0.00	0.005	3.34	0.06	0.00	0.00	9	8.01
20.56	24.35	0.00	0.00	6.82	0.01	0.00	0.00	6	5.29
0.00	0.02	0.00	0.00	0.00	0.00	0.00	0.00	5	4.19
13.32	9.54	13.52	1.03	0.41	0.40	0.00	2.4	6	5.06
0.00	4.12	0.134	.006	0.30	0.40	2.45	3.17	12	13.71

M: Measured values
P: Predicted values

Table 9 - Measured and Predicted Distress Density for Dry-Non-Freeze LTPP Sites

%Fatigue Cracking		%Longitudinal Cracking		%Transverse Cracking		%Bleeding		Rut Depth, mm	
M	P	M	P	M	P	M	P	M	P
4.18	4.35	2.69	2.54	2.55	4.31	13.54	10.11	8	7.45
3.60	4.11	8.17	8.01	3.14	5.41	2.21	2.01	3	5.16
5.78	4.99	11.31	10.52	2.34	3.92	5.32	6.15	7	6.42
5.08	5.24	3.34	3.10	4.01	5.68	0.14	0.17	6	6.06
4.58	5.94	4.48	3.75	3.65	6.08	24.63	28.61	7	7.30
4.18	5.06	7.66	7.02	3.78	5.48	2.25	2.58	8	5.91
4.32	4.89	6.45	6.44	6.89	9.28	4.31	4.92	7	5.93
4.87	3.38	11.02	11.46	4.52	6.61	13.14	11.46	6	5.95
5.44	4.85	3.64	3.21	8.44	9.98	0.15	.16	5	5.31
3.88	3.76	6.87	6.21	4.85	6.73	15.41	15.64	6	6.64
4.02	4.92	8.99	8.36	1.48	3.5	6.54	6.27	7	6.73
4.87	7.51	4.01	4.56	3.12	5.31	30.41	30.08	6	6.15
2.73	2.61	5.08	6.75	6.51	8.17	44.17	48.73	6	5.37
1.50	2.02	6.57	6.03	0.51	2.68	50.15	54.65	3	6.63
1.56	0.99	3.22	4.25	9.99	12.17	39.71	35.69	6	7.65
3.48	4.35	13.67	13.42	8.64	10.59	22.42	19.99	7	5.11
1.78	1.42	10.51	10.22	3.93	5.88	7.00	7.09	7	6.37
1.30	1.21	11.41	10.68	5.12	7.59	15.24	15.29	5	5.41
1.35	1.76	6.12	5.88	4.61	6.51	0.46	0.56	6	6.79

M: Measured values
P: Predicted values

7. COMPARISON WITH AVAILABLE PUBLISHED MODELS

The developed models of fatigue and rutting, which are considered the most important structural pavement failure, were compared with the available published models as follows and as shown in Figure 1, Figure 2, Figure 3 and Figure 4:

- **Fatigue wet-non-freeze zone**: model developed by Ker et al., 2007 [14] as shown in Table 1 versus the developed model of Equation (1). The comparison is shown in Figure 1.

- **Fatigue dry-non-freeze zone**: model developed by Ker et al., 2007 [14] as shown in Table 1 versus the developed model of Equation (2). The comparison is shown in Figure 2.

- **Rut depth wet-non-freeze zone**: model developed by Naiel, 2010 [6] as shown in Table 1 versus the developed model of Equation (9). The comparison is shown in Figure 3.

- **Rut depth dry-non-freeze zone**: model developed by Naiel, 2010 [6] as shown in Table 1 versus the developed model of Equation (10). The comparison is shown in Figure 4.
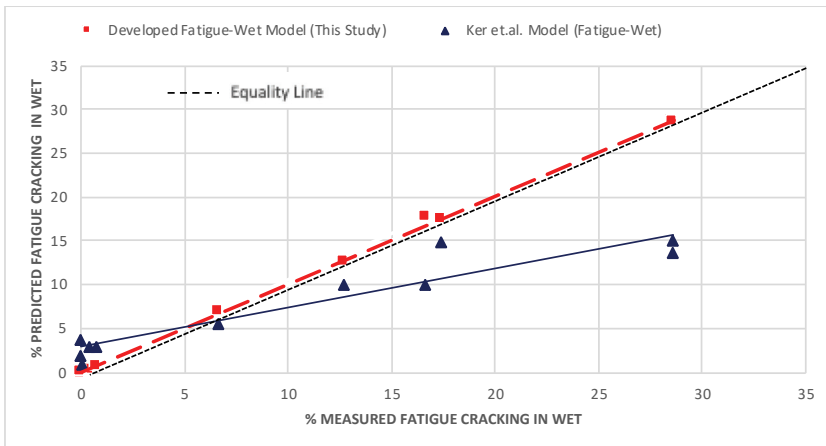
Figure 1 - Measured vs. Predicted Values using Different Fatigue-Wet Models

It can be clearly noticed that the developed models of fatigue and rutting in this study predict better than the available published models. The developed model of fatigue-wet generally overestimated the values; however, the Ker et al. model overestimated in case of %fatigue less than 7% and underestimated when %fatigue is more than 7%. On the other hand, the developed model of fatigue-dry overestimated the values when %fatigue is less than 2% and underestimated over 2%. However, the Ker et al. model overestimated when %fatigue is less than 3.5% and underestimated over 3.5%.

For rut-wet model, the developed model in this study overestimated the rut depth when the depth is less than 11.5 mm and underestimated over this value. However, the model

developed by Naiel overestimated the rut depth when the depth is less than 7.5 mm. On the other hand, the developed model of rut-dry overestimated the rut depth in case of rut depth less than 6.5 mm. However, the model by Naiel generally underestimated the values.

In conclusion, the average % error of fatigue and rutting models developed in this study is 4 times less than the average % error obtained from the available published models.
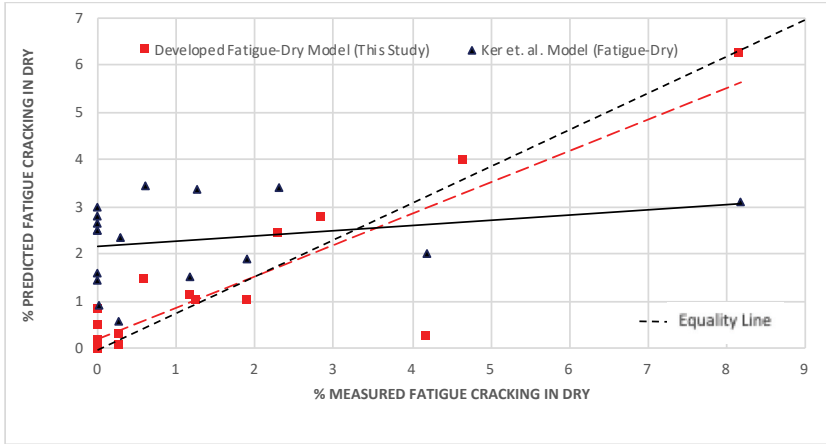
Figure 2 - Measured vs. Predicted Values using Different Fatigue-Dry Models
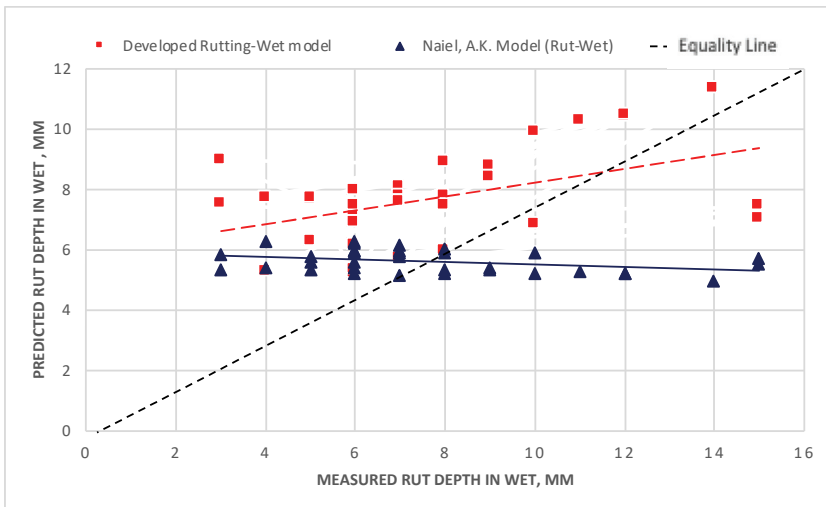
Figure 3 - Measured vs. Predicted Values using Different Rut-Wet Models
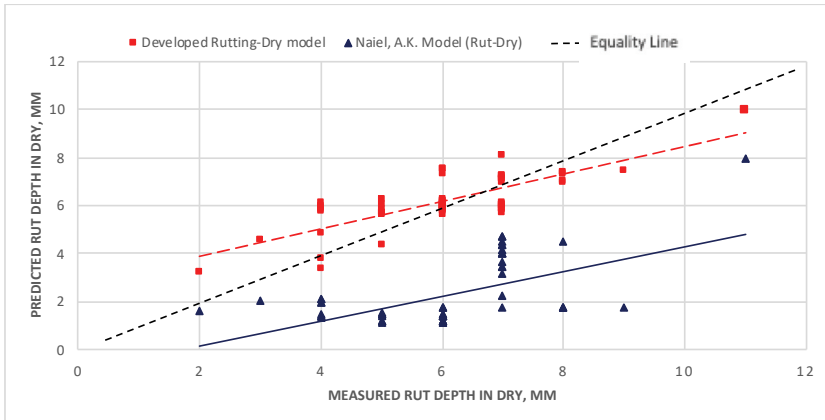
Figure 4 - Measured vs. Predicted Values using Different Rut-Dry Models

8. CONCLUSIONS

The main objective of this study is to develop pavement distress prediction models for main roads located in non-freeze climatic zones, which represent most of the Middle East countries, to be used in pavement management system. Six pavement distress prediction models were developed for fatigue cracking, longitudinal cracking, transverse cracking, raveling distress, bleeding distress and rut depth using data extracted from the Long-Term Pavement Performance (LTPP) program. It was found that pavement age factor is sensitive to most of the developed models while plasticity index and air temperature are very sensitive to fatigue cracking. Additionally, %passing the #200 sieve (0.075 mm) of subgrade soil is sensitive to longitudinal cracking, which indicates that too much fine aggregates in the mix could result longitudinal cracking. On the other hand, %air void of asphalt layer is sensitive to bleeding distress. Validation process was performed using Long-Term Pavement Performance data sets different from the database used in the model development process. The results indicate that the predicted values are fairly close to the measured values at the corresponding LTPP sites. A comparison is also made between the developed models and the available published models for fatigue and rutting models, which are assumed the most important pavement distresses. This study is considered as a crucial attempt to develop such models for the Middle East region due to lack of resources led to unavailability of such models in most of the Middle East countries. However, calibration of the developed models is recommended based on local conditions of a country whenever the pavement performance data is available.

9. FUTURE WORKS AND RECOMMENDATIONS

The results of this study are very important to the Middle East countries experiencing similar climatic conditions. However, calibration of the developed models is recommended based on local conditions, whenever pavement performance data is available. Furthermore, elastic modulus of AC layer shall be considered as possible factor that could affect the developed

models especially for fatigue, longitudinal, and transverse cracking. On the other hand, layer thickness and % voids in mineral aggregate should also be considered as possible factors that could affect rut depth models.

List of Abbreviations

ESAL : Traffic loading represented by Equivalent Single Axle Load

MCb : Moisture content of base/subbase courses

Mr : Resilient modulus of subgrade soil

MCS : Moisture content of subgrade soil

P200 : % Passing the #200 sieve (0.075 mm) of subgrade soil

PA : Pavement age since overlay

Pb : % asphalt content in the mix

PI : Plasticity index of subgrade soil

T : Asphalt pavement thickness

Ta : Air temperature

Va : % Air voids of asphalt mix

References

[1] Haas, R., Hudson, R., Zaniewski, J., Modern Pavement Management. Krieger Publishing Company, Malabor Florida, 1994.

[2] Stantec-HPMA Manual, Highway Pavement Management Application (HPMA). User Documentation, V4.50. GARBLT Research Project in Egypt, Technical Consultations Bureau, Applied Engineering Technologies (TCB/AET), Cambridge, ON, Canada, 2001.

[3] George, K. P., Rajagopal, A.S., Lim, L. K., Models for Predicting Pavement Deterioration. Transportation Research Record 1215, 1-7, 1989.

[4] Li, N., Haas, R., Xie, W-C, Investigation of Relationship Between Deterministic and Probabilistic Prediction Models in Pavement Management. Transportation Research Record 1592, 70–79, 1997.

[5] Zimmerman, K. A., Testa, D. M., An Evaluation of Idaho Transportation Department Needs for Maintenance Management and Pavement Management Software Tools, 2008.

[6] Naiel, A. K., Flexible Pavement Rut Depth Modeling For Different Climate Zones. Ph.D. Thesis, Wayne State University, 2010.

[7]   Kulkarni R.B., Miller R.W., Pavement Management Systems Past, Present, and Future. Transportation Research Record 1853, 65–71, 2002.

[8]   Li, N., Xie, W-C; Haas, R., Reliability-Based Processing of Markov Chains for Modeling Pavement Network Deterioration. Transportation Research Record 1524, 203–213, 1996.

[9]   Porras-Alvarado, J. D., Probabilistic Approach to Modeling Pavement Performance using IRI Data. In Proceedings of 93rd Annual Meeting of the Transportation Research Board, Washington, DC, 2014.

[10] ARA Inc. Guide for Mechanistic-Empirical Design of New and Rehabilitated Pavement Structures. Final Documents, NCHRP, Champaign, 2004.

[11] Göransson, N. G., Den Svenska Nationella LTPP Database, VTI, 2009.

[12] Asphalt Institute, Research and Development of the Asphalt Institute's Thickness Design Manual (MS1), 9th Ed. Research Report: 82-2, 1982.

[13] Ali, H. A., Tayabji, S. D., Evaluation of Mechanistic-Empirical Performance Prediction Models for Flexible Pavement. Transportation Research Record, 1629, 169-180, 1989. http://Doi: 10.1016/j.sbspro.2012.06.1012.

[14] Ker, H., Lee, Y., Wu, P., Development of Fatigue Cracking Performance Prediction Models for Flexible Pavements Using LTPP Database. Transportation Research Board 86th Annual Meeting, Washington, D.C, January 21-25, 2007.

[15] George, K., Vepa, T., Shekhran, A., Prediction of Pavement Remaining Life. 1996.

[16] Ali, B., Numerical Model for the Mechanical Behavior of Pavement: Application to the Analysis of Rutting. Ph.D. Thesis, University of Science and Technology Lille, 2006.

[17] Federal Highway Administration (FHWA) 2002. Available from internet: https://www.fhwa.dot.gov/research/tfhrc/programs/infrastructure/pavements/ltpp/ (Accessed August 2017).

[18] Long-Term Pavement Performance (LTPP), 2017. Available from: https://infopave.fhwa.dot.gov/ (Accessed on September 19, 2017).

[19] Abo-Hashema, M. A., Sharaf, E. A., Development of Maintenance Decision Model for Flexible Pavements. International Journal of Pavement Engineering, 10 (3), 173-187, 2009.

[20] Shahin, M. Y., Kohn, S. D., Pavement Maintenance Management for Roads and Parking Lots. United States Army Corps of Engineers, Technical Report: M-294, 1981.

[21] This reference must be added to the list because it is cited in the manuscript on page 10.

Artificial Neural Network Model to Predict Anchored Pile-Wall Displacements on Istanbul Greywackes

Özgür YILDIZ[1]
Mehmet M. BERİLGEN[2]

ABSTRACT

The greywackes are the common soil formation of Istanbul locally known as the Trakya Formation. It is mostly weathered and extensively fractured. The stress relief induced by deep excavations causes excessive displacements in horizontal direction. As a result, predicting excavation-induced wall displacements is critical for avoiding collapse. The aim of this study is to develop an Artificial Neural Network (ANN) model to predict anchored-pile-wall displacements at different stages of excavation performed on Istanbul's greywacke formations. A database was created on excavation and monitoring data from 11 individual projects. Five variables were used as input parameters, namely, excavation depth, maximum ground settlement measured behind the wall, system stiffness, standard penetration test N value of the soil depth, and index-of-observation. The proposed model was trained, validated, and tested. Finally, two distinct projects were numerically modeled by applying the finite element method (FEM) and then used to test the performance of the ANN model. The displacements predicted by the ANN model were compared with both the computed values obtained from the FEM analysis and in situ measured displacements. The proposed ANN model accurately predicted the displacement of anchored pile walls constructed in greywackes at different stages of excavation.

Keywords: Artificial neural network, anchored pile walls, finite element method, wall displacement, Istanbul greywackes.

1. INTRODUCTION

Because of the increase in urban populations, deep excavations are often required in metropolitan areas. Such excavation projects rely on rigorous analyses based on geotechnical investigations and laboratory experiments. Changes in excavation-induced stress trigger horizontal and vertical ground movements in and around the excavation area. Therefore,

accurate prediction of displacements becomes crucial to ensure the safety and serviceability of surrounding properties.

In some of the earliest works, Peck [1] investigated ground-surface settlements around excavations and subdivided the ground settlements according to the soil type and workmanship. Later, Mana and Clough [2] provided a simplified method to predict movements for braced cuts in clay and provided a relation between wall movements and the safety factor against basal heave. Finno et al. [3] investigated the performance of deep excavations in clay, and Clough and O'Rourke [4] carried out an in situ investigation of wall movements using a database containing information on conventional and new earth-retaining systems. Whittle et al. [5] applied a finite element analysis on braced excavations to predict excavation-induced soil deformations and applied the MIT-E3 effective stress soil model to describe the behavior of clay. They found that post-construction deformations led to differences between predicted and measured wall movements. Hashash and Whittle [6] performed an extensive set of numerical experiments to investigate deformations of a braced diaphragm wall in a deep clay deposit. One result of their study is that the effects of excavation depth and support conditions on ground movements are now given in design charts. Hsieh and Ou [7] proposed a method that provides good predictions of ground-surface settlements. Long [8] used a database containing several case histories to examine ground movements due to deep excavations and deduced remarkable conclusions for retaining walls in stiff and soft soils with different levels of safety factors against basal heave. Hwang et al. [9] studied the performance of wall systems by focusing on toe movements and reducing wall displacements using buttresses. Wang et al. [10] studied the relationship between ground settlements and wall displacements. Bolton et al. [11] studied ground movements and provided a set of design charts giving soil deformability, wall stiffness, and excavation geometry as a function of the soft soil depth.

The accuracy of current ground movement predictions depends on the accuracy of the soil behavior models and the parameters used [12]. In some cases, soil parameters are poorly defined, the behavior models do not reflect the in situ soil conditions, and/or the problem is too complex to be described in mathematical form. Researchers overcome such problems by using experimental data in computational processing methods. Modern techniques such as fuzzy systems and neural networks have been used to develop data-based models, which are capable of learning and recognizing trends in data patterns [13]. For example, Ghaboussi et al. [14] developed an auto-progressive algorithm to extract material behavior by exploiting force and displacement measurements, and Jan et al. [12] developed a neural network model to predict displacements of diaphragm walls. The model developed by Jan et al. [12] was based on training using wall-displacement data from 18 case histories and considered excavation stages and accurate predictions of wall displacements obtained from simulations at different stages of the excavation. Hashash et al. [15] developed a neural-network-based model to estimate ground deformations in a staged construction of a deep excavation. In another work, Hashash [16] used a self-learning simulation system to extract soil information from lateral wall deformations and surface-settlement measurements of deep excavations. Song et al. [17] used an inverse analysis approach that combined synthetically generated measurements including lateral wall displacements with surface settlement to extract soil behavior. Yıldız et al. [18] developed a neural-network approach to estimate the total lateral thrust on strip-loaded retaining walls. Johari et al. [19] established a genetic-based model to estimate lateral wall displacements of retaining walls using a database including 240 cases.

In recent years, many high-rise buildings, underground parking lots, and subway stations have been constructed in Istanbul mainly in the local soil formation-known as Istanbul greywackes. Greywackes are characterized by a high degree of weathering, with intercalated sandstone, siltstone, and claystone layers. Excavations in greywackes induce excessive wall movements, causing major problems. Although researchers have already applied artificial neural network (ANN)-based models to predict movements in soft soils, here we present an ANN-based model to predict displacements of anchored pile walls constructed on Istanbul's greywackes. In this study, a database containing information and monitoring data from 11 independent excavation projects in Istanbul was established and an ANN model was developed to predict lateral wall displacements. Four parameters that influence the performance of anchored pile wall as well as the index-of-observation were used as input variables. The created database was then used to train, validate, and test the model. The accuracy of the proposed prediction model was evaluated on the basis of mean square error (MSE) and correlation coefficient (R) values. Finally, two excavation projects not included in the database were used as testing cases. The wall displacements for these testing cases were predicted by applying the developed ANN model, and then, the excavation cases were also numerically modeled by the finite element method (FEM). The lateral displacements predicted by the ANN model were compared with the computed values obtained from the FEM analysis and in situ measurements to examine its performance.

2. CHARACTERIZATION OF THE GREYWACKES

A detailed geotechnical survey was carried out by the Istanbul Metropolitan Municipality to identify geological formations in Istanbul [20], in 2007. As a result of this comprehensive work, 24 different local soil and rock formations were identified. The Trakya formation encountered in the study area is known to have been affected by intense tectonic events and has a variety of strike-slip faults, folds, fractures, and joints every few meters. This formation is characterized by a sedimentary greywacke containing intercalated yellowish-brown-to-dark-gray sandstone, siltstone, and claystone. The Trakya formation can be seen as highly fractured and weathered and exhibits closely to moderately spaced discontinuities. The strength properties of the rock material are in the range of weak to strong. Sandstone is the.

Table 1 - Average characteristic properties of formations.

Local name	Definition of formation	c' (kPa)	$\Phi'(°)$	Ψ (°)	υ	E (kN/m²)	γ (kN/m³)
Fill	New and old, man-made material	5	28	0	0.2	20.000	18
Avcılar	Sand/sand-stone, clay/clay-stone	0	41	10	0.2	65.000	22
Trakya	Fresh/slightly weathered greywacke	157	39	0	0.2	300.000	27
	Moderately weathered greywacke	68	32	0	0.2	90.000	24
	Completely weathered greywacke	5	28	0	0.2	15.000	19

c': effective cohesion, Φ': effective friction angle, Ψ: dilatancy angle, υ : Poisson's ratio, E: deformation modulus,γ: unit weight

most common rock type in this formation, and limestone and conglomerate interbeds or lenses are occasionally found between the layers. The thickness of the formation varies between 600 and 1700 m [21]. The overlying deposits, which are variously distinguished as the Gurpınar, Cukurcesme, and Gungoren Formations, have collectively been named as a single unit recently, namely the Avcılar Formation [22]. This formation starts with a basal conglomerate layer and continues upwards with intercalated layers of sand/sandstone and clay/claystone. The properties of the soil formations encountered in the selected project sites are given in Table 1

3. CASE HISTORIES

In this study, a database was created on the basis of projects supervised by the Istanbul Metropolitan Municipality. In this context, excavation and monitoring data from seven concourse structures of metro stations, three underground parking lots, and a gymnasium building were collected. Anchored pile walls were used as retaining systems in the investigated excavations. The excavation depth of the cases varied between 11.5 to 35 m. The excavations were supported by 65 cm and 80 cm diameter pile walls having 13 m to 36.5 m length. Ground anchors served as the supporting system. The bond lengths of the anchors varied between 6 to 10 m, and the total lengths were in the range of 10 to 28 m. The vertical and horizontal spacings of the anchors varied between 1 to 2.5 m and 1.3 to 5 m, respectively. The average inclination of the anchors is 15°. The number of anchor rows used in the projects varied between 2 and 17. Three to four 0.5″ and 0.6″ diameter tendons were used. Inclinometers were used to measure the lateral displacement through a borehole casing in the walls. The number of inclinometers used in the projects depended on the geometric configuration of the sections. The excavation-induced settlements were measured by settlement markers installed on the ground behind the wall. The local formations encountered at the project sites were artificial fill layers overlying the Avcılar and Trakya formations. Figure 1 shows the typical geometry of an anchored pile wall and the displacement features, along with the notation used.
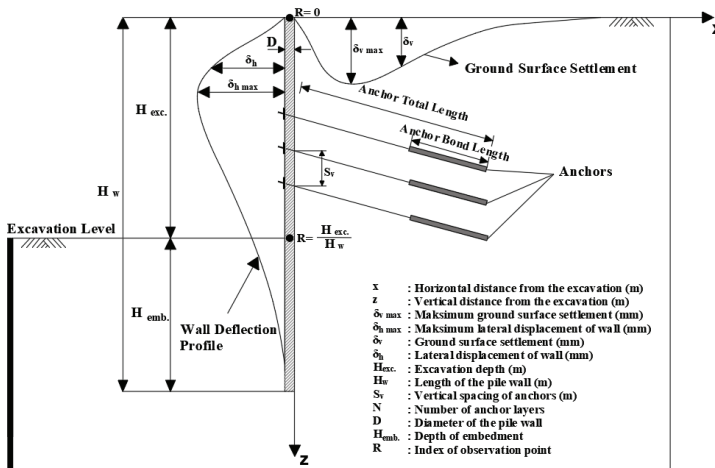
Figure 1 - Definition of variables used to describe the anchored pile walls.

4. ARTIFICIAL NEURAL NETWORKS

ANNs consist of logical software developed to perform basic functions by imitating the working mechanism of the human brain [23]. They can derive new information by learning, remembering, and generalizing. ANNs use their ability to generate new information to produce adaptive solutions to problems that cannot be solved by using a certain algorithm or formulation. The learning ability of ANNs is dependent on different learning algorithms that improve the information at each iteration, thereby achieving more accurate results. [24]

ANNs consist of interconnected process elements called neurons, and each interconnection has a weight. There are different types of ANN architectures. A widely used one is the feed-forward network, in which information flows in one direction along the connections, from the input layer via the hidden layer to the output layer. The processing data are fed forward to avoid generating feedback connections [25].

Once a network is structured for an application, it must be trained. In this process, initial weights are chosen at random before the training process begins. Two types of training rules exist, namely, supervised and unsupervised. For supervised training, both inputs and outputs are provided to the network, whereas only inputs are provided for unsupervised training [24]. A feed-forward network is commonly trained using a backpropagation learning algorithm, which is used for applications, and training a neural network with such an algorithm consists of two stages: The first one is the data feed-forward stage in which the output of a neuron is calculated. The output is defined as

$$net_j = \sum_{i=1}^{n} W_{ij} o_i + \phi_i,$$ (1)

$$o_i = f(net_i),$$ (2)

where W_{ij} is the weight associated with the input element i in the previous layer to element j in the current layer, o_i is the output of element i in the previous layer, ϕ_i is the threshold of element j in the current layer, and f is the activation function that processes inputs to determine outputs. The activation function f is usually a nonlinear function. Herein, the sigmoid function is used as activation function because it is continuous and differentiable. Its nonlinearity makes it the most frequently used function in ANN applications. The function f generates a value between 0 and 1 for each input. It is given by

$$f(x) = \frac{1}{1 + e^{-x}}$$ (3)

In the second stage, after the feed-forward network processes the inputs, the backpropagation algorithm compares the resulting outputs with the desired outputs. The errors are then propagated back through the system, and weights are adjusted. The error function for the system is given by

$$e_i = d_{ik} - y_{ik}, \tag{4}$$

$$E = \frac{1}{2} \sum_{i=1} \sum_{k=1} e_{ik}^2, \tag{5}$$

where d_{ik} is the desired output of node k for instance i and y_{ik} is the calculated output of node k for instance i. The backpropagation algorithm serves to minimize the fitness function, and since this function depends on the network weight, the algorithm consists of processes to optimize the weights. The backpropagation algorithm, which uses the gradient-descent approach to optimize the weights, is defined as

$$\Delta w_{ij} = -\gamma \frac{\partial E(w)}{\partial w_{ij}} \tag{6}$$

where the learning rate γ is a constant between 0 and 1 [26].

5. ESTABLISHING THE ANN MODEL

Stress changes induced by a deep excavation inevitably trigger displacements. Herein, an ANN model is developed to predict the displacements in anchored pile walls constructed on Istanbul greywackes by learning from the monitoring data. The displacement data cover 39 sections of 11 anchor-supported pile walls, each section being treated individually. As proposed by Jan et al. [12], each anchored pile wall is discretized into 18 uniform intervals with 19 nodal points. An index-of-observation, R, is defined as the ratio of the depth of the observed segment to the wall length. Altogether, 741 (39 × 19) instances were generated to train, validate, and test the network. The primary reason for applying the ANN model was to predict displacements of anchored pile walls constructed on Istanbul greywackes prior to construction as well as during the early and later stages of the activity. A properly established ANN model will accurately predict the wall displacements at each excavation stage. A flowchart of the ANN model is given in Figure 2.

The multilayer perceptron ANN model consists of three layers: an input layer, a hidden layer, and an output layer. The input layer contains five input parameters, namely, the depth of excavation (H_{exc}); measured maximum ground settlement behind the wall ($\delta_{v\ max}$); wall stiffness (EI); the SPT-N value of the observed soil depth; and the index of observation (R). The number of hidden layers can be changed according to the network, but the time required for the calculation and the complexity of the network both increase with the number of hidden layers. Accordingly, one hidden layer was used in this model. A series of trial-and-error processes with different numbers of neurons (between 5 and 40) was tested to find the optimum number of neurons in the hidden layer. The best performance was obtained with 15 neurons. The output layer consists of one neuron; $\delta_{h\ max}$, the maximum lateral displacement of the observation point. The available data were divided into three subsets, that is, training, validation, and testing sets. In this study, 80% of the 741 samples (593 randomly selected
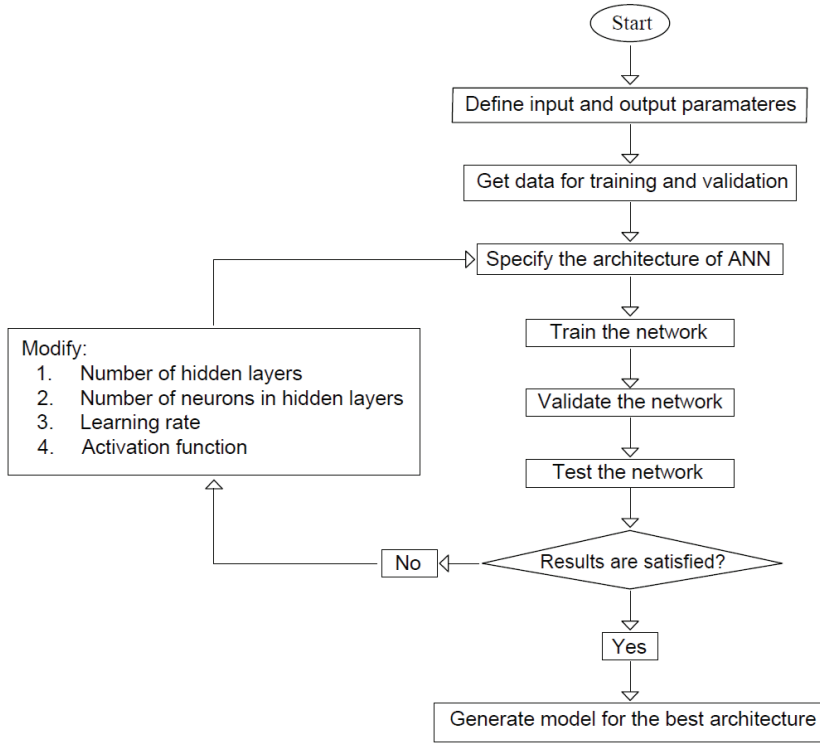
Figure 2 - Flowchart of the ANN model.
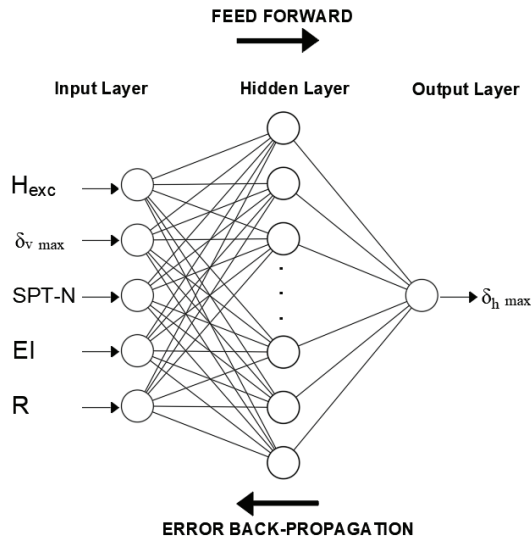
Figure 3 - Typical architecture of a feed-forward network with one hidden layer.

data) was used for training, 10% (74 randomly selected data) for validation, and 10% (74 randomly selected data) for testing of the developed network to predict the lateral displacements. The most commonly preferred algorithm [27], the feed-forward back-propagation algorithm, was used during the training process. The Levenberg–Marquardt algorithm, which is fast and has stable convergence and provides numerical solutions to nonlinear functions, was used in the training stage. In the hidden layer, the best performance of the model was obtained with the sigmoid function, which is a continuous and nonlinear function. The optimal ANN model was determined on the basis of the MSE and R values. Figure 3 shows the architecture of the developed feed-forward network.

6. COMPUTATIONAL RESULTS FOR THE ANN

A database containing 11 case histories of deep excavations was used to train, validate, and test the developed ANN model. The accuracy of the predicted wall displacements was determined by comparing them with the results of in situ measurements. Figure 4 shows the regression curves obtained for the network at the training, validation, and testing stages as well as during the entire process. The in situ measurements are shown on the x-axis, labeled as "Target," whereas the predicted displacements are given on the y-axis, labeled as "Output." The linear output demonstrates the success of the prediction model. The correlation coefficients between the maximum measured wall displacements and the predicted wall
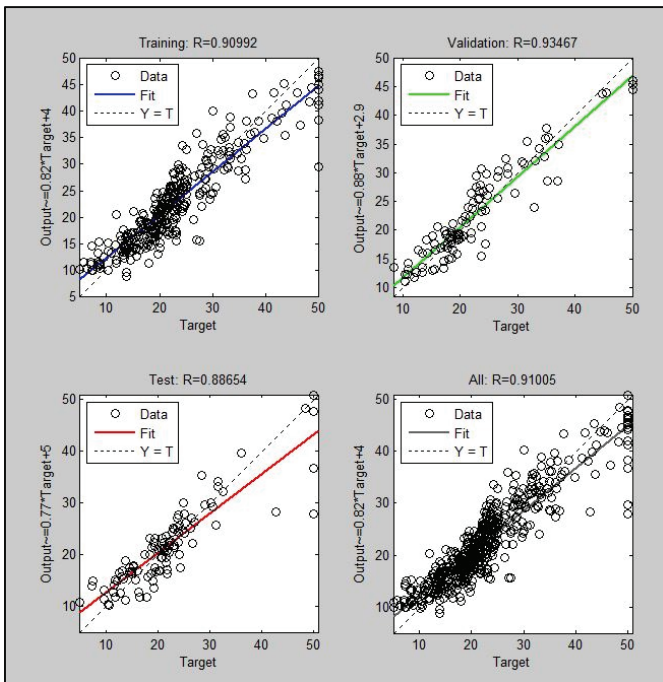
Figure 4 - Regressions curve obtained for the network at the training, validation, and testing stages as well as during the entire process.

displacements for the training, validation, and testing stages were 0.9099, 0.9347, and 0.8865, respectively, whereas the cumulative correlation coefficient for all the stages was 0.9101. The high correlation coefficients between the measured and predicted settlements obtained for all the data sets demonstrate that the adopted model performs well. The MSE values determined for the training, validation, and testing stages were 15.15, 9.65, and 17.44, respectively, showing a close relationship between the measured and ANN-predicted displacement values. The best validation performance obtained at epoch 20 (Figure 5). Ranges of test parameters with basic statistics used for ANN modelling can be seen in Table 2.
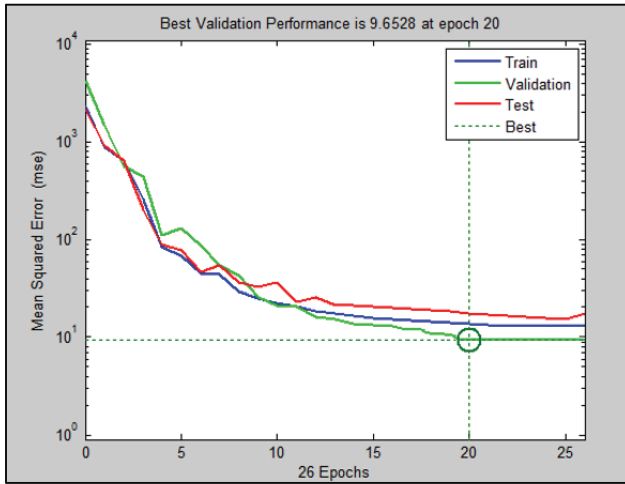
Figure 5 - MSE vs. number of epoch for validation phase

Table 2 - Ranges of test parameters with basic statistics

Number of datasets	Testing Parameters	Maximum	Minimum	Mean	STD
741 samples	$H_{exc.}$ (m)	35	9	19.5	6.2
	δ_{vmax} (mm)	44	2	9	11
	SPT-N	>50	5	27	12
	EI (kNm^2/m)	3.110.000	115.000	2.510.000	534.000
	R	32	0	1.60	3.1

7. TESTING CASES

Excavation sites not included in the database were used to validate the performance of the developed ANN model. In this context, the excavations of the two metro stations were selected as testing cases. The lateral displacements for these two stations were first predicted by the developed ANN model and then calculated by numerical modeling using the FEM method.

Table 3 - Testing cases used to evaluate the ANN model.

Project name	Section	Wall type	Soil formation	Soil profile	H_e (m)	H_w (m)	H_{emb} (m)	δ_{vmax} (mm)	δ_{hmax} (mm)	EI (kNm²/m)
Case-I	2A	Multi anchored bored pile, 65 cm	Avcılar, Trakya	Weathered claystone, mudstone	25	26	1	5	26	115000
	4C				20	22.5	2.5	30	21	
	5E				19.5	20	0.5	38	5	
	6				30.5	36	5.5	9	11	
Case-II	2G	Multi anchored bored pile, 65 cm	Trakya	Weathered, fractured sandstone	16.5	19	2.5	45	27	115000
	6A	80 cm diameter bored pile			16.5	19.5	3	4	15	312500
	10	Multi anchored bored pile, 65 cm			21.5	25	4.5	44	20	115000

In order to observe the ground profile and to determine the excavation support system, at the project sites of case I and case II, 3 boreholes for each with the depth of 35 m and 30 m were performed, respectively. A set of laboratory and in situ tests were performed to determine the geotechnical parameters. Both testing cases were constructed on Istanbul greywackes, and anchored pile walls were used as retaining systems in these projects. The plan for **case I** was rectangular (length: 61.65 m, width: 35.65 m, Figure 6.a). The excavation was completed in eight stages, and the final excavation depth varied between 19.5 and 30.5 m. Cut-and-cover construction method was applied, and according to the geometric configuration of the excavation, four different pile sections with different excavation depths and wall lengths were identified. The diameter of the pile wall was the same for each section, and the installation angle of the anchors ranged from 15° to 30°. The soil profile at the site consisted of an artificial fill layer between 0 and 1.50 m, a sandy-clay layer between 1.50 to 3.50 m, a clayey-sand layer between 3.50 and 6.50 m, a clayey-gravel-and-sand layer between 6.50 to 10.50 m, and an intercalated layer (containing claystone and mudstone) between 10.5 and 32 m. The groundwater table was measured at 8.15 m (Figure 7.a). **Case II** excavation was 21.72 m long and 27.15 to 15.05 m wide (Figure 6.b), and cut-and-cover construction method was applied here as well. In this case, the excavation was carried out in seven stages, and the final depth of excavation varied between 16.5 and 21.5 m. Three sections with different geometric configurations were modeled. The diameter of the piled wall varied depending on the

Table 4 - Properties of the anchored pile walls for the excavation of testing cases I and II.

Project name	S_v (m)	S_h (m)	Number of anchor rows	Anchor length (m)	Tendon	EA (kN/m)	Allowable tensile capacity (kN)
Case-I	1.5-2.5	1.5-2.0	6-12	13-26	4x0.6″	104000	804
Case-II	2	1.75	3-8	14-28	4x0.6″	84000	603

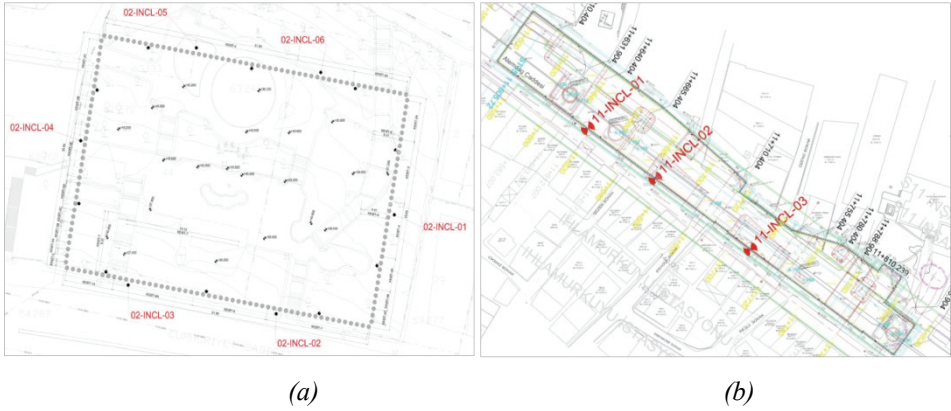*(a)*   *(b)*

Figure 6 - Plans of the excavations showing the placements of the inclinometers: (a) case I and (b) case II.

(a)   *(b)*
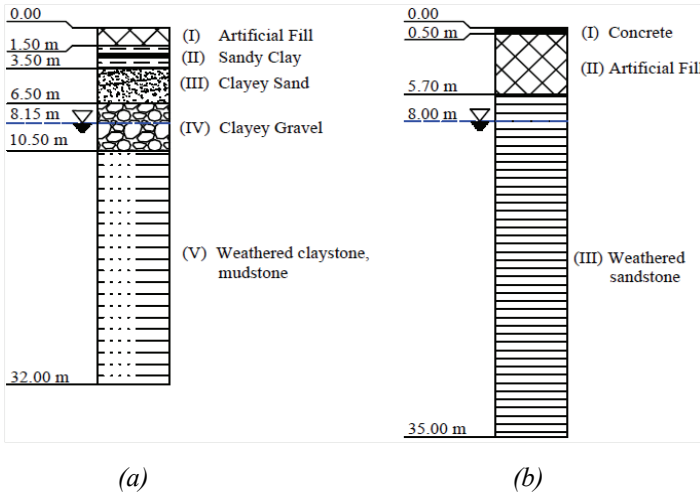
Figure 7 - Soil profiles for the testing cases: (a) case I and (b) case II.

geometric configuration of the section. The installation angle of the anchors ranged from 15° to 25°. The soil profile at the site consisted of a concrete layer between 0 and 0.40 m, a fill layer between 0.40 and 5.70 m, and a weathered and fractured sandstone layer between 5.7 and 35 m. The groundwater table was measured at 8.00 m (Figure 7.b). Table 3 summarizes the excavation data for cases I and II, and the anchor properties for both cases are given in Table 4. Inclinometers and ground-settlement markers were used to monitor the excavation areas. Six inclinometers were used for case I and three for case II. Typically, the inclinometers were denoted as "02-INCL-01," where "02" is the number of the metro station and "01" is the number of the inclinometer. Figure 6 shows plans with the placements of the inclinometers marked for each test case.

8. FINITE ELEMENT MODEL

The test cases were modeled by applying the 2D plane strain finite element analysis approach employing the PLAXIS 2D v.2018 software package. The boundaries of the finite element models were extended beyond the zone of influence induced by the excavation, in accordance with procedures recommended by Hsieh and Ou [7]. 15-node triangular elements were used in the finite element mesh, and to determine the optimum size of the elements and get precise results in a minimized time, different meshing patterns were analyzed. Since the results using fine and very fine meshes were similar, a fine meshing pattern was used. The pile wall was modeled using an elastic plate element, whereas the anchor was modeled as an elastic spring element with the far end having a fixed node. The hardening soil material model, which is an advanced model for simulating the behavior of different types of soil, was utilized. The strength parameters were obtained from laboratory test results, and the engineering parameters used in numerical analysis are given in Table 5. The vertical boundaries of the models were supported by roller fixities to prevent displacements perpendicular to the boundary, whereas the base was supported by hinges. The analyses were performed following the in situ excavation procedures, and the construction was modeled utilizing the staged construction sequence of the software. The soil–pile wall interaction was modeled by the zero-thickness interface element. Along the length of the piled wall, joints were assigned to obtain lateral displacements and displacement profile. Meshed views of the finite element models for both cases are given in Figure 8.

Table 5 - Engineering parameters used in numerical modeling.

Parameter	Case-I					Case-II		
	Soil Layer					Soil Layer		
	I	II	III	IV	V	I	II	III
E_{50}^{ref}(kPa)	10000	15000	30000	40000	75000	50000	12000	90000
E_{oed}^{ref}(kPa)	10000	15000	30000	40000	75000	50000	12000	90000
E_{ur}^{ref}(kPa)	30000	45000	90000	120000	225000	150000	36000	270000
c^{ref}(kPa)	5	5	25	30	79	200	7	90
ϕ'(°)	26	21	30	37	39	35	26	40
Ψ(°)	0	0	0	7	9	5	0	10

Table 5 - Engineering parameters used in numerical modeling. (continue)

Parameter	Case-I					Case-II		
	Soil Layer					Soil Layer		
	I	II	III	IV	V	I	II	III
γ_{sat} (kN/m³)	17,5	17	19	22	25	24	22	25
γ_{unsat} (kN/m³)	17,5	17	19	22	25	24	22	25
K_o	0,3	0,4	0,40	0,45	0,56	0,6	0,3	0,6
ν	0,3	0,2	0,25	0,25	0,2	0,2	0,3	0,2
e_{init}	0,5	0,5	0,5	0,5	0,5	0,5	0,5	0,5
R_i	0,50	0,50	0,65	0,70	0,70	0,67	0,50	0,70

E_{50}^{ref}: secant stiffness, E_{oed}^{ref}: oedometer loading stiffness, E_{ur}^{ref}: unloading–reloading stiffness, c_{ref}: effective shear strength, ϕ': effective friction angle, Ψ: dilatancy angle, γ_{sat}: saturated unit weight, γ_{unsat}: unsaturated unit weight, K_o: pressure coefficients, ν: Poisson's ratio, e_{init}: initial void ratio, R_i: stiffness reduction factor
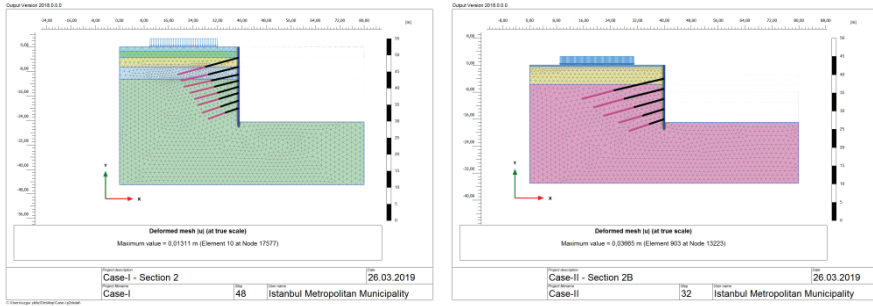
(a)   *(b)*

Figure 8 - Meshed views of the finite element models: (a) case I and (b) case II.

9. RESULTS

The lateral displacements predicted by the ANN model for the two testing cases were validated by comparison with calculated values from the FEM analysis and field measurements.

9.1. Case I

Figure 9 shows the wall displacements predicted by the ANN model, together with those computed by FEM analysis and measured by the inclinometers as a function of the excavation depth during the initial, middle, and final stages of the excavation. Five inclinometers measured lateral displacements at different sections of the excavation, and for each case, it was seen that as the excavation proceeded, the measured displacements increased and the wall gradually developed a bulging profile. The depths at which the maximum measured
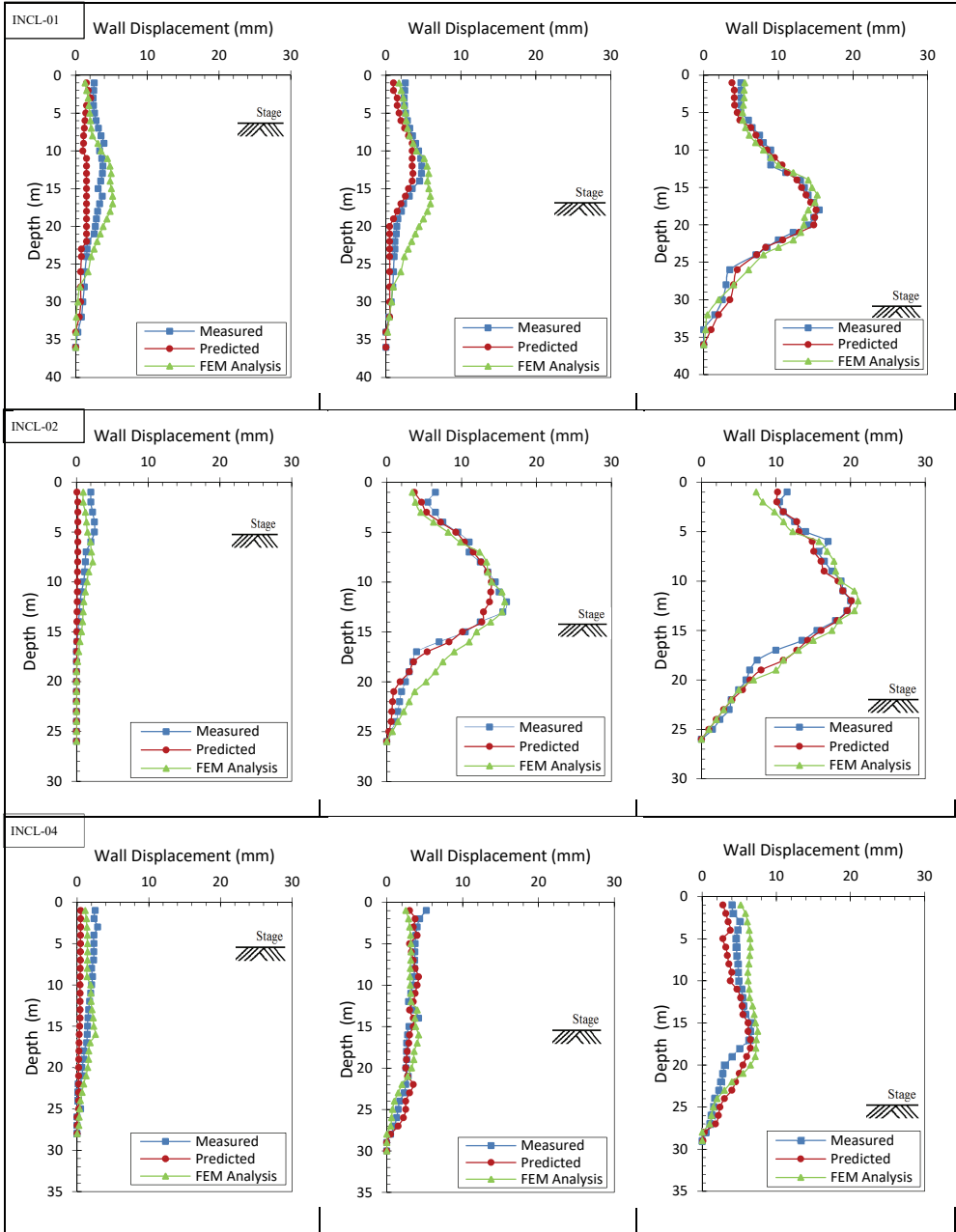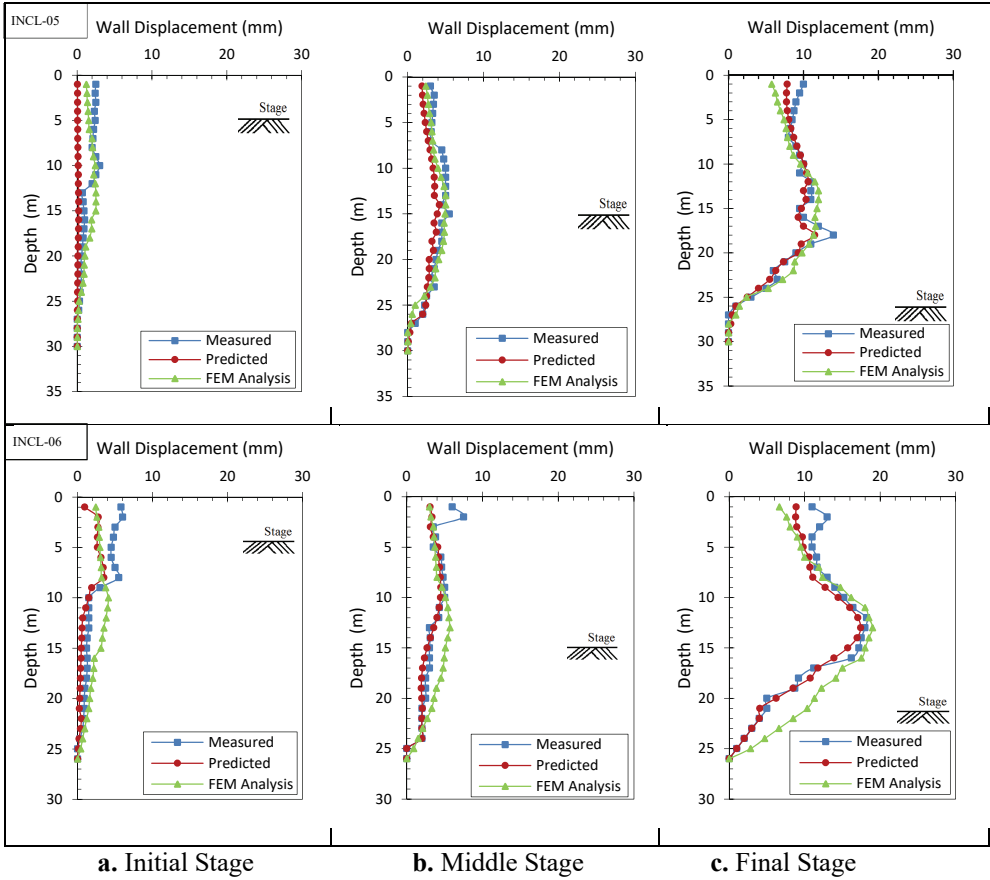
Figure 9 - Measured, ANN-predicted, and FEM-computed wall displacements for case I.

displacements occurred were not consistent, and the maximum lateral displacements were measured at different locations along the longitudinal axis. Some of the maximum displacements appeared above the excavation stage, whereas others occurred below it. At the initial excavation stage, in the upper parts of the wall, the displacements measured by the inclinometers were higher than those predicted by the ANN model and obtained from the FEM analysis. The FEM analysis gives the highest displacement values in the middle and lower parts of the wall, whereas the ANN predictions are the lowest ones in this area. The ANN model underestimates the wall displacements in the upper parts of the wall but shows a better performance in the lower parts. The differences between the measured and ANN-predicted displacements at the upper part of the wall can be attributed to the cantilevering excavation stage effect. At the middle excavation stage, the ANN-predicted displacements were very close to those measured by the inclinometers. Also, the displacement profiles matched well for all the inclinometers. In the lower parts of the wall, the displacements calculated by FEM analysis were higher than those measured by the inclinometers, which may be due to poorly defined soil parameters that do not completely reflect in situ conditions.

At the final excavation stage, the magnitudes of the displacements reached the highest values among all the inclinometers. The ANN-predicted displacements were very close to those measured by INCL-01, INCL-02, and INCL-06, whereas slight differences were observed between the predicted values and the displacements measured using the INCL-04 and INCL-05 instruments. However, a sudden increase in the displacement at 18 m wall depth (measured using INCL-05 and caused by a discontinuity in the extensively fractured greywackes) was successfully predicted by the ANN model. In general, the displacements calculated by FEM analysis were slightly higher than the ANN-predicted and measured values, which may be the result of a lack of reliance of the parameters used in numerical analysis. Overall, the ANN model provides acceptable predictions of the wall displacements. The maximum measured and predicted wall displacements and the shape of the displacement curve match well with the results obtained using all the inclinometers.

Table 6 summarizes the maximum displacements predicted by the ANN model, computed by FEM analysis and measured by the inclinometers. The ANN predicted displacements are very close to those measured by INCL-02 and INCL-04, whereas minor discrepancies were observed between the predicted values and the displacements measured using the INCL-1, INCL-05 and INCL-06. The depths at which the maximum displacements occurred were predicted with high accuracy. The maximum displacements calculated by FEM analysis provide satisfactory agreement with the field measurements.

Table 6 - Summary of the displacement data for Case-I

Method	Case-I									
	INCL-01		INCL-02		INCL-04		INCL-05		INC-06	
	Depth (m)	$\delta_{h\,max}$ (mm)	Depth (m)	$\delta_{h\,max}$ (mm)	Depth (m)	$\delta_{h\,max}$ (mm)	Depth (m)	$\delta_{h\,max}$ (mm)	Depth (m)	$\delta_{h\,max}$ (mm)
Measured	1	15.5	12	20	15	6.5	18	14	12	18.5
ANN	17	14.5	12	20,1	18	6.6	17	11,5	13	16
FEM	16	15.2	11	20,5	16	7.5	14	13	13	19

9.2. Case II

Figure 10 shows the wall displacements predicted by the ANN model, together with those computed by FEM analysis and measured by the inclinometers as a function of the excavation depth during the initial, middle, and final stages of the excavation. Three inclinometers were used to measure the lateral displacements at three distinct sections of the excavation. At the initial excavation stage, the measured wall deflections were slightly larger than the predicted ones for all the inclinometers, regardless of the depth of excavation. The maximum difference between predicted and measured displacements of about 5.5 mm was observed for INCL-01. Except for the top parts of the wall, the displacements calculated by FEM analysis were usually higher than both the ANN-predicted and measured ones. The differences between FEM results and measured displacements may have been caused by the selected geotechnical parameters that do not fully reflect the field conditions. At the middle excavation stage, the
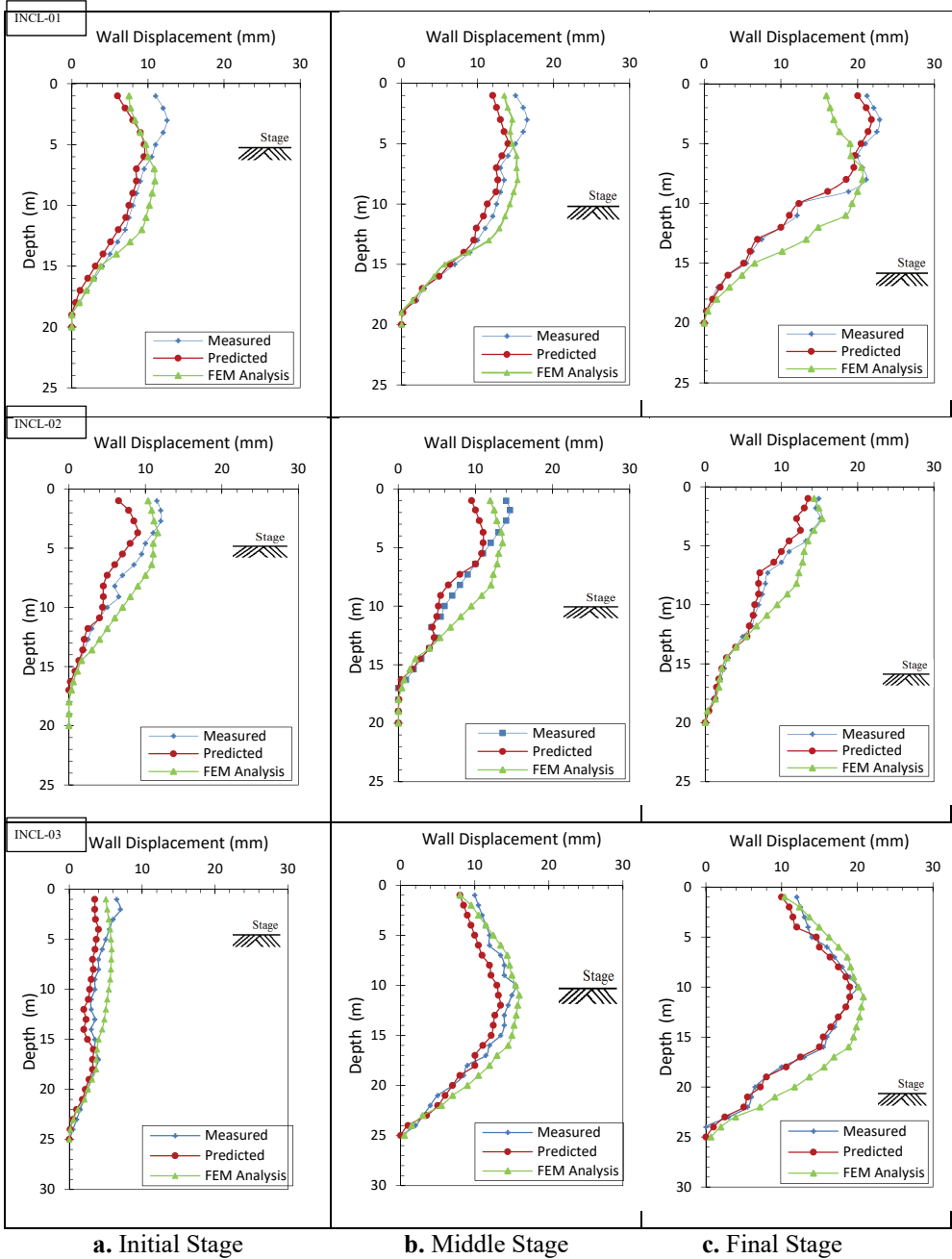
a. Initial Stage   **b.** Middle Stage   **c.** Final Stage

Figure 10 - Measured, ANN-predicted, and FEM-computed wall displacements for case II.

ANN-predicted wall deflections were lower than the values obtained from the field measurements for the upper parts of the wall, but very close to them for the lower parts. The relatively low predicted displacements could be due to the cantilever excavation stage, which sometimes causes excessive deformations. In the middle and lower parts of the wall, the displacements calculated by FEM analysis were slightly higher than the measured and predicted ones. At the final excavation stage, the differences between the predicted and measured deflections were markedly lower than those observed at the initial and middle stages. Despite the slight differences at the upper parts of the wall, the ANN-predicted displacement profile demonstrates a striking resemblance to the measured displacement profile at the lower parts of the wall. As in the previous excavation stages, the FEM analysis gives higher displacements at the lower parts of the wall compared with the field measurements and the ANN predictions. This is not the case for the upper wall parts. Overall, the wall displacements predicted by the ANN model match well with the maximum measured wall displacements over the entire range of excavation depths.

Table 7 summarizes the maximum displacements predicted by the ANN model, computed by FEM analysis and measured by the inclinometers. The maximum displacements predicted by ANN model agree well with those measured by inclinometers. The depths at which the maximum displacement occurred were successfully predicted. Also, the maximum displacements calculated by FEM analysis are very close to the field measurements.

Table 7 - Summary of the displacement data for Case-II

Method	Case-II					
	INCL-01		INCL-02		INCL-03	
	Depth (m)	$\delta_{h\,max}$ (mm)	Depth (m)	$\delta_{h\,max}$ (mm)	Depth (m)	$\delta_{h\,max}$ (mm)
Measured	3	22.9	3	15.1	10	15.5
ANN	3	21.8	1	13.5	12	13.6
FEM	8	21.4	3	15.3	11	16

10. CONCLUSIONS

We have developed an ANN model for predicting the displacements of anchored pile walls constructed in Istanbul's greywackes. The new system was trained, validated, and tested using the data collected from excavation projects in Istanbul, conducted by the Istanbul Metropolitan Municipality. The excavations of two distinct metro stations were numerically modeled by FEM, and the computed lateral displacements obtained from this analysis as well as the results of field measurements were used to validate the performance of the ANN prediction model.

The conclusions of our work can be summarized as follows:

1. The developed ANN model can accurately predict the magnitude as well as the location of the maximum wall displacement of anchored pile walls at different stages of excavation.

2. Some discrepancies observed between the measured and ANN-predicted displacements at the initial stages can be explained by cantilever stage effects.

3. Despite the slight differences between the ANN predictions and the results of the FEM analysis, the performance of the ANN-based model for predicting lateral displacements in Istanbul's greywackes was satisfactory, showing that this procedure can serve as a complementary method to FEM analysis.

4. With the ANN model being trained, tested, and validated using data from previous excavations, this method can be applied to predict anchored pile wall displacements for future projects. Predictions based on initial stage can thus be applied to excavations at subsequent stages.

5. The satisfactory performance of the developed model on Istanbul greywackes confirms the potential of ANN in the field of geotechnical engineering. The proposed model enables learning from previous regional excavations and can be applied to new projects in these areas.

References

[1] Peck, R.B., Deep excavations and tunneling in soft ground. Proceedings 7th I.C.S.M.F.E. State of Art Sayı., Mexico: 225-290, 1969

[2] Mana, A.I., Clough, G.W., Prediction of movements for braced cuts in clay. J. Geotech. Eng. Div., 107, 759-777, 1981

[3] Finno, R.J., Atmatzidis, D.K., Perkins, S.B., Observed performance of a deep excavation in clay. J. Geotech. Eng., 115(8), 1045-1064, 1989

[4] Clough, G.W., O'Rourke, T.D., Construction induced movements of in-situ walls. Geotechnical special publication: Design and performance of earth retaining structures (GSP 25)., ASCE, Reston, VA, 439-470, 1990

[5] Whittle, A.J., Hashash, Y.M.A., Whitman, R.V., Analysis of deep excavation in Boston., J. Geotech. Eng., 119(1), 69-90, 1993

[6] Hashash, Y.M.A., Whittle, A.J.,Ground movement prediction for deep excavations in soft clay., J. Geotech. Eng., 122(6), 474-486, 1996

[7] Hsieh, P.G., Ou, C.Y., Shape of ground surface settlement profiles caused by excavation., Can. Geotech. J., 35(6), 1004-1017, 1998

[8] Long, M., Database for retaining wall and ground movements due to deep excavations., J. Geotech. Geoenviron. Eng., 127(3), 203-224, 2001

[9] Hwang, R.N., Moh, Z.C., Evaluating effectiveness of buttresses and cross walls by reference envelopes., J. Geoeng. 3(1), 1-12, 2008

[10] Wang, J.H., Xu, Z.H., Wang, W.D., Wall and ground movements due to deep excavations in Shanghai soft soils., J. Geotech. Geoenviron. Eng., 136 (7), 985-994, 2010

[11] Bolton, M.D., Lam, S.Y., Vardanega, P.J., Ng, C.W., Ma, X., Ground movements due to deep excavations in Shanghai: Design charts., Front. Struct. Civ. Eng., 8(3), 201-236, 2014

[12] Jan., J.C., Hung, S.L., Chi, S.Y., Chern, J.C., Neural network forecast model in deep excavation., J. Comput. Civil Eng., 16(1), 59-65, 2002

[13] Goh, A.T.C., Goh, S.H., Support vector machines: their use in geotechnical engineering as illustrated using seismic liquefaction data.,Comput. Geotech. 34(5), 410-421, 2007

[14] Ghaboussi, J., Pecknold, D.A., Zhang, M., Haj-Ali, R., Autoprogressive training of neural network constitutive models., Int. J. Numer. Methods Fluids, 42(1), 105-126, 1998

[15] Hashash, Y.M.A., Marulanda, C., Ghaboussi, J., Jung, S., Systematic update of a deep excavation model using field performance data.,Comput. Geotech., 30(6), 477-488, 2003

[16] Hashash, Y.M.A., Marulanda, C., Ghaboussi, J., Jung, S., Novel approach to integration of numerical modeling and field observations for deep excavation., J. Geotech. Geoenviron. Eng., 132(8), 1019-1031, 2006

[17] Song, H., Osouli, A., Hashash, Y., Soil behavior and excavation instrumentation layout, 7th International symposium on field measurements in geomechanics FMGM., Boston, MA., 2007

[18] Yıldız, E., Ozyazıcıoglu, M.H, Ozkan, M.Y., Lateral Pressures on Rigid Retaining Walls: A Neural Network Approach., Gazi Univ. J. Science, 23(2), 201-210, 2010

[19] Johari, A., Javadi, A.A., Najafi, H., A genetic-based model to predict maximum lateral displacement of retaining wall in granular soil., ScienticaIranica, 23(1), 54-65, 2016

[20] Istanbul Metropolitan Municipality Department of Earthquake Risk Management and Urban Development Directorate of Earthquake and Ground Analysis, Microzonation work for the southern European side of Istanbul, Final Report, 1-88, 2007

[21] Eroskay, S.O., Graywackes of Istanbul Region, Proceedings of International Symposium on Design of Supports to Deep Excavations., Turkish Group of Soil Mechanics, Bosphorus University, 41-44, 1985

[22] Yıldırım, M., Tonaroğlu, M., Selçuk, M.E., Akgüner, C., Revised stratigraphy of the tertiary deposits of Istanbul and their engineering properties., B. Eng. Geol. Environ., 72(3-4), 413-420, 2013

[23] Shahin, M., Intelligent computing for modeling axial capacity of pile foundations., Can. Geotech. J, 47(2):230–243, 2010

[24] Öztemel,E., YapaySinirAğları, PapatyaYayıncılık, 29-162, 2012

[25] Haykin, S., Neural Networks: A Comprehensive Foundation, 1,23-71, 2001.

[26] Rojas, R., Neural Networks A systematic Introduction, Berlin, 151-184, 1996

[27] Rummelhart, D.E., Hinton, G.E., Williams, R.J., Learning Internal representation by error propagation., J. Parallel Distrib. Comput., 1(8): 318-362, 1986

Cost Efficient Design of Mechanically Stabilized Earth Walls Using Adaptive Dimensional Search Algorithm

Saeid KAZEMZADEH AZAD[1]
Ebru AKIŞ[2]

ABSTRACT

Mechanically stabilized earth walls are among the most commonly used soil-retaining structural systems in the construction industry. This study addresses the optimum design problem of mechanically stabilized earth walls using a recently developed metaheuristic optimization algorithm, namely adaptive dimensional search. For a cost efficient design, different types of steel reinforcement as well as reinforced backfill soil are treated as discrete design variables. The performance of the adaptive dimensional search algorithm is investigated through cost optimization instances of mechanically stabilized earth walls under realistic design criteria specified by standard design codes. The numerical results demonstrate the efficiency and robustness of the adaptive dimensional search algorithm in minimum cost design of mechanically stabilized earth walls and further highlight the usefulness of design optimization in engineering practice.

Keywords: Mechanically stabilized earth walls, optimum design, adaptive dimensional search, cost optimization, discrete variables, metaheuristics**.**

1. INTRODUCTION

Civil engineering projects usually require construction of soil-retaining structural systems. In general, these structures can be classified into two main groups, namely externally and internally stabilized systems. In-situ walls and gravity walls are typical instances of externally stabilized walls while reinforced soils as well as in-situ reinforcements can be categorized as internally stabilized soil-retaining systems which have been utilized since 1960 [1]. Basically, the rationale behind the use of internally stabilized systems is to enhance the tensile behavior of soil which is obviously negligible compared to its high load bearing capacity under compression. For instance, mechanically stabilized earth (MSE) walls are among the most popular internally stabilized soil-retaining systems which are constructed

---

1 Department of Civil Engineering, Atilim University, Ankara, Turkey - saeid.azad@atilim.edu.tr
  https://orcid.org/0000-0001-9309-607X

2 Department of Civil Engineering, Atilim University, Ankara, Turkey - ebru.akis@atilim.edu.tr
  https://orcid.org/0000-0001-8417-2405

through reinforcement of soil by placement of reinforcing members such as metallic strips, geotextiles, or geogrids.

Generally, the basic components of MSE wall systems can be listed as reinforcements, backfill soil, facing elements and connection parts [2, 3]. These soil-retaining structural systems are mainly low-priced compared to the conventional reinforced concrete retaining structures especially under poor foundation conditions. Although the cost of MSE walls may vary as a function of several independent parameters, it mainly depends on the cost of its principal components i.e. facing system, backfill material, placement, reinforcing material, etc. According to Ref. [2], typical relative costs of main components of MSE walls are outlined in Figure 1. Since decision making on the type of reinforcing material as well as backfill soil has a significant effect on the final cost of MSE walls, these design parameters are investigated in the present study using an optimization based approach.

- Erection of panels and contractor's profit (20% to 30% of total cost)
- Facing system (20% to 40% of total cost)
- Reinforcing materials (15% to 30% of total cost)
- Reinforced wall fill including placement (30% to 60% of total cost)
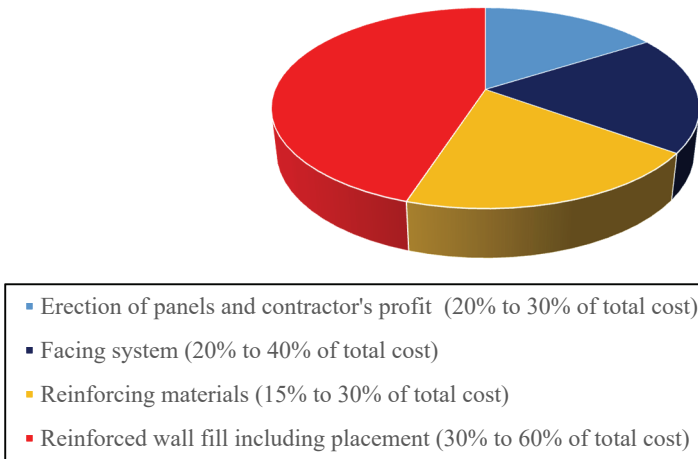
Figure 1 - Typical relative costs of main components of MSE Walls

One of the challenges in engineering design optimization is to develop efficient design optimization tools that can be used by designers to achieve cost-effective yet feasible final designs. Similarly, for optimum design of MSE walls, it is fruitful to adopt a suitable optimization method capable of handling the design variables as well as problem constraints [4-5]. Stochastic optimization techniques or the so called metaheuristics have found plenty of engineering design applications in the past decades [6-12]. The predominant characteristics of metaheuristics can be outlined as their independency on gradient information, capability of handling both discrete and continuous solution variables, and global search features to locate the optimum or near optimum solutions for challenging engineering design problems. These advantageous characteristics of stochastic search techniques make it possible to avoid cumbersome formulations of traditional structural optimization approaches, namely mathematical programming [13] and optimality criteria methods [14]. The state-of-the-art reviews of metaheuristic algorithms and their practical applications in engineering design can be found in Refs. [15, 16].

Adaptive dimensional search (ADS) algorithm is a recently developed metaheuristic algorithm for minimum weight design of truss structures [17]. This population based optimization technique is working based on an evolutionary approach where at each iteration, after generation and evaluation of candidate designs, the best design found is used to generate a new population of candidate designs. In this algorithm, in order to adjust the explorative and exploitative features of the technique, the search dimensionality ratio is adaptively updated during the optimization iterations. Regarding the promising performance of the ADS demonstrated in Ref. [17] in the present study the algorithm is revised for minimum cost design of MSE walls under realistic design constraints. For a cost efficient design, different types of steel reinforcement as well as reinforced backfill soil are considered as discrete design variables. The performance of the ADS is investigated through different cost optimization instances of MSE walls under realistic design criteria. The obtained numerical results clearly indicate the usefulness of the ADS algorithm in minimum cost design of MSE walls.

An outline of this paper is as follows. The second section provides the design procedure of MSE walls under standard code considerations. The mathematical formulation of the tackled optimization problem is stated in the third section. In the fourth section the employed metaheuristic optimization technique is described in detail. The numerical examples of MSE walls are investigated in the fifth section. A summary of the present study as well as some concluding remarks are provided in the last section.

2. DESIGN OF MECHANICALLY STABILIZED EARTH WALLS

This section outlines the main steps for design of MSE walls as recommended in Refs. [2-3] and AASHTO (2010) [18] specifications. Generally, in order to design the MSE walls, two main stability analyses, namely external and internal stability evaluations are to be performed. The external stability analyses include the checks against sliding on the base, overturning about the toe, bearing capacity of the foundation soil, settlements of the structure, and overall stability failure. In addition to external stability checks commonly used in design of retaining walls, internal stability analyses, including the check against rupture and pullout of the reinforcements within the reinforced backfill zone, must be accomplished as well.

2.1. External Stability Analyses

In order to evaluate the external stability of MSE walls, sliding, limiting eccentricity (overturning), bearing capacity, and settlement checks are carried out according to AASHTO (2010) [18] design specifications. With respect to the acting forces on the MSE walls (Figures 2 and 3) the nominal and factored resisting and sliding forces are determined along the base of the wall in order to assess the MSE wall for sliding.

Here, the vertical traffic load or live load surcharge is not included in the external forces due to the stabilizing effect. According to Refs. [1, 2, 18] the earth pressure from retained backfill F_1 and live load surcharge F_2 for MSE wall with level backfill and traffic load (Figure 2), are determined using Eqs. (1-2). Furthermore, the earth pressure from retained backfill F_T for MSE wall with sloping backfill (Figure 3) is calculated through Eq. (3) as follows.
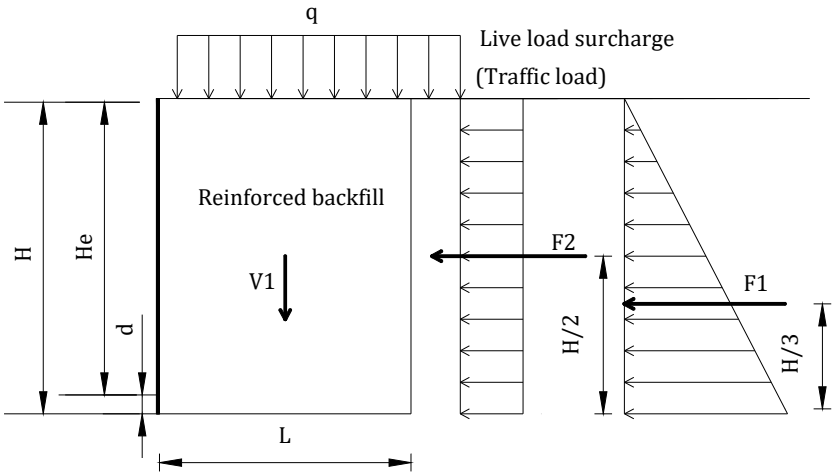
Figure 2 - External stability analysis: nominal earth pressures for MSE walls with level backfill and traffic load
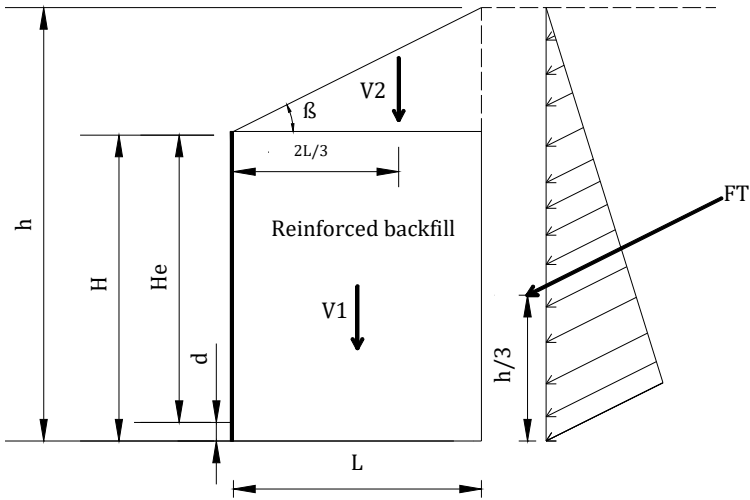

Figure 3 - External stability analysis: earth pressure for MSE walls with sloping backfill

$$F_1 = \frac{1}{2} K_{ab} \gamma_b H^2 \tag{1}$$

$$F_2 = K_{ab} q H \tag{2}$$

$$F_T = \frac{1}{2} K_{ab} \gamma_b h^2 \tag{3}$$

where, γ_b and q are moist unit weight of the retained backfill soil and the uniform live load surcharge, respectively. H is the height of the retaining wall and h is defined as the summation of the total height of the wall, H, and the slope at back of the reinforced zone. K_{ab} is the active earth pressure coefficient for the retained backfill calculated according to Eqs. (4-5).

$$K_{ab} = \frac{sin^2(\theta + \emptyset'_b)}{\Gamma \; sin^2(\theta)sin(\theta - \delta)} \tag{4}$$

$$\Gamma = (1 + \sqrt{\frac{sin(\emptyset'_b + \delta)sin(\emptyset'_b - \beta)}{sin(\theta - \delta)sin(\theta + \beta)}})^2 \tag{5}$$

where β, δ and θ are nominal slope of backfill behind the wall, angle of friction between retained backfill and reinforced soil, and inclination of the wall, respectively. Here, $\emptyset'_b$ is the effective friction angle of retained backfill in degrees. In the present study, the factored horizontal driving forces for MSE walls are computed according to Eqs. (6).

$$P_d = \gamma_{EH}F_1 + \gamma_{LL}F_2 \tag{6}$$

In this equation P_d denotes the factored horizontal driving force for MSE wall with level backfill and uniform live load, where γ_{EH} and γ_{LL} are the load factors for different load combinations presented in Table 1. In case of MSE walls with sloping backfill P_d will be determined as follows.

$$P_d = \gamma_{EH}F_H \tag{7}$$

$$F_H = F_T cos\beta \tag{8}$$

where F_H is the horizontal component of earth pressure from retained backfill, F_T. After calculation of driving forces, nominal (R_r) and factored resistance ($R_R = \emptyset_r R_r$) against sliding are calculated. Generally, resistance factors ($\emptyset$) depend on the wall type, stability mode, material type and loading conditions. In this study the corresponding resistance factors for bearing resistance and sliding are set to 0.65 and 1.00, respectively AASHTO (2010) [18].

Table 1 - Summary of load factors used for design [3]

Load combination	γ_{EV}	γ_{EH}	γ_{LL}
Strength I (max)	1.35	1.50	1.75
Strength I (min)	1.00	0.90	1.75
Service I	1.00	1.00	1.00

Furthermore, the factored resistance for MSE walls with sloping backfill is calculated using Eq. (9).

$$R_r = \{ \gamma_{EV} \; (V_1 + V_2) + \gamma_{EH} \; F_T \; sin\beta \} \; \mu \tag{9}$$

In Eqs. (9), μ is the tangent of the minimum friction angle, β is the inclination of the sloping backfill. Here, V_1 and V_2 are the vertical loads at the base of the MSE wall due to the reinforced soil zone and sloping backfill, respectively (Figure 3). In case of MSE walls with level backfill and uniform live load surcharge, Rr is computed using the following equation.

$$R_r = \gamma_{EV} \; V_1 \, \mu \tag{10}$$

Regarding the factored loads and resistance forces, the capacity demand ratio (CDR) for sliding is then determined based on the ratio of the factored resistance forces to the computed factored loads. It is apparent that the factored resistances must be greater than the factored loads i.e. CDR$\geq$1.

The eccentricity limit criterion is another external stability check that must be considered. Here, the eccentricity of the MSE walls is calculated by dividing the net moment, which is the difference between the driving and resisting moments with respect to the toe of the wall, by the vertical load. With respect to the type of foundation, two different eccentricity criteria are considered in the present study for soil and rock foundations. Accordingly, the maximum eccentricity (e_{max}) is limited to 1/4 and 3/8 of the base width for soil and rock foundations, respectively [18].

Another external stability check is to investigate the bearing capacity of foundation soil. Bearing capacity evaluations are carried out for strength as well as service limit states. Here, for strength limit state calculations, factored loads and resistances are considered, whereas in case of service limit state calculations nominal forces and capacities are taken into account. The vertical stress (σ_v) due to the presence of the MSE wall is determined as follows (Eq. 11).

$$\sigma_v = \frac{\Sigma V}{L - 2e_B} \tag{11}$$

In this equation, ΣV is the sum of factored vertical forces, L is the width of foundation, and e_B is eccentricity for bearing calculation. The bearing pressure at the base of the wall computed using the factored loads are compared to the factored bearing resistance (q_R) (Eq.12).

$$q_R = \emptyset q_n \tag{12}$$

where, $\emptyset$ is the resistance factor, and q_n is the nominal bearing resistance of the soil/rock foundation. The capacity demand ratio (CDR) for bearing capacity is then calculated based on the factored bearing resistance (q_R) and factored bearing stress (σ_v).

In this study, settlement analyses are also carried out and the results obtained are compared to the allowable limits. Although conventional settlement analyses can be performed, the settlement is evaluated at Service I limit state [2, 3]. For bearing capacity calculations based on Service I limit state, the bearing stress at the bottom of the wall is limited to the nominal bearing capacity of the soil. More specifically, through checking this criterion the settlement under the footing is limited to 2.54 cm.

2.2. Internal Stability Analyses

In case of internal stability analyses, two failure modes, namely breakage and pull out of the reinforcement due to the tensile forces should be checked. For internal stability assessments, the reinforced zone is divided into active and resistant zones based on a failure surface. In the present study, inextensible metal strips are used to reinforce the MSE walls, and the potential failure surface for walls with inextensible inclusions are depicted in Figure 4 based on Ref. [18].
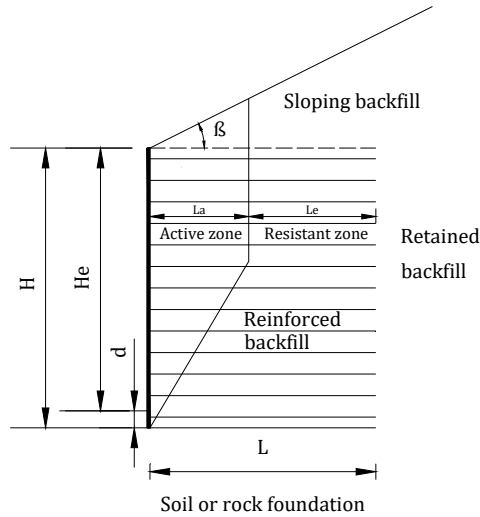
Figure 4 - Internal stability analysis: potential failure surface for walls with inextensible reinforcements.

The lateral pressure that is used to determine the maximum tension developed is determined using the simplified method [2, 18]. As presented in Figure 5 the lateral stress ratio K_r/K_a varies with depth. The active earth pressure coefficient, K_a and the horizontal stresses, σ_H, at each reinforcement layer within the reinforced soil zone for a vertical MSE wall is determined using the Rankine equation (Eqs.13-14).

$$K_a = tan^2(45 - \frac{\emptyset'_r}{2}) \tag{13}$$

$$\sigma_H = K_r(\sigma_V) + \Delta\sigma_H \tag{14}$$

where, $\emptyset'_r$ is the internal friction angle of the reinforced fill, K_r is the coefficient of lateral earth pressure in the reinforced soil zone, σ_V is the factored vertical pressure at the depth of interest, and $\Delta\sigma_H$ is the supplemental factored horizontal stress due to external surcharges.
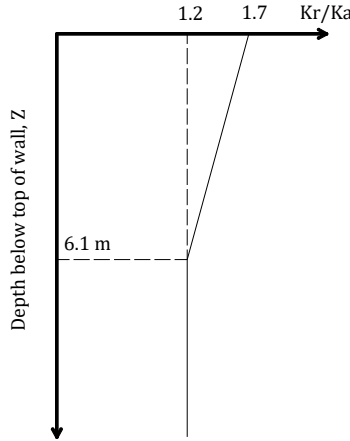
Figure 5 - Variation of the coefficient of lateral stress ratio K_r/K_a with depth for MSE walls with ribbed steel strips [18].

The maximum tension (T_{max}) in each reinforcement layer is determined by multiplying the tributary area by horizontal stress. The factored reinforcement tensile and pullout resistances are then compared with T_{max} to finalize the reinforcement pattern. In the present work, galvanized ribbed steel strips are used as reinforcement and their resistances are calculated based on 75 years of design life. Regarding the recommendations of AASHTO (2010) [18], the steel corrosion rates for the first two years are taken as 15 μm/year and thereafter 4 μm/year per side. The nominal tensile resistance (T_r) is also calculated based on the cross-sectional area at the end of the service life and yield strength of the utilized steel. The tensile resistance factor is taken as 0.75 [18] and the factored resistance (T_{rr}) is calculated by multiplying the nominal resistance by this factor.

In the course of assessment for internal stability, the pullout failure check is also accomplished. The nominal pullout resistance (P_r) is determined based on the reinforcement type, vertical stress acting on the reinforcement, and the factor F^* (Figure 6). The factored resistance (P_{rr}) is computed as follows [18].

$$P_r = \alpha F^*(2b)(L_e)(\sigma_{v-soil})\gamma_{EV} \tag{15}$$

$$P_{rr} = \emptyset P_r \tag{16}$$

In Eqs (15-16), Ø=0.90 is the resistance factor for soil reinforcement pullout, α is the scale correction factor (set to 1 for inextensible reinforcements), F^* is pullout resistance factor calculated in any depth within the reinforced backfill (see Figure 5), b and L_e are the width and length of the reinforcement in the resisting zone, respectively. Here, σ_{v-soil} is the soil load of the reinforced mass. Based on the maximum tension in each reinforcement, T_{max}, the factored tensile resistance, T_{rr}, and the factored pullout resistance P_{rr}, the number of strip reinforcements are calculated and the reinforcement pattern is determined. Generally, availability of different types of metal reinforcements as well as reinforced backfill soils

arises the need for decision making on the best solution among the numerous candidate designs for a MSE wall. Hence, to obtain a cost-effective design employing an optimization technique seems to be fruitful.
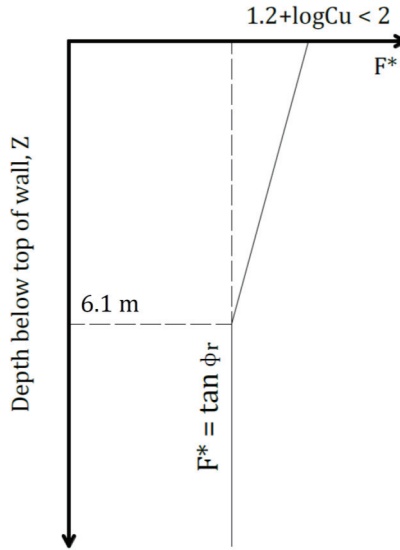
Figure 6 - F* parameter for MSE walls with ribbed steel strips [18].

3. OPTIMIZATION PROBLEM FORMULATION

Optimum design of structural systems entails decision making on the best values of the involved design variables. Meanwhile, the final design must satisfy the design constraints stipulated by a standard code of practice. Mathematically, the minimum cost design of a MSE wall considering the cost of steel strip reinforcements as well as the reinforced backfill soil can be stated as follows:

Find $\quad X^T = \left[x_1, x_2, ..., x_{nv} \right]$ $\qquad$ (17)

such that X, including nv design variables, minimizes the following cost objective function, $C(X)$:

$$C(X) = V_{soil} C_{soil} + W_{steel} C_{steel} \qquad (18)$$

where V_{soil} is the total volume of the backfill soil, C_{soil} is the cost per unit volume of the backfill soil, W_{steel} is the total weight of the steel reinforcements, and C_{steel} is the cost per unit weight of the reinforcements. Here, the minimum cost design of MSE walls is subjected to the design constraints described in the previous section. It follows that, an optimization algorithm capable of handling the aforementioned constraints is adopted for an efficient search in the solution space.

4. ADAPTIVE DIMENSIONAL SEARCH ALGORITHM

Adaptive dimensional search was first presented in Ref. [17] for design optimization of truss structures. This population based optimization technique is working based on an evolutionary approach where at each iteration, after evaluation of the generated candidate designs, the best design found is used to generate a new population of candidate designs. The robustness of the adaptive dimensional search algorithm lies in the idea of updating the search dimensionality ratio (SDR) parameter dynamically during the optimization process to achieve a satisfactory balance between the exploration and exploitation features of the technique. In general, SDR can be defined as the percentage of the design variables that are perturbed probabilistically while generating a candidate solution from the current best design as follows:

$$SDR = \frac{N_p}{N_m} \tag{19}$$

where N_p is the number of design variables perturbed for generating a new candidate design and N_m is the total number of design variables. If SDR is different for each candidate design, the average search dimensionality ratio for a population, $(SDR)_{ave}$, can be determined using the mean of *SDR* values of all the candidate designs, (Eq. 20).

$$(SDR)_{ave} = \frac{\sum_{j=1}^{N_{pop}} (SDR)_j}{N_{pop}} \tag{20}$$

In Eq. (20), $(SDR)_j$ is search dimensionality ratio for the solution j and N_{pop} is the size of population. The general outline of the *ADS* algorithm is elaborated in the following steps.

Step 1. Initial population: Generate an initial population by randomly spreading candidate solutions over the search space in a uniform manner.

Step 2. Evaluation: Evaluate the corresponding objective function value of each candidate solution. The corresponding objective function values of the feasible solutions are computed using Eq. (18). However, infeasible designs that violate the constraints of the optimization problem are penalized, and their objective function values are determined based on Eq. (21).

$$C_p(X) = C(X)\left[1 + p\left(\sum_i g_i\right)\right] \tag{21}$$

In Eq. (21), *C(X)* is the cost objective function defined in Eq. (20), $C_p(X)$ is the penalized objective function, g_i is the *i*-th problem constraint violation and *p* is the penalty constant employed for constraint handling.

Step 3. Adapting search dimensionality ratio: Determine the value of $(SDR)_{ave}$, for perturbation of candidate designs in the next step, with respect to the success of the ADS in improving the current best solution as follows.

$$(SDR)_{ave}^{(it+1)} = \begin{cases} \dfrac{(SDR)_{ave}^{(it)}}{\lambda} & \text{if the best solution is improved} \\ \\ \lambda(SDR)_{ave}^{(it)} & \text{if the best solution is not improved} \end{cases} \tag{22}$$

Considering Eq. (22) if the best candidate solution found so far is improved in the current iteration, (it), then the value of $(SDR)_{ave}$ is increased for the next iteration, (it+1), through dividing its value by an adaptation factor, λ (taken as 0.98 in this study), otherwise $(SDR)_{ave}$ is decreased through multiplying its value by λ. The high values of SDR yield a more explorative search strategy by enabling moves in the search space through the change of many design variables at a time, resulting in large, yet relatively unfettered step sizes. Meanwhile, the low values of SDR lead to a more explorative search by facilitating small, yet more conservative moves in the design space. The rationale behind Eq. (22) is to promote a more explorative search, if any of the moves in the previous iteration leads to an improved solution. This way the search dimension is increased and the algorithm is encouraged to discover new solutions in an extended region of the search space. On the other hand, if the previous iteration leads to no improvement, diverse search is somewhat limited, and the algorithm is biased towards sampling by small and judicious moves around the current design. This way the SDR parameter is updated at each iteration to benefit from a more explorative or exploitative search alternately for the most efficient optimization process. In the present study the initial value of the $(SDR)_{ave}$ is set to 0.25, and the upper and lower bounds on the values of $(SDR)_{ave}$ are set to 0.5 and $\dfrac{1}{N_m}$, respectively, where N_m is the number of solution variables.

Step 4. Generation phase: Generate new candidate solutions based on the selected *SDR* in the previous step. Here, Eq. (23) is used at each iteration to produce new solutions around the current best solution.

$$X_i^{new} = X_i^c + round\left[N(0,1)_i \left(\sqrt{(X_i^{max} - X_i^{min})} - \left(\sqrt{(X_i^{max} - X_i^{min})} - 1 \right) \frac{it}{max\_it} \right) \right] \tag{23}$$

where X_i^c is the value of i-th discrete design variable in the best candidate solution, and X_i^{min} and X_i^{max} are its lower and upper bounds, respectively. $N(0,1)_i$ is a random number generated according to a standard normal distribution with mean (μ) zero and standard deviation (σ) equal to one, it is the iteration number, and max_it is the maximum number of iterations. It is obvious that in the generation phase, in order to take the value of *SDR* into account, only some of the solution variables are selected and changed through Eq. (23).

Step 5. Elitism: Keep the current best solution in a separate place or as a member of the population.

Step 6. Termination: Go to Step 2 until a termination criterion is satisfied. In this study, a maximum number of iterations is considered as the termination criterion for the optimization process. It is worthwhile to note that, to further improve the performance of the ADS, different stagnation control strategies have been proposed in Ref. [17]. Here, the aforementioned steps are followed for implementation of the algorithm.

5. NUMERICAL EXAMPLES

This section covers the numerical experiments performed using practical examples of MSE walls under different cases. In the first design example a MSE wall with sloping backfill is optimally designed under the aforementioned design constraints. In the second example, a MSE wall with level backfill is optimally designed under traffic load. Each test instance is tackled in two different cases where in the first case (case-a) the MSE wall rests on a soil foundation, whereas in the second case (case-b) the wall is assumed to be on a rock foundation.

For design optimization, the ADS algorithm is executed using a population size of 25 individuals over 200 iterations. It is apparent that due to the stochastic nature of the optimization algorithm it is expected to obtain different solutions from independent runs of the algorithm. In this study, for each test instance the ADS optimization algorithm is independently executed 100 times, and the best solution obtained is reported as the minimum cost design. Here, a discrete optimization is performed where the algorithm selects the type of ribbed steel strip and reinforced backfill soil form the available lists provided in Tables 2 and 3. For all the investigated examples the coefficient of uniformity of the reinforced backfill soil is assumed to be C_u=7. For practical requirements, the optimal spacing and length of the strips are selected from multiplies of 0.02 m. For all the investigated MSE walls a panel width of W_p=1.5 m is chosen for the precast facing elements.

5.1. Example 1: MSE Wall with Sloping Backfill

The 9.14 m high vertical MSE wall shown in Figure 7 is considered as the first design instance. The exposed height of the structure above the finished grade (H_e) and its embedment depth (*d*) are 8.61 m and 0.53 m, respectively. In this example, the ground surface slopes behind the wall with an angle of β=26.56°. For reinforcing the wall, ribbed steel strips as inextensible reinforcements are used in this example. Generally, in case of metallic inclusions, corrosion resistance is an important parameter affecting the life of the structure. Here, expecting a service life of 75 years for the MSE wall, galvanized ribbed steel strips with zinc coating of 86**μ**m are utilized. As suggested in Ref. [2], the lower bound on the length of steel strips is set to 0.8*H* where *H* is the total height of the MSE wall. The material properties and costs of the available ribbed steel strips are presented in Table 2.

Table 2 - Material properties and costs of the available ribbed steel strips

Strip type	Designation	b (mm)	t (mm)	f_y (MPa)	ρ (ton/m^3)	Cost ($/kg)
1	ST-1	40	4	448.16	7.92	1.95
2	ST-2	40	4	509.87	8.12	2.00
3	ST-3	40	5	448.16	7.92	1.90
4	ST-4	40	5	509.87	8.12	2.00
5	ST-5	45	4	448.16	7.92	1.90
6	ST-6	45	4	509.87	8.12	2.10

Table 2 - Material properties and costs of the available ribbed steel strips (continue)

Strip type	Designation	b (mm)	t (mm)	f_y (MPa)	ρ (ton/m³)	Cost ($/kg)
7	ST-7	45	5	448.16	7.92	1.95
8	ST-8	45	5	509.87	8.12	2.05
9	ST-9	50	4	448.16	7.92	1.90
10	ST-10	50	4	509.87	8.12	2.00
11	ST-11	50	5	448.16	7.92	1.95
12	ST-12	50	5	509.87	8.12	2.00
13	ST-13	55	4	509.87	8.12	2.05
14	ST-14	55	5	509.87	8.12	2.05
15	ST-15	60	4	509.87	7.92	2.10
16	ST-16	60	5	509.87	8.12	2.10

It is generally known that in the MSE walls the performance of reinforcement mainly depends on the friction characteristics of the fill. It follows that the reinforced fill is preferred to be a well-graded soil due to its favorable strength, drainage, placement, and compaction properties. Here, the properties and costs of available soils to be used in the reinforced zone are presented in Table 3. It is worthwhile to note that shear strength parameters of the retained backfill -the fill material located behind the mechanically stabilized soil zone- are also important in the design stage to determine the coefficients of earth pressure. In this test example, friction angle and unit weight of the retained filled are taken as $\emptyset_f$=30° and γ_f= 19.64 kN/m³, respectively.
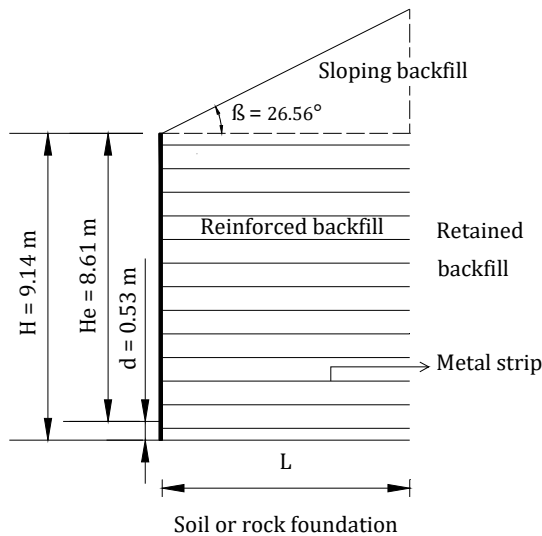

Figure 7 - MSE wall system of test example 1.

Table 3 - Properties and costs of the available reinforced backfill soils

Reinforced backfill type	Designation	ϕ_r	γ_r (kN/m³)	Cost ($/m³)
1	RB-1	34°	18.06	17.5
2	RB-2	36°	18.22	17.5
3	RB-3	38°	18.54	18.0
4	RB-4	40°	19.48	18.5
5	RB-5	42°	19.95	19.5

This test problem is solved in two different cases where in the first case (case-a) the MSE wall rests on a soil foundation, whereas in the second case (case-b) the wall is assumed to be located on a rock foundation. In case-a the foundation soil has a friction angle of $\emptyset_{fd}$=30°, and a unit weight of γ_{fd}=19.64 kN/m³. The factored bearing resistance of the foundation soil is assumed to be 359 kPa and 502 kPa for service and strength limit considerations, respectively.

Minimum cost design of the MSE wall with sloping backfill is performed using the ADS algorithm and the results obtained for case-a are summarized in Table 4. As presented in the table the ADS algorithm finds a promising final design with a cost of $ 418539.25 in case-a. In the optimum solution obtained, RB-2 is selected as the reinforced backfill soil type, and ST-2, with a length of L=7.32 m and a vertical spacing of S_v= 0.88 m, is adopted as the steel reinforcement for the investigated MSE wall. As given in Table 4 the horizontal spacing of strips (S_h) may vary for different strip layers.
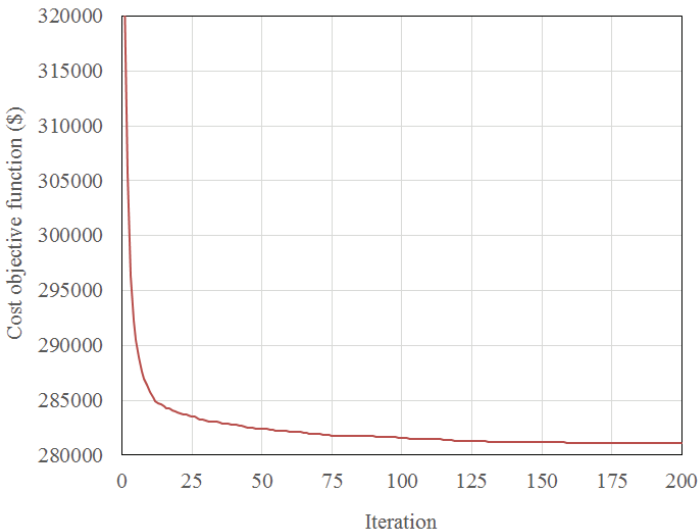

Figure 8 - Cost optimization history of test example 1-case (b)

Table 4 - Summary of cost optimization results for test example 1-case (a).

Level	Z (m)	Z_{P-ave} (m)	σ_H (kPa)	T_{max} (kN/W_p)	F^*	L_e (m)	$\emptyset_P(P_r)$ (kN/strip)	$\emptyset_T(T_n)$ (kN/strip)	N_P	N_t	N_g	S_h (m)
1	0.15	2.79	20.11	18.33	1.97	4.09	29.40	39.59	0.6	0.5	2	0.76
2	1.04	3.67	27.29	36.47	1.78	4.09	35.14	39.59	1.0	0.9	2	0.76
3	1.92	4.56	34.47	46.57	1.6	4.09	39.05	39.59	1.2	1.2	2	0.76
4	2.80	5.44	41.18	55.56	1.41	4.09	41.23	39.59	1.4	1.4	2	0.76
5	3.69	6.32	46.92	63.43	1.23	4.09	41.68	39.59	1.5	1.6	2	0.76
6	4.57	7.09	52.19	70.23	1.04	4.57	44.39	39.59	1.6	1.8	2	0.76
7	5.46	7.84	56.50	75.88	0.86	5.10	45.15	39.59	1.7	1.9	2	0.76
8	6.34	8.59	61.29	82.51	0.73	5.63	46.13	39.59	1.8	2.1	3	0.51
9	7.22	9.34	67.51	91.10	0.73	6.16	54.89	39.59	1.7	2.3	3	0.51
10	8.11	10.09	74.21	100.21	0.73	6.69	64.36	39.59	1.6	2.5	3	0.51
11	8.99	10.84	79.96	72.50	0.73	7.22	74.64	39.59	1.0	1.8	2	0.76
Cost ($) using optimum parameters (ST-2, RB-2, L=7.32 m, S_v=0.88 m)												**418539.25**

($\emptyset_P(P_r)$: Factored pullout resistance; $\emptyset_T(T_n)$: Factored tensile resistance; N_P: Number of strip reinforcements for a panel based on tensile resistance considerations; N_t: Number of strip reinforcements for a panel based on pullout resistance considerations; N_g: Governing number of strip reinforcements)

Table 5 - Summary of cost optimization results for test example 1-case (b).

Level	Z (m)	$Z_{P\text{-}ave}$ (m)	σ_H (kPa)	T_{max} (kN/W_p)	F^*	L_e (m)	$\emptyset_P(P_r)$ (kN/strip)	$\emptyset_T(T_n)$ (kN/strip)	N_P	N_t	N_g	S_h (m)
1	0.30	2.26	18.67	20.86	1.94	1.37	10.59	43.50	2.0	0.5	2	0.76
2	1.16	3.12	25.38	32.83	1.78	1.37	13.34	43.50	2.5	0.8	3	0.51
3	2.01	3.97	31.60	41.10	1.62	1.37	15.48	43.50	2.7	0.9	3	0.51
4	2.87	4.82	37.35	48.53	1.45	1.37	16.90	43.50	2.9	1.1	3	0.51
5	3.72	5.68	42.13	55.07	1.29	1.37	17.66	43.50	3.1	1.3	4	0.38
6	4.57	6.41	46.44	60.72	1.13	1.86	23.57	43.50	2.6	1.4	3	0.51
7	5.43	7.13	50.27	65.47	0.97	2.37	28.69	43.50	2.3	1.5	3	0.51
8	6.28	7.86	54.58	70.86	0.84	2.88	33.32	43.50	2.1	1.6	3	0.51
9	7.13	8.58	59.85	77.93	0.84	3.40	42.88	43.50	1.8	1.8	2	0.76
10	7.99	9.31	65.60	85.54	0.84	3.91	53.51	43.50	1.6	2.0	2	0.76
11	8.84	10.03	71.34	79.40	0.84	4.42	65.25	43.50	1.2	1.8	2	0.76

Cost ($) using optimum parameters (ST-9, RB-4, L=4.60 m, S_v=0.85 m) **280219.13**

($\emptyset_P(P_r)$: Factored pullout resistance; $\emptyset_T(T_n)$: Factored tensile resistance; N_P: Number of strip reinforcements for a panel based on tensile resistance considerations; N_t: Number of strip reinforcements for a panel based on pullout resistance considerations; N_g: Governing number of strip reinforcements)

As already noted, in case-b the foundation is selected as rock. Base on this assumption, the internal friction angle and allowable bearing pressure of the rock foundation are taken as 45° and 10 MPa, respectively. It should be noted that in case-b the lower bound on the length of steel strips is set to 0.4*H* where *H* is the total height of the MSE wall [2]. The numerical results of optimization in case-b for the MSE wall with sloping backfill are tabulated in Table 5. In this case a minimum cost of $ 280219.13 is obtained for the final design. For the optimum solution the ADS finds RB-4 as the reinforced backfill soil type, and ST-9, with a length of *L*=4.60 m and a vertical spacing of S_v= 0.85 m, as the steel reinforcement of the wall. The average cost optimization history of 100 independent runs of the ADS are plotted in Figure 8. The comparison of final results obtained in two different cases indicates a reduction of 33% in the cost of the MSE wall in case-b compared to case-a.

5.2. Example 2: MSE Wall with Level Backfill And Traffic Load

Minimum cost design of the MSE wall depicted in Figure 9, with level backfill and traffic load, is considered as the second test example. Here, similar to the previous test example in case-a the foundation soil has a friction angle of $Ø_{fd}$ =30°, and a unit weight of γ_{fd}=19.64 kN/m³. The factored bearing resistance of the foundation soil is also assumed to be 359 kPa and 502 kPa for service and strength limit considerations, respectively. In this case, the lower bound on the length of steel strips is set to 0.7*H* where *H* is the total height of the MSE wall [2].
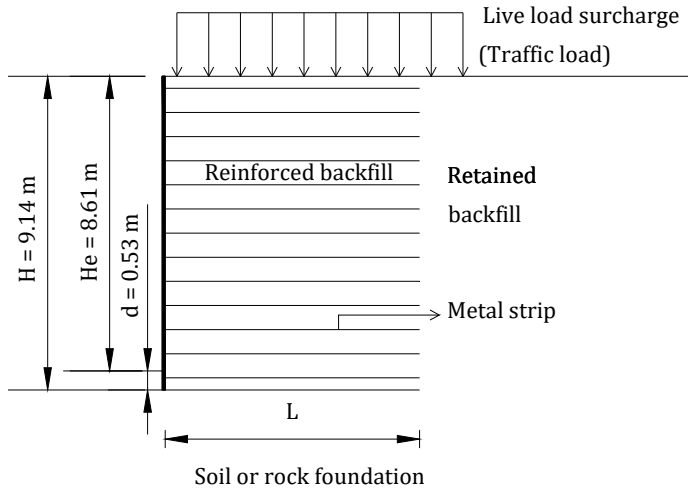

Figure 9 - MSE wall system of test example 2

Cost optimization of the MSE wall with level backfill and traffic load is carried out using the ADS algorithm and the numerical results for case-a are tabulated in Table 6. As shown in this table the algorithm locates a cost-effective design with a cost of $ 323727.76 in case-a. In the obtained optimum design, RB-2 is adopted as the reinforced backfill soil type, and ST-9, with a length of L=6.40 m and a vertical spacing of S_v= 0.84 m, is selected as the steel

reinforcement for the investigated MSE wall. As shown in Table 6 the horizontal spacing of strips (S_h) may vary for different strip layers. Figure 10 shows the average cost optimization history of the ADS algorithm in case-a.
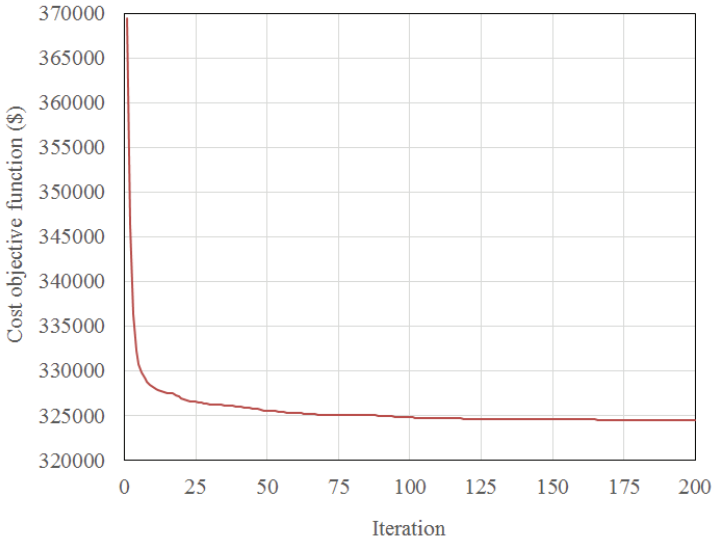

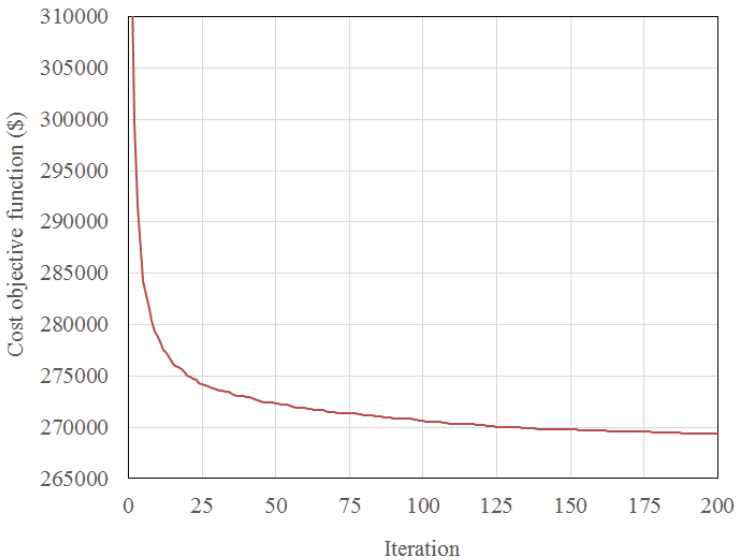*Figure 10 - Cost optimization history of test example 2-case (a)*

Figure 11 - Cost optimization history of test example 2-case (b)

Table 6 - Summary of cost optimization results for test example 2-case (a).

Level	Z (m)	$Z_{P\text{-}ave}$ (m)	σ_H (kPa)	T_{max} (kN/W_p)	F^*	L_e (m)	$\varnothing_P(P_r)$ (kN/strip)	$\varnothing_T(T_n)$ (kN/strip)	N_P	N_t	N_g	S_h (m)
1	0.38	0.38	10.53	12.99	1.92	3.66	4.40	43.50	3.0	0.3	3	0.51
2	1.22	1.22	18.67	23.75	1.75	3.66	12.77	43.50	1.9	0.6	2	0.76
3	2.06	2.06	25.86	33.18	1.57	3.66	19.39	43.50	1.7	0.8	2	0.76
4	2.90	2.90	32.56	41.72	1.4	3.66	24.24	43.50	1.7	1.0	2	0.76
5	3.73	3.73	38.78	49.28	1.22	3.66	27.31	43.50	1.8	1.1	2	0.76
6	4.57	4.57	43.57	55.91	1.04	3.66	28.65	43.50	2.0	1.3	2	0.76
7	5.41	5.41	48.36	61.56	0.87	4.16	32.11	43.50	1.9	1.4	2	0.76
8	6.25	6.25	53.15	67.70	0.73	4.66	34.74	43.50	2.0	1.6	2	0.76
9	7.09	7.09	58.89	75.35	0.73	5.17	43.63	43.50	1.7	1.7	2	0.76
10	7.92	7.92	65.60	83.53	0.73	5.67	53.51	43.50	1.6	1.9	2	0.76
11	8.76	8.76	71.82	87.40	0.73	6.17	64.45	43.50	1.4	2.0	3	0.51

Cost (\$) using optimum parameters (ST-9, RB-2, L=6.40 m, S_v=0.84 m) **323727.76**

($\varnothing_P(P_r)$): Factored pullout resistance; $\varnothing_T(T_n)$: Factored tensile resistance; N_P: Number of strip reinforcements for a panel based on tensile resistance considerations; N_t: Number of strip reinforcements for a panel based on pullout resistance considerations; N_g: Governing number of strip reinforcements)

Table 7 - Summary of cost optimization results for test example 2-case (b).

Level	Z (m)	Z_{P-ave} (m)	σ_H (kPa)	T_{max} (kN/W_p)	F^*	L_e (m)	$\emptyset_P(P_r)$ (kN/strip)	$\emptyset_T(T_n)$ (kN/strip)	N_P	N_t	N_g	S_h (m)
1	0.38	0.38	9.58	11.65	1.93	2.09	2.40	39.14	4.8	0.3	5	0.30
2	1.22	1.22	16.76	21.26	1.77	2.09	7.12	39.14	3.0	0.5	3	0.51
3	2.06	2.06	23.46	29.71	1.61	2.09	10.90	39.14	2.7	0.8	3	0.51
4	2.90	2.90	29.21	37.32	1.45	2.09	13.83	39.14	2.7	1.0	3	0.51
5	3.73	3.73	34.47	44.12	1.29	2.09	15.83	39.14	2.8	1.1	3	0.51
6	4.57	4.57	39.26	50.04	1.13	2.09	16.99	39.14	2.9	1.3	3	0.51
7	5.41	5.41	43.09	55.11	0.97	2.59	21.44	39.14	2.6	1.4	3	0.51
8	6.25	6.25	47.40	60.63	0.84	3.09	25.58	39.14	2.4	1.6	3	0.51
9	7.09	7.09	52.67	67.48	0.84	3.60	33.76	39.14	2.0	1.7	2	0.76
10	7.92	7.92	58.41	74.82	0.84	4.10	43.01	39.14	1.7	1.9	2	0.76
11	8.76	8.76	64.16	78.24	0.84	4.60	53.38	39.14	1.5	2.0	2	0.76

Cost ($) using optimum parameters (ST-5, RB-4, L=4.83 m, S_v=0.84 m)   **266275.54**

($\emptyset_T(T_n)$) : Factored tensile resistance; $\emptyset_P(P_r)$:Factored pullout resistance; N_P: Number of strip reinforcements for a panel based on tensile resistance considerations; N_t : Number of strip reinforcements for a panel based on pullout resistance considerations; N_g: Governing number of strip reinforcements)

As mentioned before, in case-b the foundation is selected as rock. Accordingly, the internal friction angle and allowable bearing pressure of the rock foundation are taken as 45° and 209 10 MPa, respectively. In this case the lower bound on the length of steel strips is set to 0.4H where H is the total height of the MSE wall [2].

The cost optimization results of case-b for the MSE wall with level backfill and traffic load are presented in Table 7. As can be seen from the table, in this case a minimum cost of $ 266275.54 is obtained for the final design. For the optimum solution, the ADS finds RB-4 as the reinforced backfill soil type, and ST-5, with a length of L=4.83 m and a vertical spacing of S$_v$= 0.84 m, as the steel reinforcement of the wall. The average cost optimization history of the ADS algorithm in case-b is plotted in Figure 11. It is worth mentioning that the comparison of final results obtained in two different cases shows a reduction of 18% in the cost of the investigated MSE wall in case-b compared to case-a.

6. CONCLUSIONS

In the present study, cost efficient design optimization of mechanically stabilized earth walls is performed using a recently proposed metaheuristic algorithm, namely adaptive dimensional search. For a minimum cost design, different types of steel reinforcement as well as reinforced backfill soil are considered as discrete solution variables. The performance of the adaptive dimensional search algorithm is evaluated through design examples of mechanically stabilized earth walls under realistic design criteria stipulated by standard design codes. The obtained numerical results indicate that the ADS algorithm can be efficiently employed for cost optimization of mechanically stabilized earth walls in real world applications. Furthermore, comparison of the final designs obtained in different test cases reveal that improving the foundation properties may be considered as an alternative way to further reduce the total cost of the mechanically stabilized earth walls in practical applications.

References

[1]   Coduto, D.P., Foundation Design Principles and Practices, 2nd Edition, 2001.

[2]   Berg R.R., Christopher B.R. and Samtani N.C. Design of Mechanically Stabilized Earth Walls and Reinforced Soil Slopes – Volume I, Department of Transportation FHWA, Washington, D.C., USA, 2009.

[3]   Berg R.R., Christopher B.R. and Samtani N.C. Design of Mechanically Stabilized Earth Walls and Reinforced Soil Slopes – Volume II, Department of Transportation FHWA, Washington, D.C., USA, 2009.

[4]   H. Ghiassian, K. Aladini, Optimum design of reinforced earth walls with metal strips; simulation-optimization approach, Asian Journal of Civil Engineering (Building and Housing), 10 (6): 641–655, 2009.

[5]   P.K. Basudhar A. Vashistha K. Deb, A. Dey, Cost optimization of reinforced earth walls, Geotech. Geol. Eng., 26: 1–12, 2008.

[6] Goldberg DE, Samtani MP. Engineering optimization via genetic algorithm. Proceeding of the Ninth Conference on Electronic Computation, ASCE, pp. 471–482, 1986.

[7] Kirkpatrick S, Gerlatt CD, Vecchi MP. Optimization by simulated annealing, Science, 220: 671–680, 1983.

[8] Kennedy J, Eberhart R. Particle swarm optimization. In: IEEE international conference on neural networks, IEEE Press, pp. 1942–1948, 1995.

[9] Colorni A, Dorigo M, Maniezzo V. Distributed optimization by ant colony. In: Proceedings of the first European conference on artificial life, USA, pp. 134–142, 1991.

[10] Dorigo M. Optimization, learning and natural algorithms, PhD thesis. Dipartimento di Elettronica e Informazione, Politecnico di Milano, Italy, 1992.

[11] Lee KS, Geem ZW. A new structural optimization method based on the harmony search algorithm, Comput. Struct., 82: 781–798, 2004.

[12] Yang X-S. Nature-inspired metaheuristic algorithms, Luniver Press, UK, 2008.

[13] Erbatur F, Al-Hussainy MM. Optimum design of frames, Comput. Struct. 45: 887–891, 1992.

[14] Tabak EI, Wright PM. Optimality criteria method for building frames, J. Struct. Div., 107: 1327–1342, 1981.

[15] Lamberti L, Pappalettere C. Metaheuristic design optimization of skeletal structures: a review, Computational Technology Reviews, pp. 1–32, 2011.

[16] Saka MP. Optimum design of steel frames using stochastic search techniques based in natural phenomena: a review, in: B.H.V. Topping (Ed.), Civil Engineering Computations: Tools and Techniques, Saxe-Coburg Publications, Stirlingshire, UK, pp. 105–147, 2007.

[17] O. Hasançebi, S. Kazemzadeh Azad, Adaptive dimensional search: A new metaheuristic algorithm for discrete truss sizing optimization, Comput. Struct. 154, 1–16, 2005.

[18] American Association of State Highway and Transportation Officials (AASHTO), LRFD Bridge Design Specifications, 5th Edition, 2010.

TEKNİK DERGİ MANUSCRIPT DRAFTING RULES

1. The whole manuscript (text, charts, equations, drawings etc.) should be arranged in Word and submitted in ready to print format. The article should be typed on A4 (210 x 297 mm) size paper using 10 pt (main title 15 pt) Times New Roman font, single spacing. Margins should be 40 mm on the left and right sides and 52.5 mm at the top and bottom of the page.

2. Including drawings and tables, articles should not exceed 25 pages, technical notes 6 pages.

3. Your contributed manuscript must be sent over the DergiPark system. (http://dergipark.gov.tr/tekderg)

4. The text must be written in a clear and understandable language, conform to the grammar rules. Third singular person and passive tense must be used, and no inverted sentences should be contained.

5. Title must be short (10 words maximum) and clear, and reflect the content of the paper.

6. Sections should be arranged as: (i) abstract and keywords, (ii) title, abstract and keywords in the other language, (iii) main text, (iv) symbols, (v) acknowledgements (if required) and (vi) references.

7. Both abstracts should briefly describe the object, scope, method and conclusions of the work and should not exceed 100 words. If necessary, abstracts may be re-written without consulting the author. At least three keywords must be given. Titles, abstracts and keywords must be fitted in the first page leaving ten line space at the bottom of the first page and the main text must start in the second page.

8. Section and sub-section titles must be numbered complying with the standard TS1212.

9. Symbols must conform to the international rules; each symbol must be defined where it appears first, additionally, a list of symbols must be given in alphabetic order (first Latin, then Greek alphabets) at the end of the text (before References).

10. Equations must be numbered and these numbers must be shown in brackets at the end of the line.

11. Tables, drawings and photographs must be placed inside the text, each one should have a number and title and titles should be written above the tables and below the drawings and photographs.

12. Only SI units must be used in the manuscripts.

13. Quotes must be given in inverted commas and the source must be indicated with a reference number.

14. Acknowledgement must be short and mention the people/ institutions contributed or assisted the study.

15. References must be numbered (in brackets) in the text referring to the reference list arranged in the order of appearance in the text. References must include the following information:

    If the reference is an article: Author's surname, his/her initials, other authors, full title of the article, name of the journal, volume, issue, starting and ending pages, year of publication.

    > Example : Naghdi, P. M., Kalnins, A., On Vibrations of Elastic Spherical Shells. J. Appl. Mech., 29, 65-72, 1962.

    If the reference is a book: Author's surname, his/her initials, other authors, title of the book, volume number, editor if available, place of publication, year of publication.

    > Example : Kraus. H., Thin Elastic Shells, New York. Wiley, 1967.

    If the reference is a conference paper: Author's surname, his/her initials, other authors, title of the paper, title of the conference, location and year.

    If the source is a thesis: Author's surname, his/her initials, thesis title, level, university, year.

    If the source is a report: Author's surname, his/her initials, other authors, title of the report, type, number, institution it is submitted to, publication place, year.

16. Discussions to an article published in Teknik Dergi should not exceed two pages, must briefly express the addressed points, must criticize the content, not the author and must be written in a polite language. Authors' closing remarks must also follow the above rules.

17. A separate note should accompany the manuscript. The note should include, (i) authors' names, business and home addresses and phone numbers, (ii) brief resumes of the authors and (iii) a statement "I declare in honesty that this article is the product of a genuinely original study and that a similar version of the article has not been previously published anywhere else" signed by all authors.

18. Copyright has to be transferred to UCTEA Turkish Chamber of Civil Engineers. The standard copyright form signed by the authorised author should therefore be submitted together with the manuscript.

CONTENTS

OBITUARY - ENDER ARKUN